nature cancer

Article

https://doi.org/10.1038/s43018-023-00594-z

The Akt/mTOR and MNK/eIF4E pathways rewire the prostate cancer translatome to secrete HGF, SPP1 and BGN and recruit suppressive myeloid cells

Received: 9 May 2022

Accepted: 13 June 2023

Published online: 17 July 2023

Check for updates

Daniela Brina[1], Adele Ponzoni[1,17], Martina Troiani[1,2], Bianca Calì[1], Emiliano Pasquini[1], Giuseppe Attanasio[1], Simone Mosole[1], Michela Mirenda[1,18], Mariantonietta D'Ambrosio[1,19], Manuel Colucci[1], Ilaria Guccini[1,20], Ajinkya Revandkar[1,21], Abdullah Alajati[1,22], Toma Tebaldi[3], Deborah Donzel[4], Fabio Lauria[4], Nahjme Parhizgari[1,23], Aurora Valdata[1], Martino Maddalena[1], Arianna Calcinotto[1], Marco Bolis[2,5,6], Andrea Rinaldi[1], Simon Barry[7], Jan Hendrik Rüschoff[8], Marianna Sabbadin[9], Semini Sumanasuriya[10], Mateus Crespo[10], Adam Sharp[10], Wei Yuan[10], Mathew Grinu[11], Alexandra Boyle[11], Cynthia Miller[11], Lloyd Trotman[11], Nicolas Delaleu[12], Matteo Fassan[9,13], Holger Moch[8], Gabriella Viero[4], Johann de Bono[10,14] & Andrea Alimonti[1,2,15,16]

Cancer is highly infiltrated by myeloid-derived suppressor cells (MDSCs). Currently available immunotherapies do not completely eradicate MDSCs. Through a genome-wide analysis of the translatome of prostate cancers driven by different genetic alterations, we demonstrate that prostate cancer rewires its secretome at the translational level to recruit MDSCs. Among different secreted proteins released by prostate tumor cells, we identified Hgf, Spp1 and Bgn as the key factors that regulate MDSC migration. Mechanistically, we found that the coordinated loss of Pdcd4 and activation of the MNK/eIF4E pathways regulate the mRNAs translation of *Hgf*, *Spp1* and *Bgn*. MDSC infiltration and tumor growth were dampened in prostate cancer treated with the MNK1/2 inhibitor eFT508 and/or the AKT inhibitor ipatasertib, either alone or in combination with a clinically available MDSC-targeting immunotherapy. This work provides a therapeutic strategy that combines translation inhibition with available immunotherapies to restore immune surveillance in prostate cancer.

Prostate cancer is the second most commonly occurring cancer in men and the fourth most commonly occurring cancer overall. While immune-checkpoint inhibitor therapies are effective in several tumors, patients with prostate cancer do not respond to this treatment[1]. Indeed, the tumor microenvironment of prostate cancers is characterized by an increased number of MDSCs and tumor-associated macrophages that dampen T-cell and natural killer (NK) cell activation[2,3]. MDSCs are the predominant immune cell subset infiltrating prostate cancer with

A full list of affiliations appears at the end of the paper. e-mail: andrea.alimonti@ior.usi.ch

previous findings demonstrating that these cells lead to (1) immunosuppression[4]; (2) evasion of chemotherapy-induced senescence[5]; and (3) onset of castration-resistance prostate cancer (CRPC)[6]. A direct relationship between tumor burden and MDSC frequency has been demonstrated in clinical studies and an inverse correlation between MDSCs and circulating T-cell counts has been described as a negative prognostic factor in patients affected by different tumors, including prostate cancer[7–15]. Previous findings from additional research teams and us have identified interleukin (IL)-8 and its cognate receptor CXCR2 as the key mediators of MDSCs recruitment in prostate tumors[16–18]. Ongoing clinical trials based on the CXCR2 antagonist AZD5069 (ref. 19) or anti-IL-8 antibody treatment are under clinical evaluation in individuals who are hormone-sensitive and those with CRPC (ClinicalTrials.gov identifiers NCT03177187 and NCT03689699). Nonetheless, preclinical studies showed that these compounds only partially affect the recruitment of MDSCs in vivo and that prolonged administration of CXCR2 antagonists ultimately leads to treatment resistance[5,20]. Thus, identifying mechanisms by which tumor cells recruit MDSCs could lead to the discovery of clinically relevant therapeutic targets.

Tumor cells rely on great demand for protein synthesis to grow, invade the surrounding tissues and control the tumor secretome[21,22]. PTEN is one of the most altered tumor suppressor genes in human prostate cancer[23–25]. Preclinical studies have demonstrated that loss of PTEN leads to PI3K/AKT/mTOR activation, thereby promoting increased protein synthesis, a cause of tumor initiation and progression[26]. In cancer cells, translation is regulated by the AKT/mTOR and MNK pathways[27]. Both pathways control the function of eIF4E, a key member of the eIF4F complex, which binds to the 7-methylguanylate cap at the 5′ end of messenger RNA and sustains protein synthesis[28]. 4EBP1 phosphorylation increases the availability of eIF4E in the eIF4F complex, whereas MNK1/2 kinase promotes eIF4E phosphorylation[29–34]. AKT also regulates the formation of the eIF4F complex through PDCD4, a protein that binds and sequesters eIF4A[35–37]. Thus, eIF4F is a central hub for protein synthesis and both the PI3K/AKT/mTOR and the MNK pathways converge to eIF4F to regulate protein synthesis. Here, using polysome profiling and bioinformatic analyses, we have characterized the extracellular interactome of Pten-deficient prostate cancers to assess the mechanisms by which prostate tumor cells recruit and activate MDSCs. We report the identification of hepatocyte growth factor (HGF), osteopontin (SPP1) and biglycan (BGN) as three translationally regulated key players in the interaction between prostate cancer cells and MDSCs. Previous studies using classical transcriptomic analysis did not identify these factors concomitantly in the secretome of prostate cancer[38]. Indeed, transcriptomic analysis does not entirely reflect the proteome of cancer cells[39], whereas polysome profiling phenocopies more faithfully changes at the proteome level[40], especially downstream of oncogenic signaling activated in cancer[41]. Mechanistically, we show that loss of PDCD4 and phosphorylation of eIF4E in prostate tumor cells allow eIF4F to translate *Hgf*, *Spp1* and *Bgn*, promoting the intratumoral recruitment of MDSCs. Therapeutically, we report that clinically available inhibitors of translation function as potent immunotherapies that block MDSCs recruitment and activation, thereby enhancing tumor immune surveillance in prostate cancer.

Results

The extracellular interactome between prostate cancer and MDSCs

Prostate tumors of different disease aggressiveness, benign ($Pten^{pc-/-}$), invasive ($Pten^{pc-/-}$;TMPRSS2-$Erg^{pc+/+}$ (ref. 42), $Pten^{pc-/-}$;$Trp53^{pc-/-}$ (ref. 43)) and metastatic ($Pten^{pc-/-}$;$CDCP1^{pc+/+}$ (ref. 44), $Pten^{pc-/-}$;$Timp1^{-/-}$ (ref. 45)) were resected from mice of five different genetic backgrounds, between 20 and 25 weeks of age. FACS analysis was performed to characterize the immune landscape of these prostate tumors. In line with previous data[5,6], we found that polymorphonuclear (PMN)-MDSCs ($CD45^+$/$CD11b^+$/$Ly6G^{high}$/$Ly6C^{low}$) cover the higher percentage among the tumor-infiltrating immune cell subsets analyzed and the percentage of these cells increased with disease aggressiveness, whereas $CD45^+$/$CD11b^+$/$Ly6G^{neg}$/$Ly6C^{high}$ (M-MDSCs) are a minority (Fig. 1a). To identify tumor-specific factors responsible for PMN-MDSC recruitment, we performed a genome-wide analysis of the translatome in these tumors by polysome profiling analysis and RNA-seq (Fig. 1b). Contrary to transcriptomic analysis, polysome profiling allows identifying actively translated ribosome-bound mRNAs in cancers, a measure of protein abundance[46,47]. Three prostates for each genetic background for a total of 18 samples were used for the polysome profiling. Principal-component analysis (PCA) of healthy and prostate tumor samples demonstrated good reproducibility of the samples in the different genetic backgrounds and between total and polysomal RNA pools (Extended Data Fig. 1a–c). The scatter-plots summarizing the translational changes obtained by the polysome profiling in the different genetic backgrounds are shown in Extended Data Fig. 1d. Bioinformatic analysis showed that most of the translated mRNAs in prostate tumors carry a long 5′ untranslated region (UTR) and have increased folding energy, which requires the helicase activity of eIF4A to be efficiently translated[48,49] (Fig. 1c). In addition, Gene Ontology (GO) analysis revealed that these upregulated mRNAs were involved in biological processes regulating myeloid/leukocytes migration and response to cytokines (Fig. 1d; polysomal RNA and total RNA GO biological processes, Extended Data Fig. 2a,b). To identify the key interactors responsible for the recruitment and activation of MDSCs, we applied a bioinformatic algorithm to identify secreted and membrane-tethering factors upregulated (log_2 fold change > 1; false discovery rate (FDR) < 0.05) in prostate cancer with a corresponding receptor upregulated (log_2 fold change > 1; FDR < 0.05) in the tumor and present on the plasma membrane of MDSCs (Extended Data Fig. 2c). By matching the ligands with the receptors, we identified 13 ligand–receptor couples overexpressed in the tumors with a cognate receptor expressed in MDSCs (Fig. 1e). Among these couples, we found CXCL5, a ligand of the CXCR2 receptor expressed on MDSCs, a known recruiter of these immune cells, thereby demonstrating the reliability of this analysis (Fig. 2a and Supplementary Tables 1 and 2). Finally, we determined the translational efficiency of the differentially expressed 13 targets (ratio between polysomal mRNA and total mRNA expression) to identify factors enriched in ribosome-bound mRNAs (Fig. 2a).

HGF, SPP1 and BGN recruit MDSCs in prostate cancer

Among the most translationally upregulated ligands identified, we found HGF, SPP1 and BGN (Fig. 2b,c and Supplementary Tables 1 and 2), secreted

Fig. 1 | Genome-wide analysis of the translatome is exploited to identify the extracellular interactome of prostate cancer - PMN-MDSCs. **a**, Immunophenotype of $Pten^{pc-/-}$ ($n = 4$), $Pten^{pc-/-}$;TMPRSS2/$Erg^{pc+/+}$ (at least $n = 3$), $Pten^{pc-/-}$;$CDCP1^{pc+/+}$ (at least $n = 2$), $Pten^{pc-/-}$;$Timp1^{-/-}$ ($n = 3$) and $Pten^{pc-/-}$;$Trp53^{pc-/-}$ ($n = 5$) prostate cancers. **b**, Scheme of the polysome profiling analysis. **c**, Features of the 5′ UTRs of the translationally regulated mRNAs: 5′ UTR estimated length (top) and folding energy comparison (bottom). The mRNAs with an increased translation efficiency (TE) and the mRNAs with a decreased TE (down) were compared to mRNAs with a not significantly changed TE (inv) for each indicated genetic background ($n = 3$ mice) compared to wild-type prostates ($n = 3$ mice). In box whisker plots, center shows median of the distribution, box shows lower and upper quartile, whiskers show 1.5 interquartile range and outliers are not displayed. The statistical test used was a Wilcoxon rank-sum test (two-sided). **d**, GO biological processes enriched among the translationally upregulated mRNAs in $Pten^{pc-/-}$, $Pten^{pc-/-}$;TMPRSS2/$Erg^{pc+/+;}$ $Pten^{pc-/-}$;$CDCP1^{pc+/+}$, $Pten^{pc-/-}$;Timp1−/− and $Pten^{pc-/-}$;$Trp53^{pc-/-}$ prostate cancer compared to wild-type prostate, determined by the DAVID software ($n = 3$ mice for each genetic background for a total of 18 samples). The log_{10} adjusted P values using the linear step-up method of Benjamini are reported. **e**, Bioinformatic algorithm applied to identify the extracellular interactome of prostate cancer - PMN-MDSCs.

https://doi.org/10.1038/s43018-023-00594-z

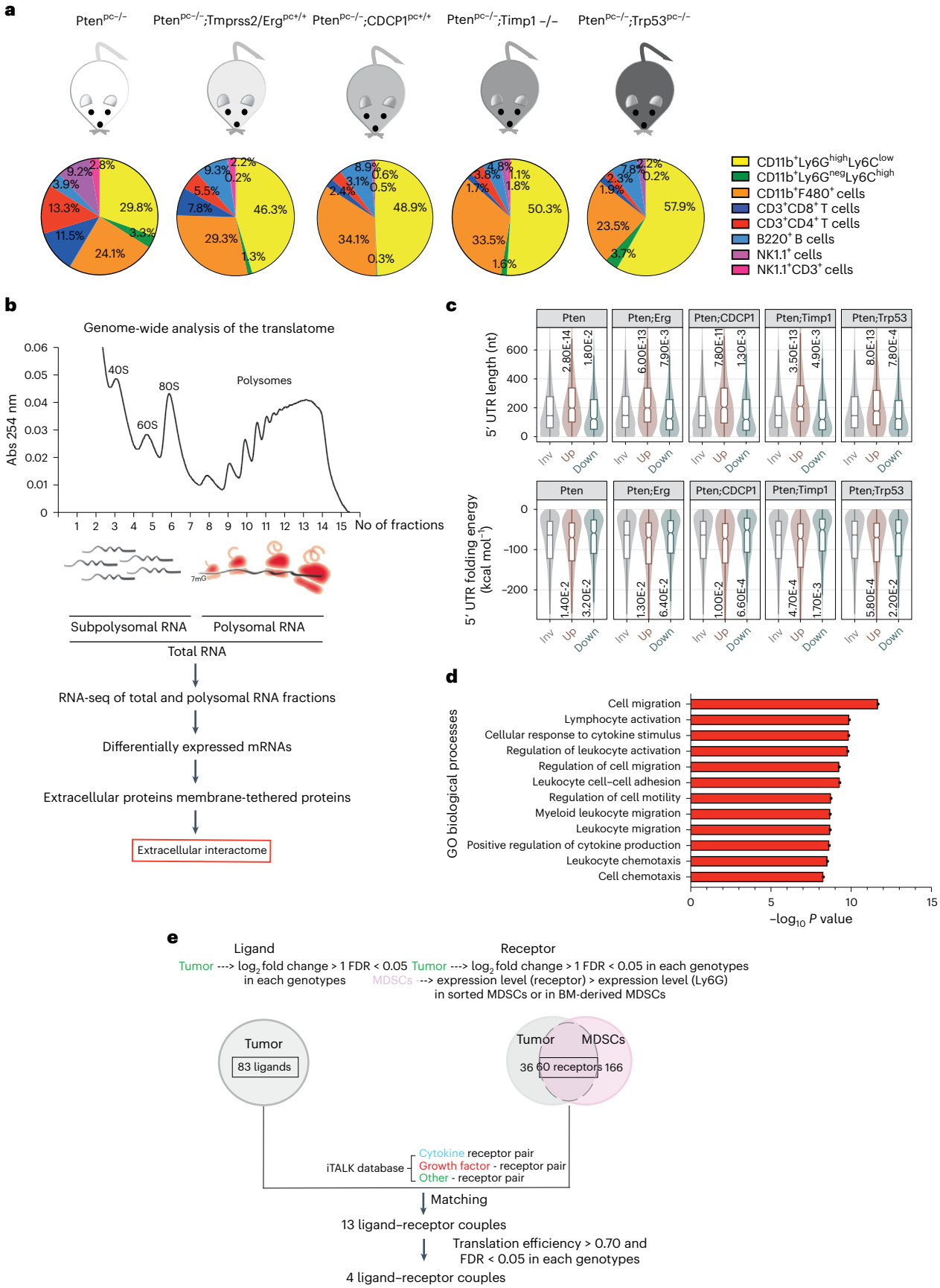

https://doi.org/10.1038/s43018-023-00594-z

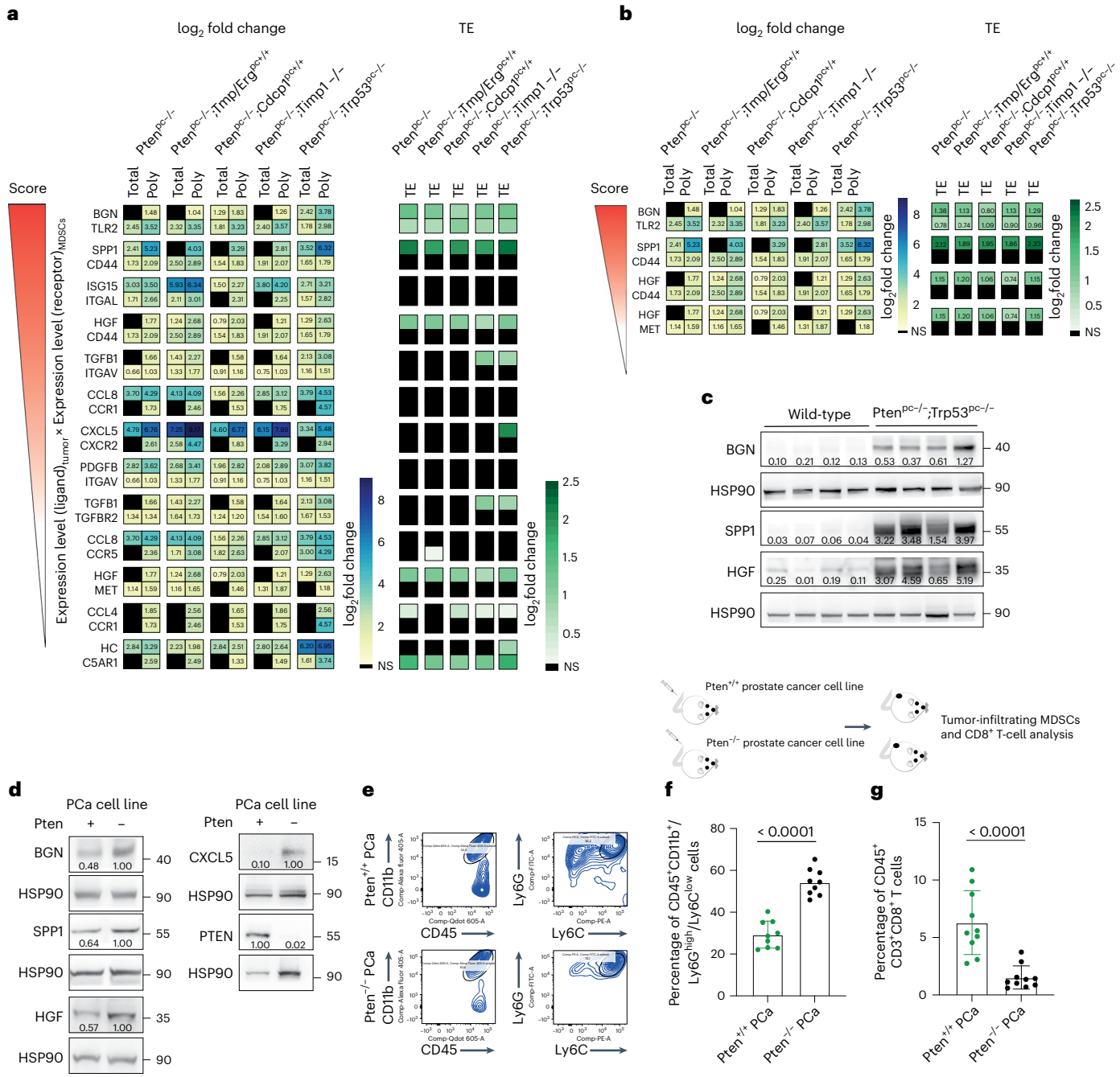

Fig. 2 | HGF, SPP1 and BGN are the most expressed, translationally regulated secreted factors in Pten-null-driven prostate cancer. a, List of ligand–receptor couples upregulated in the indicated genetic backgrounds of prostate cancer. The $\log_2$ fold change of polysome-bound RNA (poly) and total RNA (total) expression (threshold fold change >1; threshold significant FDR < 0.05) (left). The $\log_2$ fold change TE (threshold fold change >0.70; threshold significant FDR < 0.05) ($n = 3$ for each genetic background for a total of 18 samples) (right). See also Supplementary Table 1 for the fold change of total RNA and polysomal RNA. **b**, Translationally regulated ligand–receptor pairs upregulated in the indicated genetic backgrounds of prostate cancer (threshold fold change >0.70; threshold significant FDR < 0.05) ($n = 3$ for each genetic background for a total of 18 samples). The $\log_2$ fold change is indicated in the heat map. See Supplementary Table 2 for the fold change of the TE. **c**, Western blot showing the levels of HGF, SPP1 and BGN in wild-type prostates and $Pten^{pc-/-}$;$Trp53^{pc-/-}$ prostate cancers. The experiment was performed once with $n = 4$ mice for each group. Densitometry values normalized to the respective loading control are indicated for each band. **d**, Western blot showing the levels of HGF, SPP1, BGN, CXCL5 and PTEN in Pten wild-type or Pten-sh TC1 cell line. Densitometry values normalized to the respective loading control are indicated for each band. The experiment was repeated three times independently with similar results. **e**, Scheme of the experiment of Pten wild-type or Pten-sh TC1 prostate cancer cell injection (top), representative FACS plots of the $CD45^+/CD11b^+$ population and $Ly6G^{high}/Ly6C^{low}$ cells inside the $CD45^+/CD11b^+$ population (bottom left). **f**, Percentage of $CD45^+/CD11b^+/Ly6G^{high}/Ly6C^{low}$ cells inside the $CD45^+$ population in Pten wild-type and Pten-sh TC1 allograft tumors ($n = 9$ mice in each group). Statistical analysis was carried out by unpaired two-sided Student's *t*-test. **g**, Percentage of $CD45^+/CD3^+/CD8^+$ cells inside the $CD45^+$ population in Pten wild-type and Pten-sh TC1 allograft tumors ($n = 10$ mice in each group). Statistical analysis was carried out by a Mann–Whitney *U*-test. NS, not significant.

https://doi.org/10.1038/s43018-023-00594-z

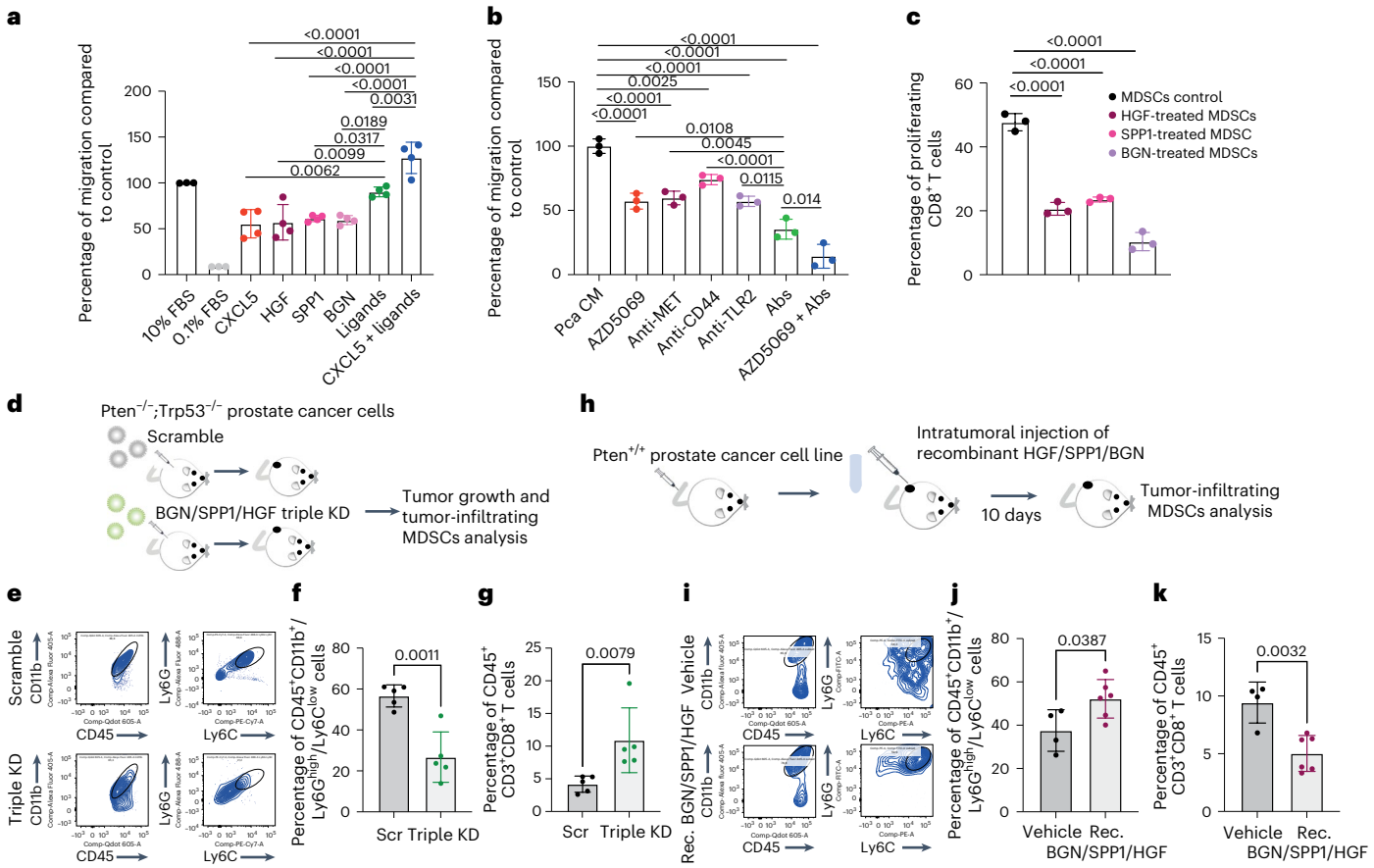

Fig. 3 | HGF, SPP1 and BGN induce PMN-MDSC migration and a T-cell suppressive function. a, Transwell migration assay with bone-marrow-derived MDSCs tested for the capability to migrate toward RPMI medium supplemented with the indicated secreted factors. Ligands were HGF + SPP1 + BGN; $n = 4$ biological replicates. The experiment was repeated twice independently with similar results. **b**, Transwell migration assay with bone-marrow-derived MDSCs tested in the presence of blocking antibodies (Abs) for MET, CD44 and TLR2 with or without CXCR2 antagonist AZD5069, toward prostate cancer (PCa) conditioned medium (CM) derived from Pten$^{-/-}$;Trp53$^{-/-}$ (RapidCap) PCa cells. Antibodies were anti-MET + anti-CD44 + anti-TLR2; $n = 3$ biological replicates. The experiment was repeated twice independently with similar results. **c**, Flow cytometric analysis of T-cell suppression assay, analyzed as CFSE dilution, of splenocytes co-cultured with bone-marrow-derived MDSCs; MDSCs were incubated for 24 h with the indicated secreted factors before performing the experiment ($n = 3$ biological replicates). The experiment was repeated twice independently with similar results. **d**, Scheme of the experiment of Hgf, Spp1 and Bgn shRNAs in Pten$^{-/-}$;Trp53$^{-/-}$ (RapidCap) cells. **e**, Representative FACS plots of CD45$^+$/CD11b$^+$ population and Ly6G^{high}/Ly6C^{low} cells inside the CD45$^+$/CD11b$^+$ population in scramble and triple KD in Pten$^{-/-}$;Trp53$^{-/-}$ (RapidCap) allografts. **f**, Percentage of CD45$^+$/CD11b$^+$/Ly6G^{high}/Ly6C^{low} cells (PMN-MDSCs) inside the CD45$^+$ population in Pten$^{-/-}$;Trp53$^{-/-}$ (RapidCap) allografts tumors ($n = 5$ mice in each group). Scr, scramble. **g**, Percentage of CD45$^+$/CD3$^{+/-}$CD8$^+$ cells inside the CD45$^+$ population in Pten$^{-/-}$;Trp53$^{-/-}$ (RapidCap) allografts tumors ($n = 5$ mice in each group). **h**, Scheme of the experiment of rec. BGN/SPP1/HGF-treated Pten wild-type TC1 allografts (10-d treatment). **i**, Representative FACS plots of CD45$^+$/CD11b$^+$ population and Ly6G^{high}/Ly6C^{low} cells (PMN-MDSCs) inside the CD45$^+$/CD11b$^+$ population in vehicle-treated or recombinant (Rec.) BGN/SPP1/HGF-treated Pten wild-type TC1 allografts. **j**, Percentage of CD45$^+$/CD11b$^+$/Ly6G^{high}/Ly6C^{low} cells (PMN-MDSCs) inside the CD45$^+$ population in Rec. BGN/SPP1/HGF-treated Pten wild-type TC1 allografts for 10 d (vehicle $n = 4$ mice; Rec. BGN/SPP1/HGF $n = 6$ mice). **k**, Percentage of CD45$^+$/CD3$^+$/CD8$^+$ cells inside the CD45$^+$ population in Rec. BGN/SPP1/HGF-treated Pten wild-type TC1 allografts ($n = 4$ vehicle; $n = 6$ Rec. protein-treated mice). Statistical analyses were conducted between all groups by ordinary one-way analysis of variance (ANOVA) followed by Tukey's multiple comparisons test (**a**–**c**), unpaired two-sided Student's *t*-test (**f**,**j**,**k**) and Mann–Whitney *U*-test (**g**). Data are mean ± s.d. (**a**–**c**,**f**,**g**,**j**,**k**).

factors previously known as regulators of extracellular matrix remodeling and epithelial-to-mesenchymal transition[50–52]. Ribosome profiling also detected an increased ribosome occupancy of *Hgf*, *Spp1* and *Bgn* mRNAs in Pten$^{pc-/-}$ tumors compared to wild-type prostates (Extended Data Fig. 3a). Finally, western blot analysis showed that HGF, SPP1 and BGN were more upregulated at protein levels in aggressive (Pten$^{pc-/-}$;TrpP53$^{pc-/-}$) than benign prostate tumors correlating with increased infiltration of PMN-MDSCs (Extended Data Fig. 3b–d). Inhibition of Pten by means of a Pten-shRNA (Pten-sh TC1) in TRAMP-C1 prostate tumor cells resulted in increased tumor cell production of HGF, SPP1 and BGN. This increase was associated with enhanced recruitment of PMN-MDSCs and decreased CD8$^+$ T-cell infiltration compared to TRAMP-C1 control cells (Fig. 2d–g).

HGF, SPP1 and BGN were mainly expressed by epithelial tumor cells and by the stroma (Extended Data Fig. 4a), whereas the corresponding receptors TLR2, CD44 and MET were predominantly expressed by tumor-infiltrating myeloid cells, as detected by FACS analysis (Extended Data Fig. 4b–c). Notably, in human prostate tumor samples, we found a direct correlation between TLR2, CD44 and MET and a previously published PMN-MDSC signature composed of 50 genes[4], both in primary tumors and CRPCs[53] (Extended Data Fig. 4d). We next assessed whether HGF, SPP1 and BGN could promote the recruitment of MDSCs by performing an in vitro migration assay. We found that recombinant HGF, SPP1 and BGN were capable of driving the migration of MDSCs, similarly to CXCL5 (Fig. 3a). Moreover, MDSC migration was enhanced when these three factors were administered in combination and in addition to CXCL5 (Fig. 3a). In line with these findings, inhibition of TLR2, CD44 and MET by treatment of MDSCs with three blocking antibodies arrested MDSCs migration toward conditioned medium derived

https://doi.org/10.1038/s43018-023-00594-z

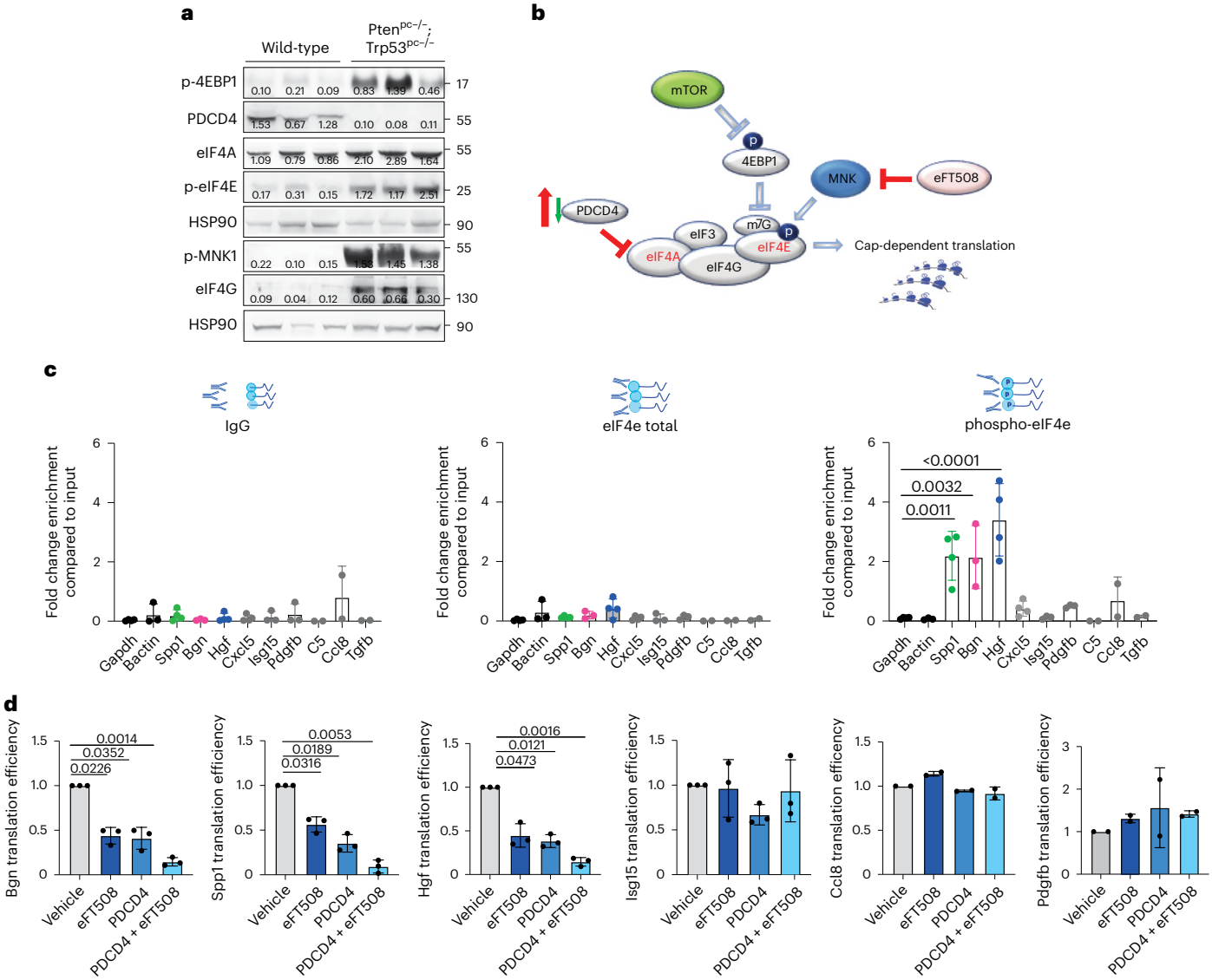

Fig. 4 | PDCD4 and phospho-eIF4E control the translation of *Hgf*, *Spp1* and *Bgn*. **a**, Western blot showing the levels of p-4EBP1, PDCD4, eIF4A, p-MNK, p-eIF4E, eIF4G and representative HSP90 in Pten$^{pc-/-}$;Trp53$^{pc-/-}$prostate cancers compared to wild-type prostates. Densitometry values normalized to the respective loading control are indicated for each band. The experiment was performed once with $n = 3$ mice for each group. **b**, Model depicting the proposed mechanism by which PDCD4 loss and phosho-eIF4E cooperate to regulate translation and modulate the tumor microenvironment. **c**, Fold change enrichment for the indicated mRNAs in Pten-sh TC1 determined by RNA immunoprecipitation using, from right to left, control anti-IgG, total eIF4E antibody or phospho-eIF4E antibody, followed by qRT–PCR performed (at least $n = 2$ independent experiments). Data are mean ± s.d. Statistical analysis between all groups was conducted by ordinary one-way ANOVA followed by Dunnett's multiple comparisons test. **d**, TE (polysomal mRNA expression/ total mRNA expression) of *Hgf*, *Spp1*, *Bgn*, *Isg15*, *Ccl8* and *Pdgfb* upon 500 nM eFT508 treatment and Pdcd4 rescue in Pten-sh TC1 PCa cell line, determined by qRT–PCR (at least $n = 2$ independent experiments). Data are mean ± s.d. Statistical analysis between all groups was conducted by a repeated measures one-way ANOVA followed by Tukey's multiple comparisons test.

from prostate tumor cells in vitro. This effect was more pronounced when the three antibodies were used in combination and in addition to the CXCR2 antagonist AZD5069 (Fig. 3b and Extended Data Fig. 4e). Finally, MDSCs exposed to HGF, SPP1 and BGN showed increased T-cell suppressive functions in vitro and increased Arg1, Nos2 and Vsir mRNA levels, thereby demonstrating that these factors are not only involved in the recruitment of MDSCs but also regulate their function (Fig. 3c and Extended Data Fig. 4f).

To address the relevance of HGF, SPP1 and BGN in mediating MDSC recruitment, we generated a triple *Hgf*, *Spp1* and *Bgn* knockdown (triple KD) Pten$^{-/-}$;Trp53$^{-/-}$ cell line using different short-hairpin RNAs (shRNAs). We did not observe differences in cell growth in vitro between scramble and the triple KD tumor cells even though these cells produce high levels of the ligands (Extended Data Fig. 4g–h); however, when these cells were injected in vivo we found a significant difference in the growth of the triple KD tumor cells than scramble-sh (Fig. 3d and Extended Data Fig. 4i). This was associated with a decreased recruitment of PMN-MDSCs (Fig. 3e–f) and increased tumor-infiltrating CD8^{+} T cells (Fig. 3g and Extended Data Fig. 4j). Together, these experiments demonstrate that HGF, SPP1 and BGN affect prostate cancer cell proliferation by altering the tumor microenvironment.

We next assessed whether enhanced levels of HGF, SPP1 and BGN in the prostate tumor microenvironment could also result in increased recruitment of MDSCs in vivo (Fig. 3h). Intratumoral injection of recombinant HGF, SPP1 and BGN proteins into TRAMP-C1 allograft tumors increased PMN-MDSCs infiltration, promoting an immunosuppressive

tumor microenvironment (Fig. 3i–k and Extended Data Fig. 4k). In summary, these data suggest that HGF, SPP1 and BGN can directly recruit MDSCs in vivo and loss of Pten in prostate tumor cells enhances the levels of these factors, leading to increased tumor infiltration of MDSCs.

PDCD4 and phospho-eIF4E control *Hgf*, *Spp1* and *Bgn* translation

To characterize the mechanism by which prostate tumor cells control MDSC recruitment, we analyzed different targets involved in the translation machinery of tumor cells by performing western blot analysis in $Pten^{pc-/-}$;$Trp53^{pc-/-}$ prostate tumors. In Pten-null tumors, we found hyperactivation of the AKT/mTOR signaling as demonstrated by increased levels of pAkt, p-S6 and p-4EBP1 and increased phosphorylation of both MNK1 and eIF4E in line with previous data[29]. Moreover, we found downregulation of programmed cell death 4 (PDCD4) at both mRNA and protein levels (Fig. 4a–b and Extended Data Fig. 5a–b). PDCD4 is a protein that binds and sequesters eIF4A, limiting the formation of the eIF4F complex. Previous evidence demonstrates that eIF4A is required to unwind high folding energy mRNAs[48]. Downregulation of Pten in TRAMP-C1 cells by means of a Pten-sh (Pten-sh TC1) resulted in decreased levels of PDCD4 when compared to control cells (scramble-sh TC1) (Extended Data Fig. 5c). Cap pull-down assays in scramble-sh TC1 and Pten-sh TC1 cells showed increased binding of eIF4A to the eIF4F complex. On the contrary, overexpression of PDCD4 in Pten-sh TC1 reduced the binding of eIF4A to the complex (Extended Data Fig. 5c). Thus, in Pten-null tumors, the lack of PDCD4 increases the availability of eIF4A for the eIF4F complex formation.

We next performed RNA immunoprecipitation for eIF4E and phospho-eIF4E in Pten-sh TC1 prostate cancer cells to assess whether phospho-eIF4E specifically increased the affinity for *Hgf*, *Spp1* and *Bgn* mRNAs. Indeed, although eIF4E is a general initiation factor, an increase in its activity only marginally affects global protein synthesis but strongly stimulates the translation of a subset of mRNAs referred to as 'phospho-eIF4E sensitive'[22]. We found significant and specific enrichment of the mRNAs encoding for *Hgf*, *Spp1* and *Bgn* in the RNA pool obtained by the immunoprecipitation of phospho-eIF4E compared to total eIF4E. Additional secreted factors identified in our previous analysis (Fig. 2a) were not bound to phospho-eIF4E, indicating the specificity of phospho-eIF4E for the translation of *Hgf*, *Spp1* and *Bgn* (Fig. 4c and Extended Data Fig. 5d).

To further corroborate these data, Pten-sh TC1 prostate cancer cells were treated with eFT508, a potent and selective MNK1/2 inhibitor[54], tested in clinical trials for prostate (NCT03690141), breast (NCT04261218) and lung (NCT04622007) cancers. eFT508 treatment decreased the levels of phospho-eIF4E both in mouse and human prostate cancer cells in a dose-dependent manner. This effect was associated with decreased HGF, SPP1 and BGN protein levels (Extended Data Fig. 5e), validating the results obtained with the phospho-eIF4E immunoprecipitation. We next assessed whether Pdcd4 loss could cooperate with phospho-eIF4E to promote the translation of *Hgf*, *Spp1* and *Bgn* by performing a Pdcd4 rescue experiment in Pten-sh TC1 cells. Polysome profiling and western blot analysis demonstrated that treatment with eFT508 inhibited translation of *Hgf*, *Spp1* and *Bgn* to a similar extent to Pdcd4 rescue; however, by combining inhibition of eIF4E phosphorylation with Pdcd4 rescue, the levels of *Hgf*, *Spp1* and *Bgn* were further decreased compared to controls (Fig. 4d and Extended Data Fig. 5f–h for the quantitative PCR with reverse transcription (qRT–PCR) analysis on the single fractions derived from the polysome profiles). These data were further validated in human PC3 cell lines that carry biallelic PTEN deletions by polysome profiling analysis (Extended Data Fig. 5i–j).

PDCD4 downregulated HGF, SPP1 and BGN protein levels without affecting cell growth in vitro (Extended Data Fig. 6a). Notably, Pdcd4 rescue, specifically in $Pten^{-/-}$;$TrpP53^{-/-}$ prostate cancer cells, leads to reduced tumor growth in vivo (Extended Data Fig. 6b), inhibition of HGF, SPP1 and BGN protein levels (Extended Data Fig. 6c) and decreased PMN-MDSCs infiltration (Extended Data Fig. 6d–f). Interestingly, in human prostate cancer, we found that PDCD4 mRNA levels correlate with poor disease-free survival (Extended Data Fig. 6g). Moreover, PTEN deletions were significantly associated with decreased PDCD4 mRNA levels (Extended Data Fig. 6h). Taken together, these findings demonstrate that eIF4E phosphorylation and Pdcd4 loss cooperate to regulate the translation of *Hgf*, *Spp1* and *Bgn* in prostate cancer.

eFT508 blocks PMN-MDSCs in $Pten^{pc-/-}$;$Trp53^{pc-/-}$ prostate tumors

We next investigated whether treatment with eFT508 could promote inhibition of PMN-MDSCs recruitment in vivo (Fig. 5a). $Pten^{pc-/-}$;$Trp53^{pc-/-}$ mice were treated with the MNK1/2 inhibitor eFT508 at standard dosage (10 mg kg^{-1}) for 6 weeks before being sacrificed. Histopathological analysis showed that eFT508 inhibited prostate cancer growth (Fig. 5b–d). Polysome profiling and western blot analyses confirmed that *Hgf*, *Spp1* and *Bgn* mRNA levels were decreased (Fig. 5e,f and Extended Data Fig. 7a,b). In parallel, immunohistochemistry (IHC) and FACS analysis showed that PMN-MDSC infiltration in prostate tumors was decreased upon eFT508 treatment (Fig. 5b,g). Of note, the percentage of $CD8^+$ T cells increased upon eFT508 treatment compared to the vehicle (Fig. 5h). This effect was associated with increased tumor mRNA levels of the T-cell cytotoxic markers interferon (IFN)-γ, granzyme B, perforin and decreased Foxp3 expression (Extended Data Fig. 7c). In line with these findings, MDSCs cultured in vitro with conditioned medium from prostate tumor cells treated

Fig. 5 | eFT508 treatment inhibits tumor growth and PMN-MDSC infiltration in $Pten^{pc-/-}$;$Trp53^{pc-/-}$ prostate cancer. a, Model depicting the proposed mechanism by which MNK1/2 inhibition by eFT508 may inhibit translation and modulate the tumor microenvironment. **b**, Representative hematoxylin and eosin (H&E), Gr-1 and CD3 staining ($n = 3$ mice in each group). Scale bar, 50 µm. **c**, Volume of the anterior prostate glands ($n = 3$ mice in each group). **d**, Histopathological score ($n = 3$ mice in each group). Summary table with statistical analysis (bottom) (two-way ANOVA followed by Šídák's multiple comparisons test; top). PIN, prostatic intraepithelial neoplasia. **e**, TE (polysomal mRNA expression/total mRNA expression) of *Bgn*, *Spp1* and *Hgf* in eFT508-treated and vehicle-treated prostate cancer ($n = 3$ prostate tumors for each group). Statistical analysis (two-tailed ratio paired *t*-test). **f**, Western blot analysis showing the protein levels of HGF, SPP1, BGN, p-eIF4E, eIF4E and representative HSP90 in eFT508-treated and vehicle-treated prostate cancer. Densitometry values normalized to the respective loading control are indicated for each band. The experiment was repeated three times independently with similar results. **g**, Percentage of $CD45^+$/$CD11b^+$/$Ly6G^{high}$/$Ly6C^{low}$ cells (PMN-MDSCs) inside the $CD45^+$ population ($n = 3$ mice in each group). **h**, Percentage of $CD45^+$/$CD3^+$/$CD8^+$ cells inside the $CD4^{5+}$ population ($n = 3$ mice in each group). **i**, Flow cytometric analysis of CFSE dilution in spleen-derived T cells co-cultured with bone-marrow-derived MDSCs in a T-cell suppression assay; MDSCs were incubated for 24 h with CM of eFT508-treated PCa cells ($n = 3$ biological replicates). The experiment was repeated twice independently with similar results. pretr., pretreated. **j**, Tumor growth of RapidCap allografts in C57BL6 mice treated with eFT508 (20 mg kg^{-1}) or the indicated depleting-antibodies: anti-Ly6G (150 µg kg^{-1}) and anti-CD8 (200 µg kg^{-1}) (from the top of the legend, $n = 8$, $n = 9$, $n = 4$, $n = 5$, $n = 5$ and $n = 5$). Data are mean ± s.e.m. Statistical analysis between all groups and time points (multiple unpaired *t*-test). **k**, Percentage of $CD45^+$/$CD11b^+$/$Ly6G^{high}$/$Ly6C^{low}$ cells (PMN-MDSCs) inside the $CD45^+$ population (from the left, $n = 6$, $n = 9$, $n = 4$, $n = 5$, $n = 3$ and $n = 4$). **l**, Percentage of $CD45^+$/$CD3^+$/$CD8^+$ cells inside the $CD45^+$ population (from the left, $n = 4$, $n = 7$, $n = 4$, $n = 4$, $n = 3$ and $n = 4$). Data are mean ± s.d. (**c**–**e**,**g**–**i**,**k**,**l**). Statistical analyses were carried out by two-sided unpaired Student's *t*-test (**c**,**g**,**h**), ordinary one-way ANOVA followed by Tukey's multiple comparisons test between all groups (**k**,**i**) and one-way ANOVA followed by Dunnett's multiple comparisons test (**l**).

https://doi.org/10.1038/s43018-023-00594-z

with eFT508 showed an impaired migration and decreased capability to suppress T-cell proliferation than MDSCs treated with control conditioned medium (Fig. 5i and Extended Data Fig. 7d,e). Of note, while treatment with eFT508 in Pten$^{-/-}$;Trp53$^{-/-}$ allografts mice efficiently decreased PMN-MDSC infiltration and increased T-cell activity, it did not promote tumor suppression in mice co-treated with an anti-CD8 antibody (Fig. 5j and Extended Data Fig. 8a). In addition, anti-Ly6G treatment in the same mice decreased tumor growth and increased T-cell infiltration to a similar extent to eFT508 (Fig. 5j–l and Extended Data Fig. 8b); however, eFT508 and anti-Ly6G co-treatment did not

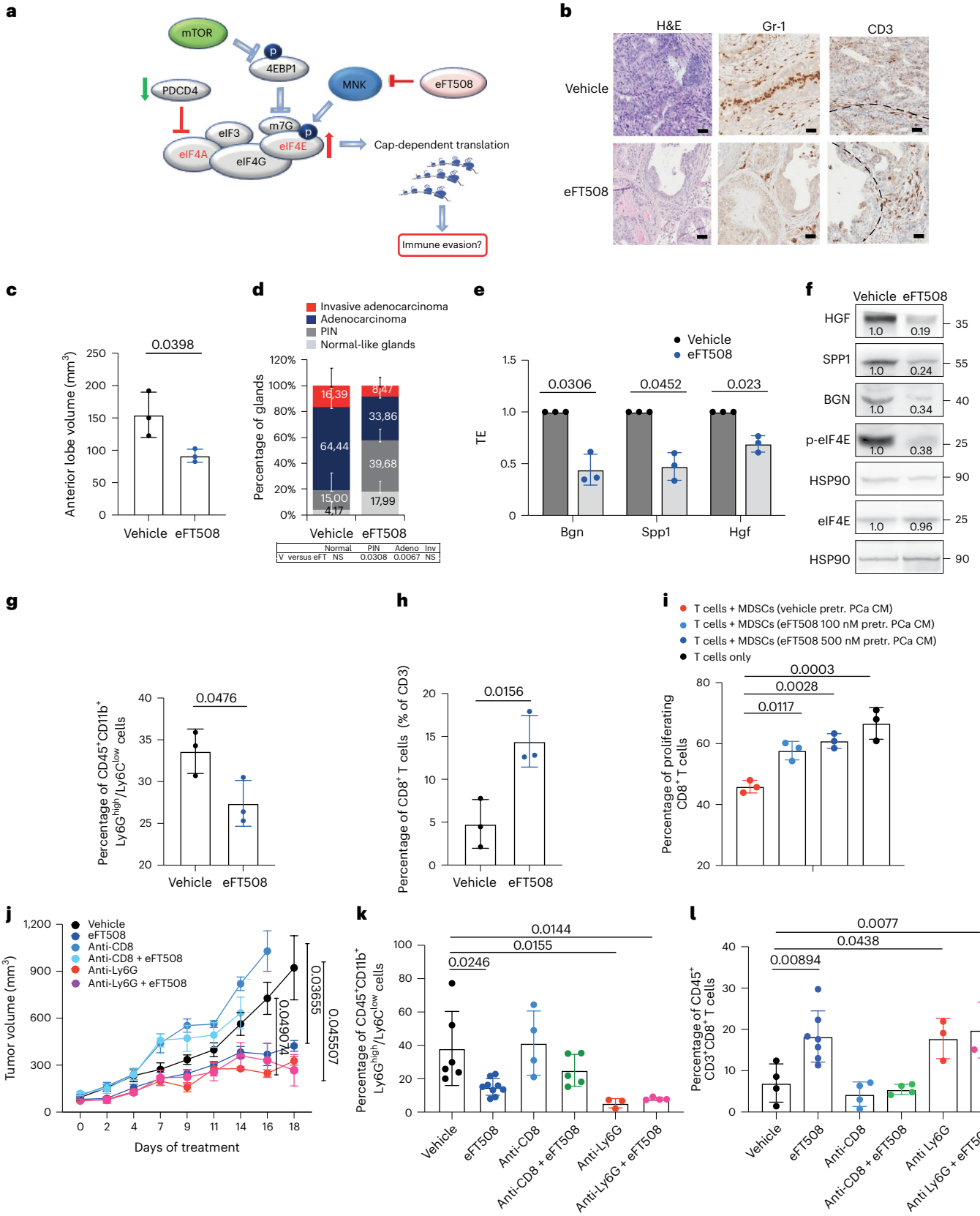

https://doi.org/10.1038/s43018-023-00594-z

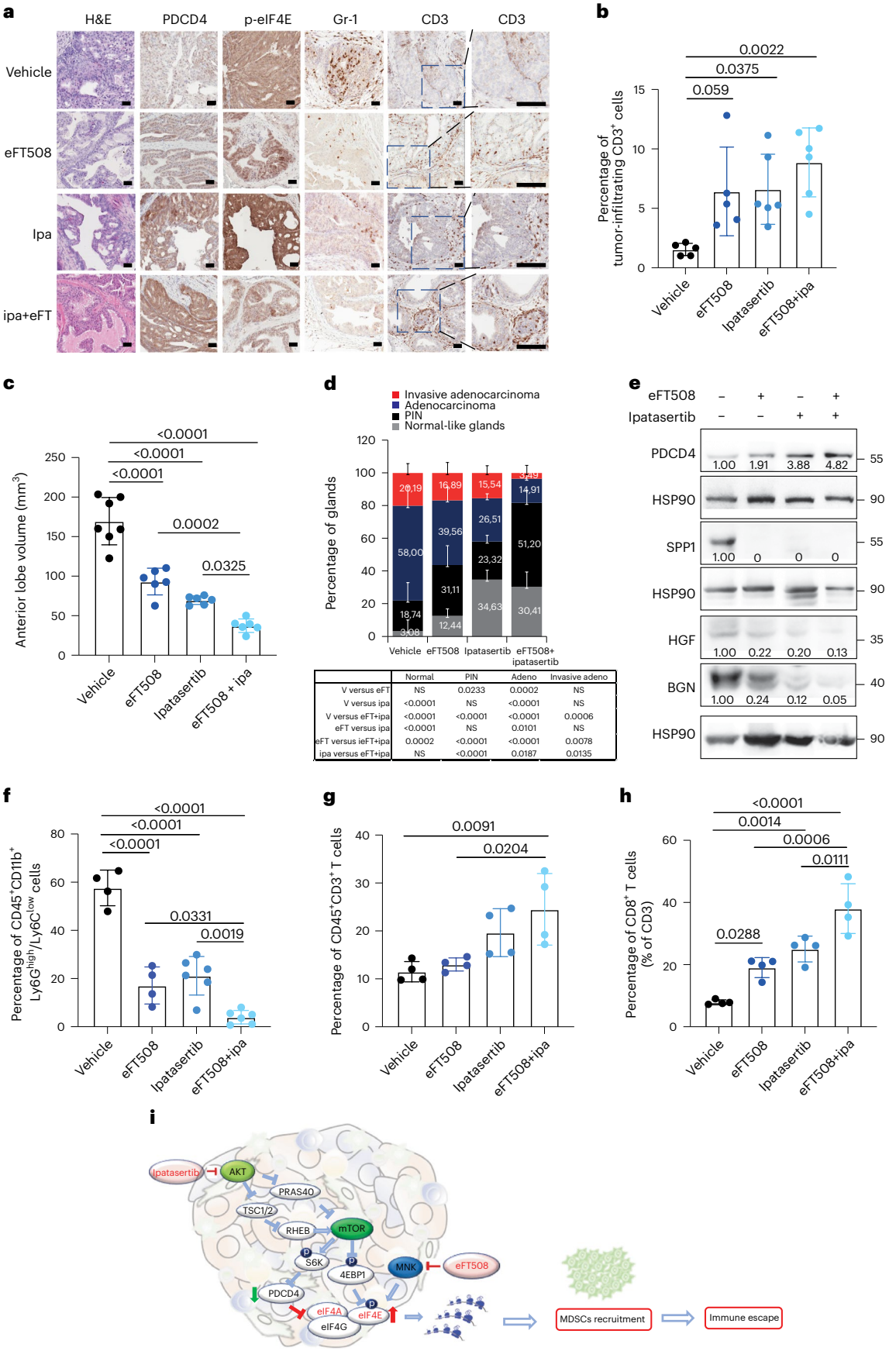

Fig. 6 | Dual eFT508 and ipatasertib treatment dampens tumor growth, tumor-infiltrating PMN-MDSCs and increases CD8$^+$ T cells in Pten$^{pc-/-}$Trp53$^{pc-/-}$ prostate cancer. a, Representative H&E, PDCD4, p-eIF4E, Gr-1 and CD3 staining in the tumor at the completion of the study (vehicle $n = 5$, eFT508 $n = 5$, Ipa $n = 6$ and eFT + Ipa $n = 6$). Scale bar, 50 µm. **b**, Quantification of the percentage of CD3$^+$ cells infiltrating the glands in the tumors of the indicated treatment groups (from the left, $n = 5$, $n = 5$, $n = 6$ and $n = 6$). **c**, Volume of the anterior prostate glands in Pten$^{pc-/-}$;Trp53$^{pc-/-/-}$ mice randomly assigned to the indicated treatment groups (from the left, $n = 7$, $n = 6$, $n = 6$ and $n = 6$). **d**, Histopathological score of Pten$^{pc-/-}$;Trp53$^{pc-/-}$ prostate tumor glands in the indicated treatment groups (from the left, $n = 5$, $n = 5$, $n = 6$ and $n = 6$). Summary table with statistical analysis (two-way ANOVA followed by Tukey's multiple comparisons test) on the bottom. **e**, Western blot analysis showing the protein levels of PDCD4, HGF, SPP1 and BGN in Pten$^{pc-/-}$;Trp53$^{pc-/-}$ whole tumor lysates in the indicated treatment groups. Densitometry values normalized to the respective loading control are indicated for each band. The experiment was repeated twice independently with similar results. **f**, Percentage of CD45$^+$/CD11b$^+$/Ly6G^{high}/Ly6C^{low} cells (PMN-MDSCs) inside the CD45$^+$ population in Pten$^{pc-/-}$;Trp53$^{pc-/-}$ PCa (from the left, $n = 4$, $n = 4$, $n = 6$, $n = 6$). **g**, Percentage of CD45$^+$/CD3$^+$ cells inside the CD45$^+$ population in Pten$^{pc-/-}$;Trp53$^{pc-/-}$ PCa ($n = 4$ in each group). **h**, Percentage of CD45$^+$/CD3$^+$/CD8$^+$ T cells (% of CD3$^+$ T cells) inside the CD45$^+$ population determined by flow cytometric analysis in Pten$^{pc-/-}$;Trp53$^{pc-/-}$ PCa in the indicated treatment groups ($n = 4$ in each group). **i**, Model depicting the proposed mechanism by which ipatasertib and eFT508 inhibit protein synthesis of the immunosuppressive secretome. Data are mean ± s.d. Statistical analysis between all groups was conducted by ordinary one-way ANOVA followed by Tukey's multiple comparisons test (**b**,**c**,**f**–**h**).

further reduce prostate tumor growth (Fig. 5j), thereby demonstrating that in these tumors, the activation of T cells associated with eFT508 (Extended Data Fig. 8c) is controlled by MDSCs. Of note, treatment with eFT508 did not affect the proliferation of prostate tumor cells when this compound was administered in vitro (Extended Data Fig. 8d). In summary, these findings suggest that the antitumor effect observed in vivo in mice treated with eFT508 depends on the modulation of the tumor immune response. Inhibition of MDSCs mediated by eFT508 increases T-cell recruitment and activation in prostate cancer, thereby promoting tumor inhibition.

Combined eFT508 and ipatasertib treatment in Pten$^{pc-/-}$;Trp53$^{pc-/-}$ prostate tumors

The findings that the translation machinery of prostate tumor cells controls MDSC recruitment through PDCD4 loss and eIF4E phosphorylation prompted us to hypothesize that inhibitors acting on different translation factors of the eIF4F complex could be used in combination to enhance treatment efficacy. Treatment of mouse and human prostate tumor cells with ipatasertib (Ipa), a highly selective pan-AKT inhibitor[55], promoted a dose-dependent increase in PDCD4 levels (Extended Data Fig. 9a). A recent phase III clinical trial demonstrated that Ipa, in combination with standard of therapy in prostate cancer, improved radiographical progression-free survival in patients with metastatic CRPC (mCRPC) with PTEN-loss tumors, without affecting patient survival[56,57]. Treatment with eFT508 in combination with Ipa in murine Pten$^{-/-}$;Trp53$^{-/-}$ and human PC3 prostate tumor cells blocked eIF4E phosphorylation and promoted the upregulation of PDCD4 levels triggering a more robust inhibition of HGF, SPP1 and BGN than in cells treated with the single inhibitors (Extended Data Fig. 9b,c). Moreover, the migratory capability of MDSCs was strongly reduced when exposed to conditioned medium from tumor cells treated with Ipa and eFT508. This defect was rescued when HGF, SPP1 and BGN were added back to the conditioned medium of tumor cells treated with eFT508 and Ipa (Extended Data Fig. 9d). In vivo, the combination treatment was well tolerated in Pten$^{pc-/-}$;Trp53$^{pc-/-}$ mice. eFT508 (10 mg kg^{-1}) in combination with Ipa (100 mg kg^{-1}) led to a strong reduction in tumor volume and number of prostate glands affected by invasive adenocarcinoma (Fig. 6a,c,d), efficiently decreasing the tumor levels of HGF, SPP1 and BGN also in vivo (Fig. 6e). Notably, eFT508 and Ipa co-treatment reduced tumor-infiltrating PMN-MDSCs to a greater extent than the single treatments (Fig. 6a,f and Extended Data Fig. 9e). Inhibition of PMN-MDSC recruitment was also associated with increased CD8$^+$ T cells in prostate tumors treated with the combination (Fig. 6g–h). Note that in tumors treated with Ipa and eFT508, T cells were found within the prostate tumor glands, whereas in tumors treated with monotherapy, T cells were confined to the stroma (Fig. 6a,b). Thus, the dual targeting of both AKT and MNK promotes a more potent inhibition of the eIF4F initiation complex, reprogramming the tumor immune response of prostate cancer (Fig. 6i).

eFT508 or Ipa combined with AZD5069 in Pten$^{pc-/-}$;TMPRSS2/Erg$^{pc+/+}$ prostate cancer

We and others have previously demonstrated that inhibition of the CXCR2 receptor partially inhibits MDSC recruitment in prostate cancer (Extended Data Fig. 10a)[5]. Treatment with AZD5069 consistently increases the tumor levels of HGF but not of SPP1 and BGN in Pten$^{pc-/-}$ mice (Extended Data Fig. 10b). Given that eFT508 inhibits the levels of HGF, SPP1 and BGN but not of CXCL5 (Extended Data Fig. 10c), which is transcriptionally regulated in prostate tumors, we speculated that eFT508 efficacy could be enhanced by AZD5069 treatment. As a model system to validate this hypothesis, we used the Pten$^{pc-/-}$;TMPRSS2/Erg$^{pc+/+}$ mouse model. As shown by our bioinformatic analyses, Pten$^{pc-/-}$;TMPRSS2/Erg$^{+/+}$ tumors present the highest transcriptional levels of CXCL5 when compared to prostate tumors of the other genetic backgrounds (Extended Data Fig. 10d). Pten$^{pc-/-}$;TMPRSS2/Erg$^{pc+/+}$ mice were treated with the MNK1/2 inhibitor eFT508 (10 mg kg^{-1}), AZD5069 (30 mg kg^{-1}) or the combination of the two compounds at the same concentration for 6 weeks before being sacrificed. The combined treatment

Fig. 7 | eFT508 or ipatasertib enhances the antitumor immune response of AZD5069 in Pten$^{pc-/-}$;TMPRSS2/Erg$^{pc+/+}$ prostate cancer. a, Representative H&E, Gr-1 and CD3 staining in the tumor. Scale bar, 50 µm (vehicle $n = 5$, AZD5069 $n = 4$, eFT508 $n = 9$, AZD5069 + eFT508 $n = 7$). **b**, Volume of the anterior prostate glands (from the left, $n = 6$, $n = 7$, $n = 10$ and $n = 7$). **c**, Histopathological score of prostate cancer glands (top). (from the left, $n = 5$, $n = 4$, $n = 9$ and $n = 7$). Summary table with statistical analysis (two-way ANOVA followed by Tukey's multiple comparisons test; bottom). **d**, Western blot showing the protein levels of HGF, SPP1, BGN, CXCL5, p-eIF4E, eIF4E and representative HSP90 in tumor lysates. Densitometry values normalized to the respective loading control are indicated for each band. The experiment was repeated twice independently with similar results. **e**, Percentage of tumor-infiltrating CD45$^+$/CD11b$^+$/Ly6G^{high}/Ly6C^{low} cells (PMN-MDSCs) inside the CD45$^+$ population (from the left, $n = 4$, $n = 4$, $n = 7$ and $n = 7$). **f**, Percentage of tumor-infiltrating CD45$^+$/CD3$^+$/CD8$^+$ inside the CD45$^+$ population (from the left, $n = 4$, $n = 4$, $n = 7$ and $n = 7$). **g**, Representative H&E, Gr-1 and CD3 staining in the tumor. Scale bar, 50 µm. (vehicle $n = 4$, AZD5069 $n = 4$, Ipa $n = 6$ and AZD5069 + Ipa $n = 8$). **h**, Volume of the anterior prostate glands (from the left, $n = 5$, $n = 4$, $n = 7$ and $n = 8$). **i**, Histopathological score of prostate tumor glands (top). (from the left, $n = 4$, $n = 4$, $n = 6$ and $n = 8$). Summary table with statistical analysis (two-way ANOVA followed by Tukey's multiple comparisons test; bottom). **j**, Western blot showing the protein levels of HGF, SPP1, BGN, CXCL5 and representative HSP90 in whole tumor lysates. Densitometry values normalized to the respective loading control are indicated for each band. The experiment was repeated twice independently with similar results. **k**, Percentage of tumor-infiltrating CD45$^+$/CD11b$^+$/Ly6G^{high}/Ly6C^{low} cells (PMN-MDSCs) inside the CD45$^+$ population (from the left, $n = 5$, $n = 4$, $n = 7$ and $n = 8$). **l**, Percentage of tumor-infiltrating CD45$^+$/CD3$^+$/CD8$^+$ inside the CD45$^+$ population (from the left, $n = 5$, $n = 4$, $n = 7$ and $n = 8$). Data are mean ± s.d. Statistical analysis between all groups was conducted by ordinary one-way ANOVA followed by Tukey's multiple comparisons test (**b**,**e**,**f**,**h**,**k**,**l**).

https://doi.org/10.1038/s43018-023-00594-z

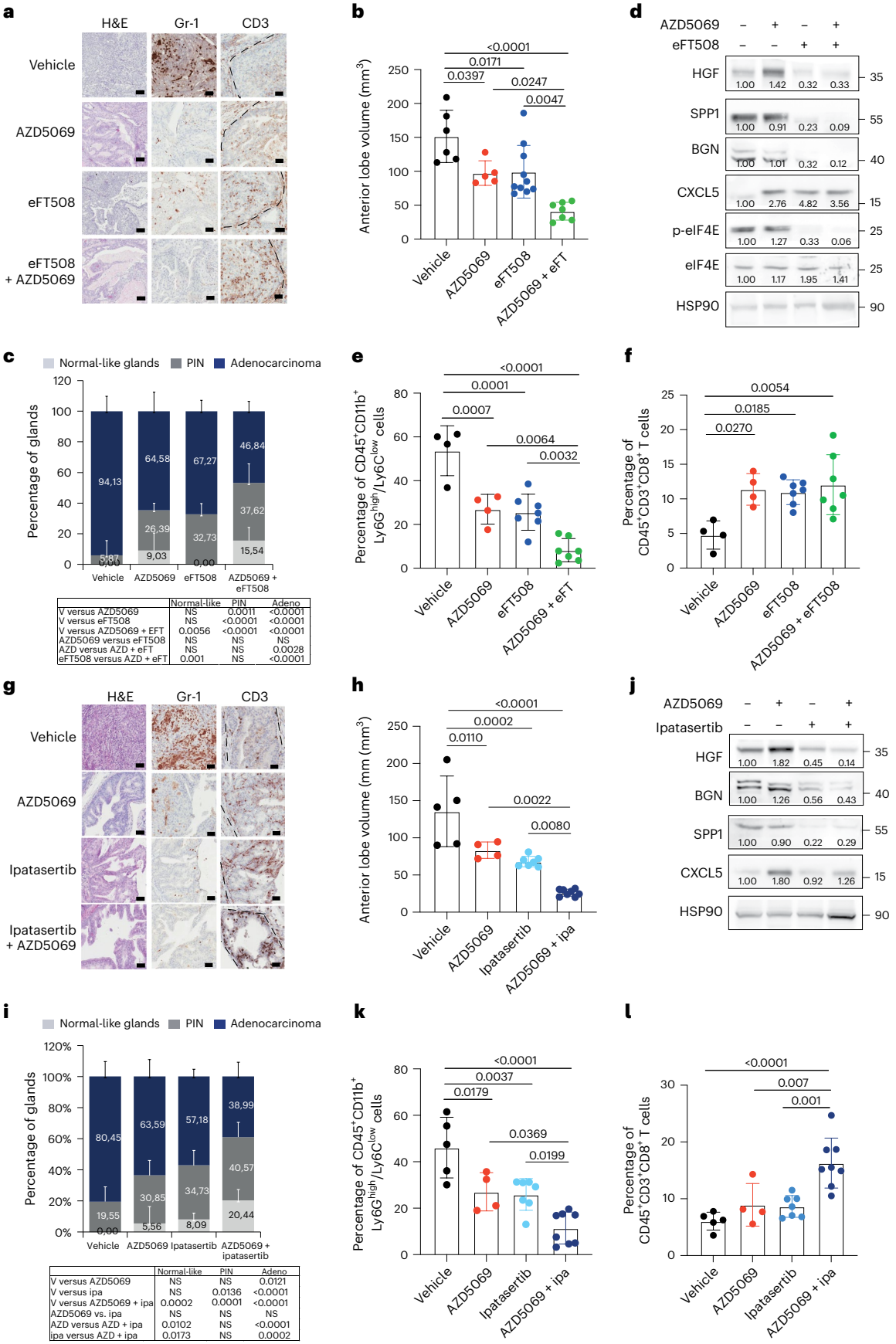

https://doi.org/10.1038/s43018-023-00594-z

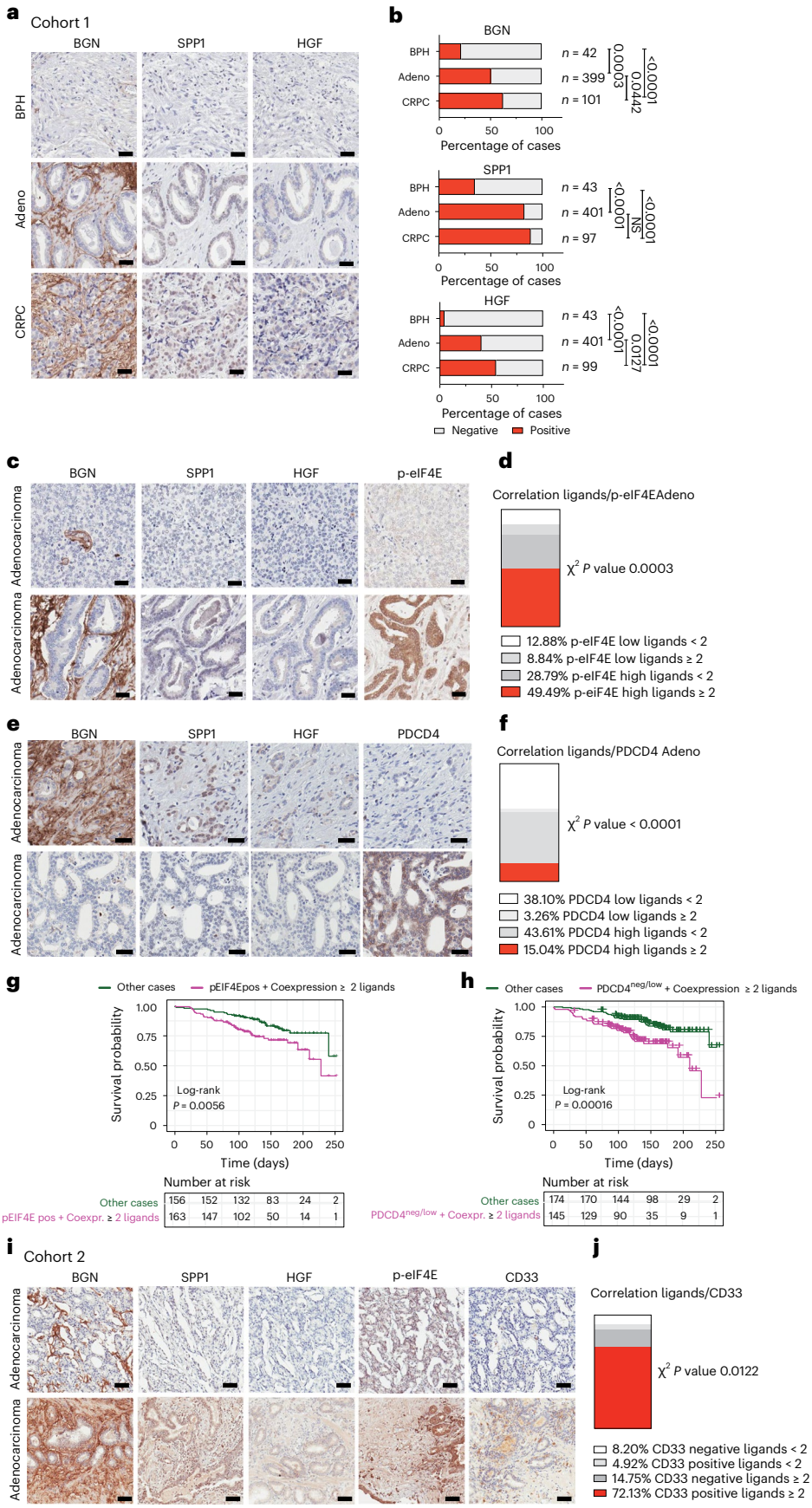

Fig. 8 | BGN, SPP1 and HGF are highly expressed in human prostate cancer and correlate with p-eIF4E and CD33 density. a, Representative IHC of BGN, SPP1 and HGF in BPH, prostate adenocarcinoma and CRPC in cohort 1 ($n = 545$). Scale bar, 50 µm. **b**, Percentage of BGN, SPP1 and HGF-negative and -positive cases in BPH, prostate adenocarcinoma and CRPC in cohort 1 for the indicated number of patients. Two-sided Fisher's exact test. **c**, Representative IHC of BGN, SPP1, HGF and p-eIF4E showing negative (top) and positive (bottom) cases in prostate adenocarcinoma in cohort 1. Scale bar, 50 µm. **d**, Correlation between the coexpression of ≥2 ligands and p-eIF4E in prostate adenocarcinoma in cohort 1 ($n = 401$). Two-sided Fisher's exact test. **e**, Representative IHC of BGN, SPP1, HGF and PDCD4 showing the negative correlation in prostate adenocarcinoma in cohort 1. Scale bar, 50 µm. **f**, Correlation between the coexpression of ≥2 ligands and PDCD4 in prostate adenocarcinoma in cohort 1 ($n = 401$); Two-sided Fisher's exact test. **g**, Correlation between overall survival and coexpression of p-eIF4E and ≥2 ligands in prostate adenocarcinoma. The number of cases is indicated in the table below for each comparison. **h**, Correlation between overall survival and concomitant PDCD4 loss and expression of ≥2 ligands in prostate adenocarcinoma; The number of cases is indicated in the table below for each comparison. **i**, Representative IHC of BGN, SPP1, HGF and CD33 showing a positive correlation of BGN, SPP1 and HGF with p-eIF4E and CD33 in prostate adenocarcinoma in cohort 2. Scale bar, 50 µm. **j**, Correlation between the coexpression of ≥2 ligands and CD33 in prostate adenocarcinoma in cohort 2. Two-sided Fisher's exact test.

of AZD5069 with eFT508 promoted a potent tumor growth inhibition as assessed by decreased tumor volume and tumor aggressiveness compared to the single treatments (Fig. 7a–c). eFT508 treatment also decreased HGF, SPP1 and BGN protein levels without affecting CXCL5 levels (Fig. 7d). Consistently, PMN-MDSC infiltration was reduced in tumors treated with the combination therapy compared to the single treatments (Fig. 7e). Finally, T-cell infiltration increased in tumors treated with the combination of eFT508 and AZD5069 to a greater extent than in tumors treated with the single treatments (Fig. 7f).

AZD5069 was also tested in combination with Ipa in vivo. Treatment with Ipa and AZD5069 in Pten$^{pc-/-}$;TMPRSS2/Erg$^{pc+/+}$ mice was more effective than treatment with Ipa and AZD5069 alone, as detected by reduced tumor growth and tumor aggressiveness (Fig. 7g–i). HGF, SPP1 and BGN protein levels were reduced upon Ipa treatment (Fig. 7j). Ipa treatment combined with AZD5069 strongly decreased PMN-MDSCs compared to the single treatments (Fig. 7g,k). This was associated with increased CD8$^+$ T-cell infiltration in prostate tumors (Fig. 7g,l). Taken together, these findings demonstrate that both eFT508 and Ipa treatment decrease PMN-MDSC infiltration and that co-treatment with AZD5069 further increases the antitumor immune response, providing an effective therapeutic strategy for the treatment of patients with prostate cancer.

HGF, SPP1 and BGN correlate with p-eIF4E and CD33 in human prostate cancer

To corroborate our findings in human prostate tumors, we analyzed two tissue microarrays from a total cohort of 614 (cohort 1 $n = 545$ and cohort 2 $n = 69$) patients with prostate cancer at different stages of the disease. IHC analysis in cohort 1 found that HGF, SPP1 and BGN levels were overexpressed in prostate adenocarcinoma and CRPC samples compared to benign prostate hyperplasia (BPH) (cohort 1 $n = 545$) (Fig. 8a,b). Moreover, the coexpression of the MDSC recruiters directly correlated with p-eIF4E levels in prostate adenocarcinoma and CRPC samples (cohort 1 $n = 401$) (Fig. 8c,d and Extended Data Fig. 10e,f). The coexpression of phospho-eIF4E and the ligands correlated with poor survival in patients with prostate cancer (Fig. 8g). In addition, we found a significant negative correlation between PDCD4 levels and the expression of the ligands (cohort 1 $n = 401$) (Fig. 8e,f). Notably, patients with prostate cancer carrying PDCD4 loss and overexpression of the ligands showed reduced overall survival compared to patients with high PDCD4 levels and low expression of the ligands (Fig. 8h).

HGF, SPP1 and BGN levels were also correlated with increased CD33 density in cohort 2, with included samples with available CD33 staining ($n = 69$) (Fig. 8i,j). In patient-derived organoids, we also detected different protein levels of the three MDSC recruiters, thereby validating the findings in the two cohorts of tissue microarrays (TMAs) (Extended Data Fig. 10g). Last, we tried to correlate the plasma levels of HGF, SPP1 and BGN in patients affected by prostate cancer with the neutrophil-to-lymphocyte ratio, a clinically established prognostic marker that correlates with circulating MDSCs[12,58] and we found that only HGF plasma levels correlated with the neutrophil-to-lymphocyte ratio in CRPCs (Extended Data Fig. 10h). In summary, these data confirm that the immunosuppressive secretome, constituted by HGF, SPP1 and BGN is increased in human prostate cancer and associated with increased CD33 density.

Discussion

Despite advances in prostate cancer care, there is an urgent unmet need for new therapeutic strategies to improve the outcome for patients with prostate cancer[59]. Immune-checkpoint inhibitors dramatically improved the prognosis of patients with certain types of tumors[60]. Nevertheless, the anticancer activity of immune-checkpoint inhibitors in prostate cancer is very limited[61]. This lack of efficacy is probably due to the strong infiltration of immunosuppressive MDSCs that exclude T cells from the tumor[2]. Thus, new immunotherapeutic strategies targeting MDSCs are needed to restore immune surveillance in prostate cancer. Here, we have demonstrated that the genome-wide analysis of the translatome of prostate cancer identifies a specific signature of translationally regulated MDSC recruiters that promote the establishment of an immunosuppressive tumor microenvironment. Mechanistically we found that prostate cancer cells build up a translational apparatus that is functional to its immune escape. The increased activity of the eIF4F complex, triggered by decreased PDCD4 and increased phosphorylation of eIF4E, upregulates the expression of *Hgf*, *Spp1* and *Bgn* mRNAs that work as potent recruiters of MDSCs, as demonstrated by functional experiments in vitro and in vivo (Fig. 6i). Notably, we found that eIF4E phosphorylation promotes the selective translation of *Hgf*, *Spp1* and *Bgn* mRNAs and that pharmacological inhibition of MNK1/2 through eFT508 decreases the translation of phospho-eIF4E-sensitive mRNAs, depriving cancer cells of MDSCs. In line with these findings, previous papers demonstrate that phosphorylation of eIF4E marginally affects global translation, but it stimulates the translation of a subset of mRNAs, known as phospho-eIF4E sensitive. Notably, secreted and membrane-associated proteins are between the factors controlled by phospho-eIF4E[62]. In different tumors, the types of translationally regulated secreted factors vary according to the cell context[63], the available pool and features of mRNAs and the presence of inhibitory RBPs[22].

Our findings also demonstrate that the translation of factors capable of recruiting PMN-MDSCs partially depends on PDCD4, whose levels are downregulated in Pten-deficient cells. As demonstrated, PDCD4 rescue in prostate cancer cells is associated with decreased protein synthesis of HGF, SPP1 and BGN despite the elevated levels of phospho-eIF4E. Of note, a previous paper demonstrated that PDCD4 KD was associated with increased production of protumorigenic cytokines in a spontaneous lymphoma model[64]. This finding suggests that PDCD4 downregulation, common in multiple types of cancer[65,66], is necessary to establish an anti-inflammatory immune response[67]. In line with these findings in human prostate tumors, characterized by increased infiltration of PMN-MDSCs, we found decreased PDCD4 levels associated with increased HGF, SPP1 and BGN levels. Moreover, PDCD4 mRNA levels correlated with decreased disease-free survival in human prostate cancer (Extended Data Fig. 6g).

Our findings are also noteworthy because of their implications for research in the field of cancer immunotherapy. Recent work

demonstrates that Ipa combined with abiraterone improved radiographical progression-free survival compared to abiraterone alone among patients with mCRPC with PTEN-loss tumors; however, in this trial, there was no significant difference between the groups in the intention-to-treat population[57]. One possible explanation of the partial efficacy of Ipa is that the MNK1/2–phospho-eIF4E axis remains active and promotes the recruitment of PMN-MDSCs, allowing cancer cells to escape immunosurveillance. Our findings provide evidence that the efficacy of Ipa can be enhanced by eFT508 treatment by reshaping the tumor microenvironment, leading to decreased PMN-MDSCs, increased $CD8^+$ T-cell infiltration and tumor suppression.

These findings are also relevant for future personalized therapies in prostate cancer. Contrary to tumors of other genetic backgrounds, in the $Pten^{pc-/-}$;TMPRSS2/$Erg^{pc+/+}$ tumors, we found a transcriptional upregulation of CXCR2 ligands. This finding prompted us to hypothesize that this genetic background could be specifically sensitive to AZD5069 treatment. Indeed, PMN-MDSC infiltration was significantly reduced upon AZD5069 administration. When AZD5069 was combined with eFT508 or Ipa, PMN-MDSC infiltration was further reduced due to the inhibition of the translationally regulated recruiters HGF, SPP1 and BGN.

In conclusion, our findings demonstrate that the translation apparatus of cancer cells control the tumor immune response via PMN-MDSCs and that translation inhibition represents a valuable therapeutic approach to improve the treatment outcome of patients affected by aggressive prostate cancer.

Methods

Mouse strains

The research complies with all relevant ethical regulations and inclusion and ethics recommendations. The animal experiments were approved by the local ethical committee ('Dipartimento della Sanità e Socialità, Esperimenti su animali' Canton Ticino), authorization nos. TI13/2015, TI25/2016, TI51/2018 and TI08/2021. Male $Pten^{pc-/-}$ mice were generated by crossing female Pten loxP/loxP mice with male Pten loxP/WT;PB-Cre4 transgenic mice and genotyped as previously described[5]. $Pten^{pc-/-}$;TMPRSS2/$Erg^{pc+/+}$, $Pten^{pc-/-}$;$Trp53^{pc-/-}$, $Pten^{pc-/-}$;$CDCP1^{pc+/+}$ and $Pten^{pc-/-}$;TIMP1−/− mice were generated as described previously[42–45], respectively. Four-week-old male C57BL6 male mice were purchased from Charles River and acclimatized for 4 weeks before experimentation. For allograft experiments, 2.5×10^6 TRAMP-C1 cells, 2.5×10^6 Pten-shTRAMP-C1 or 2×10^6 $Pten^{-/-}$;$Trp53^{-/-}$ (RapidCap) cells[68] were injected subcutaneously into the flank of 8-week-old male C57BL/6 mice. When tumors were approximately 100 mm^3, mice were randomized to the treatment groups. Tumor growth was monitored every 2–3 d by measuring the tumor size with a caliper. The following formula was applied to measure tumor volume = (width^2 × length) / 2. The local ethics committee approved the conduction of the in vivo experiments with maximal tumor sizes of 1,500 mm^3. The maximal tumor size was not exceeded.

Cell cultures

HEK-293T (CRL-3216 ATCC), TRAMP-C1 cell line (ATCC CRL-2730), PC3 (ATCC CRL-1435) and LNCaP (ATCC CRL-1740) were obtained from the ATCC. No further authentications were performed. No commonly misidentified cell lines were used in the study.

The TRAMP-C1 Pten-sh cell line was generated in the laboratory using the murine Pten Plasmid shRNA (sc-36326-SH, Santa Cruz) and validated by western blotting. $Pten^{-/-}$;$Trp53^{-/-}$ Rapid Cap cells, kindly provided by L. Trotman, were obtained as previously described[68].

Differentiation of myeloid-derived suppressor cells from bone marrow in vitro

Mouse bone-marrow-derived MDSCs were differentiated in vitro as previously described[69]. Briefly, bone-marrow precursors were flushed from the femurs of C57BL/6 with RPMI 1640 medium. Red blood cells were lysed with ACK buffer (Gibco, cat. no. A10492-01). The cell pellet was filtered through a 40-µm cell strainer (Falcon, cat. no. 352340) and resuspended in 10 ml in RPMI 1640 containing 10% heat-inactivated FBS, 40 ng ml^{-1} granulocyte–macrophage colony-stimulating factor and 40 ng ml^{-1} IL-6.

Treatments

eFT508 (MedChem Express) was administered daily by oral gavage at a final concentration of 10 mg kg^{-1} in 12–14-week-old transgenic mice and 20 mg kg^{-1} in C57BL6 mice on a Monday through Friday schedule. Ipa (MedChem Express) was administered daily by oral gavage at a final concentration of 100 mg kg^{-1} in 12–14-week-old transgenic mice on a Monday through Friday schedule. The CXCR2 antagonist AZD5069 (AstraZeneca) was administered daily by intraperitoneal injections at a final concentration of 100 mg kg^{-1} in 12–14-week-old transgenic mice on a Monday through Friday schedule. The 12–14-week-old control mice received vehicle solutions. For in vivo depletion, InVivoPlus anti-mouse CD8 antibody (200 µg per mouse; BioXCell, BP0061-5MG-A), InVivoPlus anti-mouse Ly6G (150 µg per mouse; BioXCell, BP0075-1-5MG-A) or InVivoMab rat IgG2b isotype control (200 µg per mouse; BioXCell, BE0090-5MG-A) was administered three times a week via intraperitoneal injection.

Recombinant Murine HGF (315-23, Peprotech; 0.04 mg kg^{-1}), Recombinant Human SPP1 (120-35, Peprotech; 0.2 mg kg^{-1}) and Recombinant Mouse BGN Protein, CF (8128-CM-050, R&D systems; 0.2 mg kg^{-1}), were dissolved in sterile PBS and administered daily by intratumoral injection to TRAMP-C1-injected mice.

In vitro culture experiments

For western blotting, RNA extraction and polysome profiling experiments, the cells were serum-starved for 18 h, then stimulated for 2 h with 10% FBS and lysed in the appropriate buffer or TRIzol for proteins or RNA extraction, respectively. Cell growth was analyzed in the indicated conditions and time using the Incucyte system.

Transwell migration assay

The 5-µm Boyden chambers (Millipore, MCMP24H48) were placed in a 24-well plate containing the appropriate medium or recombinant proteins (Recombinant Murine CXCL5 SRP3219, Sigma-Aldrich; 40 ng ml^{-1}); Recombinant Murine HGF 315-23, Peprotech; 40 ng ml^{-1}; Recombinant Human SPP1 120-35, Peprotech; 40 ng ml^{-1}; and Recombinant Mouse BGN Protein, CF 8128-CM-050, R&D systems; 40 ng ml^{-1}) and incubated for 30 min at 37 °C. An equal number of MDSCs under serum-starved conditions or pre-conditioned as indicated were placed on the top chamber of the Transwell system. Cells were allowed to migrate to the bottom well for 6 h at 37 °C with 5% CO_2. Migrated MDSCs in the lower wells of the membrane were collected, acquired by Fortessa (BD Biosciences) and analyzed using FlowJo software (TreeStar).

In vitro T-cell suppression assay

In vitro T-cell suppression assays were carried out with naive murine splenocytes, labeled with 5 µM CFSE (Molecular Probes, C34554) and activated in vitro with anti-CD3 and anti-CD28 beads (Invitrogen, 11452D), as described previously[6]. Bone-marrow-derived MDSCs were pretreated where indicated with the following recombinant proteins: Recombinant Murine HGF 315-23, Peprotech; Recombinant Human SPP1 120-35, Peprotech; Recombinant Mouse BGN Protein, CF 8128-CM-050, R&D systems. Then, the recombinant proteins were washed out and MDSCs were co-cultured with the splenocytes. The proliferation of CFSE-labeled $CD8^+$ T cells stained with an anti-CD8 antibody (BioLegend, clone 53-6.7) was assessed by BD Fortessa (BD Biosciences) and analyzed using FlowJo software (TreeStar).

ELISA assay

Prostate cancer-derived CM from mouse prostate cancer cell lines was tested for the quantification of HGF, SPP1 and BGN by ELISA assay (Mouse BGN ELISA kit 48-strip-wells MBS2602124; Mouse Osteopontin ELISA kit MBS263335; and Mouse HGF ELISA kit MBS268751).

CRPC serum samples were analyzed to assess HGF concentration using the HU HGF ELISA kit 96 tests Biosource (Life Technologies, KAC2211), following the manufacturer's instructions.

Immunophenotyping by flow cytometry

Tumors were minced and digested in collagenase D (5 μg ml^{-1}, Roche, Cat. 11088858001) for 1 h at 37 °C, followed by incubation in Trypsin and DNase (20 μg ml^{-1}, Roche, cat. no. 4716728001) for 5 min. Then, 10% FBS-containing RPMI medium was added and the cells were filtered through a cell strainer (Falcon, 352340) to obtain a single-cell suspension. Unspecific binding was neutralized with a CD16/CD32 antibody (BioLegend, clone 93, cat. no. 101302). Single-cell suspensions were stained with specific antibodies for 15 min at 4 °C in FACS buffer (PBS containing 1% FCS and 1 mM EDTA). The primary antibodies are listed in the Reporting Summary.

For the EpCAM$^+$ epithelial separation from the CD45$^+$ immune cell fraction and from the EpCAM$^-$/CD45$^-$ population, the single-cell suspension from Pten$^{pc-/-}$;Trp53$^{pc-/-}$ prostate tumors were stained with the FITC-EpCAM antibody (Thermo Fisher Scientific, clone G8.8, 11-5791-82). Then, the single-cell suspension was incubated with anti-FITC MicroBeads (Miltenyi Biotec, 130-048-701) and purified through the MACS column in a QuadroMACS separator. The EpCAM- population was stained with PE-CD45 antibody (BioLegend, clone 30-F11, 103106), further incubated with the anti-PE MicroBeads (Miltenyi Biotec, 130-048-801) and purified through the MACS column. The EpCAM$^+$, CD45$^+$ and EpCAM$^-$/CD45$^-$ population was resuspended in RIPA buffer and further analyzed for protein analysis.

Transduction of prostate cancer cells with lentiviral vectors

For PDCD4 overexpression, the Precision Lenti ORF Human PDCD4 (Horizon Discovery, OHS5897-202618618) and Precision Lenti ORF positive control (Horizon Discovery, OHS5832) were used. For the triple knockdown, Scramble[shRNA#1], mHgf[shRNA#1, mSpp1[shRNA#1] and] mBgn[shRNA#1] (VectorBuilder) were used. The transfection was performed using jetPRIME reagent (Polyplus-transfection, 114-07/712-60) according to the manufacturer's protocol at the 1:2 DNA:jet PRIME ratio in 293T cells. After 48 h, each lentiviral-containing medium was collected, filtered through 0.45-μM filters and added to 70% confluent prostate cancer cells. After 48 hours from the transduction, antibiotics selection was performed for 48 hours. The efficiency of PDCD4 expression or Hgf/Spp1/Bgn silencing was confirmed by western blotting.

Immunohistochemistry

Tissues were fixed in formalin 10% and processed for H&E staining and IHC according to standard procedures, as described elsewhere[70]. Sections were stained for anti-p-eIF4E (ab7626, Abcam, 1:100 dilution), anti-PDCD4 (Cell Signaling Technology, cat. no. 9535S, 1:400 dilution), anti-Ly6G (Gr-1) (BD Pharmingen, clone 1A8, cat. no. 551459, 1:1,500 dilution) and anti-CD3 (Dako, cat. no. A0452, 1:800 dilution). Images were obtained with Aperio ScanScope, Leica Biosystems. All quantifications were performed with ImageScope v.12.3.2.8013 Leica Biosystems.

Polysome profiling, library synthesis and RNA-seq

Polysome profiles analysis of prostate tumor was performed in six different genetic backgrounds: wild-type, Pten$^{pc-/-}$, Pten$^{pc-/-}$;TMPRSS2-ERG$^{pc+/+}$, Pten$^{pc-/-}$;CDCP1$^{pc+/+}$, Pten$^{pc-/-}$;Timp1$^{-/-}$ and Pten$^{pc-/-}$;Trp53$^{pc-/-}$. For each genotype, three mice of 20–25 weeks of age were analyzed. Prostate tumor tissues were quickly excised and homogenized in polysome lysis buffer (30 mM Tris-HCl, pH 7.5, 100 mM NaCl, 30 mM $MgCl_2$, 1% sodium deoxycolate, 1% Triton X-100, 100 mg ml^{-1} cycloheximide, 1 mM dithiothreitol (DTT) and 30 U ml^{-1} RNasin) using a sterile pestle.

For MDSC polysome profiling analysis, bone-marrow-differentiated MDSCs were collected and sorted in CD11b^{high}; Ly6G^{high};Ly6C^{low} and CD11b^{high}; Ly6G^{neg};Ly6C^{high} after 5 d of differentiation. Sorted cells were plated and collected the day after for polysome profiling analysis after incubation with PMA (20 ng ml^{-1})/ionomycin (1 μM) for 15 min and cycloheximide 100 μg ml^{-1} in the last 5 min. Bone marrow from three mice was flushed from the femurs of C57BL/6 with RPMI 1640 medium. Red blood cells were lysed with ACK buffer (Gibco, cat. no. A10492-01). The cell pellet was filtered through a 40-μm cell strainer (Falcon, cat. no. 352340), resuspended and lysed in polysome lysis buffer.

Cells were seeded in two 15-cm dishes 1 d before collection to reach a 70% confluence by the time of the experiment. Cells were treated with 100 μg ml^{-1} cycloheximide (Sigma, C7692) 5 min before collection. After a quick wash in ice-cold PBS containing cycloheximide (100 μg ml^{-1}; PBS-CHX), cells were scraped in polysome lysis buffer. Cytoplasmic extracts with equal amounts of RNA were loaded on a 15–50% sucrose gradient and centrifuged at 4 °C for 3.5 h at *187,813 g* in a SW41Ti Beckman rotor using a Beckman Optima L-90K ultracentrifuge. Gradients were read at 254 nm by the BioLogic LP system (BioRad) and acquired by the BioLogic LP Dataview v.2.0. The fractions (1.0 ml each) were collected for subsequent RNA extraction to isolate the polysomal RNA fractions. Total and polysomal RNA fractions were incubated with 200 μg ml^{-1} proteinase K and SDS 1% for 1 h at 37 °C. RNA was extracted by phenol:chloroform at 5:1 (Sigma-Aldrich; P1944), followed by overnight isopropanol precipitation at −80 °C, centrifugation at 19,090*g* for 45 min and resuspension in 10 μl DEPC water. At the end of the procedure, DNase digestion was carried out with Turbo DNase (Thermo Fisher Scientific, AM2238) for 30 min at 37 °C and RNA purification was performed with RNA Clean and Concentrator kit (Zymo Research, R1015). The purified RNA was measured using Nanodrop and the quality was assessed using the Agilent 2100 Bioanalyzer. After random primer annealing, whole library preparation was performed using the Illumina TruSeq Stranded Total RNA with Ribo Zero. Completed libraries were then submitted for sequencing. RNA-seq was constructed with barcodes to allow multiplexing of 12 samples per lane. Sequencing was carried out on NextSeq 500 Illumina platform. Sequence alignments of paired-end 75-bp reads to the reference mouse genome (GRCm38) were performed using STAR (v.2.5.2a)[71]. Gene expression was quantified using the comprehensive annotations made available by Gencode[72]. Specifically, we used v.20 release of the Gene Transfer File. Raw counts were further processed in the R Statistical environment and downstream differential expression analysis was performed using the DESeq2 pipeline[73]. Genes characterized by low mean normalized counts were filtered out by the independent filtering feature embedded in DESeq2 (α = 0.05). The polysomal RNA and total RNA expression for each genetic background were compared to the wild-type. For the PCA of Extended Data Fig. 1b,c, the R function plotPCA was applied considering the top 500 genes selected by the highest variance between samples. To measure the TE for each comparison shown in the scatter-plots of Extended Data Fig. 1d, anota2seq package was used, specifically the anota2seqRun function[74].

Gene expression bioinformatic analysis

For the 5′ UTR length and 5′ UTR folding energy, genes with altered TE were identified based on FDR < 0.05 and TE > 0.7 (up) or <−0.7 (down). The 5′ UTR lengths were retrieved from ENSEMBL annotations (*Mus musculus*, v.90). Secondary structure minimum free energies were calculated with Vienna RNAfold (v.2.4). Differences in 5′ UTR features of genes with altered TE were tested against the distributions of genes with invariant TE (inv) with the Wilcoxon rank-sum test (two-sided).

GO biological processes enriched among the translationally upregulated mRNAs (threshold for polysomal mRNA expression $\log_2$ fold change ≥ 1.0; FDR < 0.05; threshold for TE $\log_2$ fold change ≥ 0.5;

FDR < 0.1), polysomal mRNAs (threshold $\log_2$ fold change ≥ 1.0; FDR < 0.05) and total mRNAs (threshold $\log_2$ fold change ≥ 1.0; FDR < 0.05) were determined by the DAVID v.6.8 software; adjusted *P* values for multiple comparisons by using the linear step-up method of Benjamini are reported.

For the selection of the ligand–receptor couples, the upregulated mRNAs encoding for extracellular proteins were selected from the RNA-seq of the five different genetic backgrounds of PCa compared to wild-type prostate. In addition, the expressed membrane-tethered protein-encoding mRNAs in bone-marrow-differentiated MDSCs were filtered and merged with the upregulated membrane-tethered proteins in PCa to select the target receptors. The matching of the upregulated ligands in the tumors with the expressed receptors in the MDSCs was performed by the iTALK database (https://doi.org/10.1101/507871). The first 61 couples in the cytokines, growth factors and 'other factors' were selected. The ligands and the receptors with a $\log_2$ fold change >1 in all genotypes were filtered. Among the 'other factors', the first 20 couples were further filtered and ligand–receptor couples were positively selected if (1) the ligands were extracellular proteins based on Uniprot and Human Protein Atlas annotation and (2) the ligands were not downregulated in human Pten-loss prostate cancer by using the TCGA dataset. The confirmation of the interaction of the pairs based on the STRING network database[75] was used as further validation for all the categories. Isg15-Itgal[76] and C5-C5ar1 (ref. 77) were added to the list based on the literature.

For the analysis of human samples, we used two different human datasets of patients with PCa (https://www.cancer.gov/tcga and elswhere[25]). In these datasets of patients, survival analysis has been performed using Kaplan–Meier estimator and Cox regression model based on PDCD4 mRNA expression and protein levels (survival, survminer and rms packages). For the RNA-seq data, samples were classified into quartiles based on expression levels of PDCD4 and first (PDCD4_LOW) and fourth (PDCD4_HIGH) quartiles were used for the analysis. Additionally, correlation analysis was performed using ggscatter function and chisq.test function.

Ribosome profiling

Cytoplasmic lysates from control and $Pten^{pc-/-}$ prostates were prepared as described previously[78]. Endonuclease digestion was performed using RNase I (10 U per unit of absorbance at 260 nm in the lysate) at room temperature for 45 min. The reaction was stopped by adding SUPERase-In RNase inhibitor (Thermo Fisher Scientific). Samples were loaded on a sucrose gradient and ultracentrifuged as described previously[78]. The fraction containing the 80S was collected and RNA was extracted using phenol–chloroform as described previously[79]. Ribosome protected fragments were isolated on Novex TBE-Urea Gel, 15% (Thermo Fisher Scientific) and used for library preparation. SMARTer sm-RNA-Seq kit for Illumina (Takara Bio) and SMARTer RNA Unique Dual Index kit (Takara Bio) were used according to manufacturer's instructions to prepare Ribo-seq libraries. Libraries were further purified on Novex TBE Gel, 8% (Thermo Fisher Scientific). The library's quality was assessed using a high-sensitivity DNA chip on the BioAnalyzer (Agilent) according to the manufacturer's protocol and Qubit v.2.0 (Thermo Fisher Scientific). Then, the libraries were sequenced using a NovaSeq 6000 system.

Analysis of ribosome profiling data

The 100-bp single-end reads were processed by removing poly(A) sequences in each read, trimming the first three nucleotides and discarding reads shorter than 15 nucleotides (Cutadapt v.2.5). Reads mapping on the collection of *M. musculus* rRNAs (from the SILVA rRNA database) and tRNAs (from the Genomic tRNA database) were removed. The remaining reads were aligned to the mouse genome (GRCm39) using the Gencode M28 gene annotation based on ENSEMBL release 105. Antisense and duplicate reads were removed. All alignments were performed with STAR (v.2.5.3a).

The ribosome occupancy for each gene has been computed using the riboWaltz R package (v.1.2.0)[80] and collapsing all isoforms of the same transcript. Only genes with gene count >1 in all the replicates of at least one condition were kept for subsequent analysis. To remove possible size or compositional differences between libraries coming from multiple conditions, gene counts were normalized using the trimmed mean of M-values normalization method implemented in the edgeR Bioconductor package (v.3.32)[81]. Differential analyses were performed with generalized linear models implemented in edgeR (glmQLFTest function) and genes with significantly different ribosome occupancy were selected with a triple threshold on the $\log_2$ fold change (absolute value > 0.75), the correspondent statistical significance ($P < 0.05$) and mean counts per million >0.05 for both conditions.

RNA extraction and quantitative real-time PCR

RNA was isolated from tissues and cells using TRIzol (Ambion, Life Technologies, 15596026). cDNA was synthesized by using IMPROM II kit (Promega, A3800) according to the manufacturer's instructions. qPCR reactions were performed using GoTAQ qPCR Master Mix (Promega, A6002) on Step One Real-Time PCR systems (Applied Biosystems). Each expression value was calculated using the ΔΔCT method[82] and normalized to 18S, Actinb or Gapdh level as reference. The primer sequences were obtained by the Primer Bank database (http://pga.mgh.harvard.edu/primerbank/index.html) and are listed in Supplementary Table 3.

RNA immunoprecipitation

Cells at 70% confluency are lysed in RNA immunoprecipitation buffer (20 mM Tris-HCl, pH 7.5, 200 mM NaCl, 5 mM $MgCl_2$, 0.5% Triton X-100, protease/phosphatase inhibitor cocktail, 800 U RiboLock RNase inhibitor (Thermo Fisher Scientific, EO0381), 10% BSA and 0.5 µM DTT). IgG control (Cell Signaling Technology, 2729S), eIF4E (Thermo Fisher Scientific, MA1089) and p-Ser209 eIF4E (Abcam, ab76256) were incubated with Dynabeads Protein G (Thermo Fisher Scientific, 10004D) for 2.5 h. RNA immunoprecipitation was conducted by incubating the antibody-Dynabeads complex with the cell lysates for 30 min at 4 °C in rotation. After the immunoprecipitation, three washes with RNA immunoprecipitation buffer were performed. The resulting elution was divided for protein extraction or RNA extraction by TRIzol (Ambion, Life Technologies, 15596026).

Cap column pull-down

The 500 µg proteins were incubated with 50 µl of m^7GTP agarose (Jena Biosciences), in a total volume of 1 ml cap pull-down buffer (50 mM MOPS-KOH, pH 7.4, 100 mM NaCl, 0.5 mM EDTA, 0.5 mM EGTA, 7 mM β-mercaptoethanol, 0.5 mM phenylmethylsulfonyl fluoride (PMSF), 1 mM Na_3VO_4, 0.1 mM GTP and 1× protease/phosphatase inhibitor cocktail), for 90 min at 4 °C with rotation. The beads were washed three times in cap pull-down buffer. The cap-bound fraction was eluted in 50 µl of 2× SDS sample buffer by boiling at 70 °C for 10 min, followed by western blotting.

Western blotting

Proteins from tissue and cell lysates were extracted with RIPA buffer (Cell Signaling Technology, 9806) supplemented with PMSF (Millipore Sigma, 329-98-6) and Pierce Protease and Phosphatase Inhibitor Mini Tablets (Thermo Fisher Scientific, A32959). Protein concentration was measured using a BCA Protein Assay kit (Thermo Fisher Scientific, 23227). The same amounts of proteins underwent electrophoresis by SDS–PAGE and were transferred onto a 0.45-mm nitrocellulose membrane (Thermo Fisher Scientific, 88018). Membranes were probed with diluted antibodies and incubated overnight at 4 °C. The primary antibodies are listed in the Reporting Summary. Secondary antibodies conjugated to horseradish peroxidase anti-rabbit IgG (Promega, W4011, 1:5,000 dilution) or anti-mouse IgG (Cell signaling Technology, W4021, 1:5,000 dilution) were used. The protein band signals were

developed using the ECL Western Blotting Substrate (Thermo Fisher Scientific, 32106). Membranes were exposed to the Fusion Solo S imaging system (Vilber). Blots were analyzed for the densitometry analysis using ImageJ v.1.52 (National Institutes of Health).

Patient-derived samples and human tissue microarrays

CRPC plasma (collected as described previously[6]) and organoids from patient-derived-xenografts (generated as described elsewhere[83,84]) were obtained from patients identified from a population of men with CRPC treated at the Royal Marsden NHS Foundation Trust. All patients had given written informed consent and were enrolled in institutional protocols approved by the Royal Marsden NHS Foundation Trust Hospital ethics review committee (ref. no. 04/Q0801/60)

Human TMA samples of cohort 1 were obtained and processed from Universitatsspital Zurich[85]. Three independent TMAs (ZTMA76, ZTMA80 and ZTMA204) were stained with the antibodies listed in the Reporting Summary.

Human TMA samples of cohort 2 were obtained and processed from the University of Padova. Five independent TMAs were stained with the antibodies listed in the Reporting Summary.

All patients had given written informed consent and were enrolled in institutional protocols approved by the Padova Province Clinical Experimentation Ethics Committee (ref. no. 5480/AO/22). Patients did not receive compensation.

Statistics and reproducibility

Data analyses were carried out using GraphPad Prism v.7 or Microsoft Excel 2018. The data are mean ± s.d. or s.e.m. where indicated. Two-sided, paired or unpaired *t*-tests, according to the experimental setting, were used to compare two groups in the indicated experiments. One-way ANOVA with Tukey's post hoc test was used to compare three or more groups in the indicated experiments. The correlation between p-eIF4E, PDCD4 and CD33 status with HGF, SPP1 and BGN was performed using the chi-squared tests with Yates correction[86]. The survival probability of Fig. 8g,h was calculated using the log-rank test. Normality test was calculated using GraphPad for most of the datasets. Otherwise, data were assumed to be normally distributed. No statistical method was used to predetermine sample size. Group sizes were determined based on the results of preliminary experiments. No data points were excluded from the analysis. All samples meeting proper experimental conditions were included in the analysis. Group allocation was performed in a randomized fashion. Data collection and analysis were not performed blind to the conditions of the experiments.

Reporting summary

Further information on research design is available in the Nature Portfolio Reporting Summary linked to this article.

Data availability

RNA-seq data that support the findings of this study have been deposited in ArrayExpress under accession code E-MTAB-9624 (RNA-seq on total RNA of wild-type, Pten$^{pc-/-}$, Pten$^{pc-/-}$;P53$^{pc-/-}$) and Gene Expression Omnibus (GEO) under accession code GSE202910 (RNA-seq on total RNA of Pten $^{pc-/-}$; TMPRSS2/Erg$^{pc+/+}$; Pten $^{pc-/-}$; CDCP1$^{pc+/+}$; Pten$^{pc-/-}$; Timp1$^{-/-}$; RNA-seq on polysomal RNA of wild-type, Pten$^{pc-/-}$, Pten$^{pc-/-}$;P53$^{pc-/-}$, Pten $^{pc-/-}$; TMPRSS2/Erg$^{pc+/+}$; Pten $^{pc-/-}$; CDCP1$^{pc+/+}$; Pten$^{pc-/-}$; Timp1$^{-/-}$). The data published in the Array Express are the results of the RNA-seq on total RNA of the same samples for which the results of the RNA-seq on polysomal RNA are published in GEO and they were processed at the same time.

GEO accession code GSE202907 contains data for RNA-seq on total and polysomal RNA of undifferentiated bone marrow, PMN-MDSCs (CD11b^{+}/Ly6G^{high}/Ly6C^{low}) and M-MDSCs (CD11b^{+}/Ly6G^{neg}/Ly6C^{low}).

The datasets used in this study were Uniprot, https://www.uniprot.org/; the Human Protein Atlas, https://www.proteinatlas.org/; STRING, https://string-db.org/; and DAVID v.6.8, https://david.ncifcrf.gov/. The human prostate cancer transcriptomic data were derived from the TCGA Research Network at http://cancergenome.nih.gov/ and elsewhere[25].

Source Data for Figs. 1–8 and Extended Data Figs. 2–10 have been provided as Source Data files. All other data supporting the findings of this study are available from the corresponding author upon reasonable request. Source data are provided with this paper.

Code availability

All packages used for the bioinformatics analysis are described in Methods.

References

1. Kwon, E. D. et al. Ipilimumab versus placebo after radiotherapy in patients with metastatic castration-resistant prostate cancer that had progressed after docetaxel chemotherapy (CA184-043): a multicentre, randomised, double-blind, phase 3 trial. *Lancet Oncol.* **15**, 700–712 (2014).
2. de Bono, J. S. et al. Prostate carcinogenesis: inflammatory storms. *Nat. Rev. Cancer* **20**, 455–469 (2020).
3. Feng, S. et al. Myeloid-derived suppressor cells inhibit T cell activation through nitrating LCK in mouse cancers. *Proc. Natl Acad. Sci. USA* **115**, 10094–10099 (2018).
4. Veglia, F., Sanseviero, E. & Gabrilovich, D. I. Myeloid-derived suppressor cells in the era of increasing myeloid cell diversity. *Nat. Rev. Immunol.* **21**, 485–498 (2021).
5. Di Mitri, D. et al. Tumour-infiltrating Gr-1+ myeloid cells antagonize senescence in cancer. *Nature* **515**, 134–137 (2014).
6. Calcinotto, A. et al. IL-23 secreted by myeloid cells drives castration-resistant prostate cancer. *Nature* **559**, 363–369 (2018).
7. Lu, X. et al. Effective combinatorial immunotherapy for castration-resistant prostate cancer. *Nature* **543**, 728–732 (2017).
8. Porembka, M. R. et al. Pancreatic adenocarcinoma induces bone marrow mobilization of myeloid-derived suppressor cells which promote primary tumor growth. *Cancer Immunol. Immunother.* **61**, 1373–1385 (2012).
9. Wang, L. et al. Increased myeloid-derived suppressor cells in gastric cancer correlate with cancer stage and plasma S100A8/A9 proinflammatory proteins. *J. Immunol.* **190**, 794–804 (2013).
10. Donkor, M. K. et al. Mammary tumor heterogeneity in the expansion of myeloid-derived suppressor cells. *Int. Immunopharmacol.* **9**, 937–948 (2009).
11. Leibowitz-Amit, R. et al. Clinical variables associated with PSA response to abiraterone acetate in patients with metastatic castration-resistant prostate cancer. *Ann. Oncol.* **25**, 657–662 (2014).
12. Lorente, D. et al. Baseline neutrophil-lymphocyte ratio (NLR) is associated with survival and response to treatment with second-line chemotherapy for advanced prostate cancer independent of baseline steroid use. *Ann. Oncol.* **26**, 750–755 (2015).
13. Templeton, A. J. et al. Simple prognostic score for metastatic castration-resistant prostate cancer with incorporation of neutrophil-to-lymphocyte ratio. *Cancer* **120**, 3346–3352 (2014).
14. Kaur, H. B. et al. Association of tumor-infiltrating T-cell density with molecular subtype, racial ancestry and clinical outcomes in prostate cancer. *Mod. Pathol.* **31**, 1539–1552 (2018).
15. van Soest, R. J. et al. Neutrophil-to-lymphocyte ratio as a prognostic biomarker for men with metastatic castration-resistant prostate cancer receiving first-line chemotherapy: data from two randomized phase III trials. *Ann. Oncol.* **26**, 743–749 (2015).
16. Sharma, J. et al. Elevated IL-8, TNF-α, and MCP-1 in men with metastatic prostate cancer starting androgen-deprivation therapy (ADT) are associated with shorter time to castration-resistance and overall survival. *Prostate* **74**, 820–828 (2014).

17. Chi, N., Tan, Z., Ma, K., Bao, L. & Yun, Z. Increased circulating myeloid-derived suppressor cells correlate with cancer stages, interleukin-8 and -6 in prostate cancer. *Int. J. Clin. Exp. Med.* **7**, 3181–3192 (2014).
18. Lopez-Bujanda, Z. A. et al. Castration-mediated IL-8 promotes myeloid infiltration and prostate cancer progression. *Nat. Cancer* **2**, 803–818 (2021).
19. Nicholls, D. J. et al. Pharmacological characterization of AZD5069, a slowly reversible CXC chemokine receptor 2 antagonist. *J. Pharmacol. Exp. Ther.* **353**, 340–350 (2015).
20. Dominguez, C., McCampbell, K. K., David, J. M. & Palena, C. Neutralization of IL-8 decreases tumor PMN-MDSCs and reduces mesenchymalization of claudin-low triple-negative breast cancer. *JCI Insight* https://doi.org/10.1172/jci.insight.94296 (2017).
21. Silvera, D., Formenti, S. C. & Schneider, R. J. Translational control in cancer. *Nat. Rev. Cancer* **10**, 254–266 (2010).
22. Piccirillo, C. A., Bjur, E., Topisirovic, I., Sonenberg, N. & Larsson, O. Translational control of immune responses: from transcripts to translatomes. *Nat. Immunol.* **15**, 503–511 (2014).
23. Jamaspishvili, T. et al. Clinical implications of PTEN loss in prostate cancer. *Nat. Rev. Urol.* **15**, 222–234 (2018).
24. The Cancer Genome Atlas Research Network. The molecular taxonomy of primary prostate cancer. *Cell* **163**, 1011–1025 (2015).
25. Taylor, B. S. et al. Integrative genomic profiling of human prostate cancer. *Cancer Cell* **18**, 11–22 (2010).
26. Hsieh, A. C. et al. The translational landscape of mTOR signalling steers cancer initiation and metastasis. *Nature* **485**, 55–61 (2012).
27. Bhat, M. et al. Targeting the translation machinery in cancer. *Nat. Rev. Drug Discov.* **14**, 261–278 (2015).
28. Chu, J., Cargnello, M., Topisirovic, I. & Pelletier, J. Translation initiation factors: reprogramming protein synthesis in cancer. *Trends Cell Biol.* **26**, 918–933 (2016).
29. Furic, L. et al. eIF4E phosphorylation promotes tumorigenesis and is associated with prostate cancer progression. *Proc. Natl Acad. Sci. USA* **107**, 14134–14139 (2010).
30. Xu, Y. et al. Translation control of the immune checkpoint in cancer and its therapeutic targeting. *Nat. Med.* **25**, 301–311 (2019).
31. Knight, J. R. P. et al. MNK inhibition sensitizes KRAS-mutant colorectal cancer to mTORC1 inhibition by reducing eIF4E Phosphorylation and c-MYC expression. *Cancer Discov.* **11**, 1228–1247 (2021).
32. Huang, F. et al. Inhibiting the MNK1/2-eIF4E axis impairs melanoma phenotype switching and potentiates antitumor immune responses. *J .Clin. Invest.* https://doi.org/10.1172/JCI140752 (2021).
33. Robichaud, N. et al. Phosphorylation of eIF4E promotes EMT and metastasis via translational control of SNAIL and MMP-3. *Oncogene* **34**, 2032–2042 (2015).
34. Robichaud, N., Sonenberg, N., Ruggero, D. & Schneider, R. J. Translational control in cancer. *Cold Spring Harb. Perspect. Biol.* https://doi.org/10.1101/cshperspect.a032896 (2019).
35. Schmid, T. et al. Translation inhibitor Pdcd4 is targeted for degradation during tumor promotion. *Cancer Res.* **68**, 1254–1260 (2008).
36. Parsyan, A. et al. mRNA helicases: the tacticians of translational control. *Nat. Rev. Mol. Cell Biol.* **12**, 235–245 (2011).
37. Sheth, S. et al. Resveratrol reduces prostate cancer growth and metastasis by inhibiting the Akt/MicroRNA-21 pathway. *PLoS ONE* **7**, e51655 (2012).
38. Tomlins, S. A. et al. Integrative molecular concept modeling of prostate cancer progression. *Nat. Genet.* **39**, 41–51 (2007).
39. Sinha, A. et al. The proteogenomic landscape of curable prostate cancer. *Cancer Cell* **35**, 414–427 (2019).
40. Fabbri, L., Chakraborty, A., Robert, C. & Vagner, S. The plasticity of mRNA translation during cancer progression and therapy resistance. *Nat. Rev. Cancer* **21**, 558–577 (2021).
41. Rajasekhar, V. K. et al. Oncogenic Ras and Akt signaling contribute to glioblastoma formation by differential recruitment of existing mRNAs to polysomes. *Mol. Cell* **12**, 889–901 (2003).
42. Chen, Y. et al. ETS factors reprogram the androgen receptor cistrome and prime prostate tumorigenesis in response to PTEN loss. *Nat. Med.* **19**, 1023–1029 (2013).
43. Chen, Z. et al. Crucial role of p53-dependent cellular senescence in suppression of Pten-deficient tumorigenesis. *Nature* **436**, 725–730 (2005).
44. Alajati, A. et al. CDCP1 overexpression drives prostate cancer progression and can be targeted in vivo. *J. Clin. Invest.* **130**, 2435–2450 (2020).
45. Guccini, I. et al. Senescence reprogramming by TIMP1 deficiency promotes prostate cancer metastasis. *Cancer Cell* **39**, 68–82 (2021).
46. Ingolia, N. T., Ghaemmaghami, S., Newman, J. R. & Weissman, J. S. Genome-wide analysis in vivo of translation with nucleotide resolution using ribosome profiling. *Science* **324**, 218–223 (2009).
47. Schwanhausser, B. et al. Global quantification of mammalian gene expression control. *Nature* **473**, 337–342 (2011).
48. Rozen, F. et al. Bidirectional RNA helicase activity of eucaryotic translation initiation factors 4A and 4F. *Mol. Cell. Biol.* **10**, 1134–1144 (1990).
49. Cerezo, M. et al. Translational control of tumor immune escape via the eIF4F-STAT1-PD-L1 axis in melanoma. *Nat. Med.* **24**, 1877–1886 (2018).
50. Fu, J. et al. HGF/c-MET pathway in cancer: from molecular characterization to clinical evidence. *Oncogene* **40**, 4625–4651 (2021).
51. Appunni, S. et al. Biglycan: an emerging small leucine-rich proteoglycan (SLRP) marker and its clinicopathological significance. *Mol. Cell. Biochem.* **476**, 3935–3950 (2021).
52. Zhao, H. et al. The role of osteopontin in the progression of solid organ tumour. *Cell Death Dis.* **9**, 356 (2018).
53. Bolis, M. et al. Dynamic prostate cancer transcriptome analysis delineates the trajectory to disease progression. *Nat. Commun.* **12**, 7033 (2021).
54. Reich, S. H. et al. Structure-based design of pyridone-aminal eFT508 targeting dysregulated translation by selective mitogen-activated protein kinase interacting kinases 1 and 2 (MNK1/2) inhibition. *J. Med. Chem.* **61**, 3516–3540 (2018).
55. Lin, J. et al. Targeting activated Akt with GDC-0068, a novel selective Akt inhibitor that is efficacious in multiple tumor models. *Clin. Cancer Res.* **19**, 1760–1772 (2013).
56. de Bono, J. S. et al. Randomized phase II study evaluating Akt blockade with ipatasertib, in combination with abiraterone, in patients with metastatic prostate cancer with and without PTEN loss. *Clin. Cancer Res.* **25**, 928–936 (2019).
57. Sweeney, C. et al. Ipatasertib plus abiraterone and prednisolone in metastatic castration-resistant prostate cancer (IPATential150): a multicentre, randomised, double-blind, phase 3 trial. *Lancet* **398**, 131–142 (2021).
58. de Wit, R. et al. Baseline neutrophil-to-lymphocyte ratio as a predictive and prognostic biomarker in patients with metastatic castration-resistant prostate cancer treated with cabazitaxel versus abiraterone or enzalutamide in the CARD study. *ESMO Open* **6**, 100241 (2021).
59. Rebello, R. J. et al. Prostate cancer. *Nat. Rev. Dis. Primers* **7**, 9 (2021).
60. Wei, S. C., Duffy, C. R. & Allison, J. P. Fundamental mechanisms of immune checkpoint blockade therapy. *Cancer Discov.* **8**, 1069–1086 (2018).
61. Rescigno, P. & de Bono, J. S. Immunotherapy for lethal prostate cancer. *Nat. Rev. Urol.* **16**, 69–70 (2019).
62. Aguilar-Valles, A. et al. Translational control of depression-like behavior via phosphorylation of eukaryotic translation initiation factor 4E. *Nat. Commun.* **9**, 2459 (2018).

63. Genuth, N. R. & Barna, M. Heterogeneity and specialized functions of translation machinery: from genes to organisms. *Nat. Rev. Genet.* **19**, 431–452 (2018).
64. Hilliard, A. et al. Translational regulation of autoimmune inflammation and lymphoma genesis by programmed cell death 4. *J. Immunol.* **177**, 8095–8102 (2006).
65. Dorrello, N. V. et al. S6K1- and βTRCP-mediated degradation of PDCD4 promotes protein translation and cell growth. *Science* **314**, 467–471 (2006).
66. Asangani, I. A. et al. MicroRNA-21 (miR-21) post-transcriptionally downregulates tumor suppressor Pdcd4 and stimulates invasion, intravasation and metastasis in colorectal cancer. *Oncogene* **27**, 2128–2136 (2008).
67. Sheedy, F. J. et al. Negative regulation of TLR4 via targeting of the proinflammatory tumor suppressor PDCD4 by the microRNA miR-21. *Nat. Immunol.* **11**, 141–147 (2010).
68. Cho, H. et al. RapidCaP, a novel GEM model for metastatic prostate cancer analysis and therapy, reveals myc as a driver of Pten-mutant metastasis. *Cancer Discov.* **4**, 318–333 (2014).
69. Marigo, I. et al. Tumor-induced tolerance and immune suppression depend on the C/EBPβ transcription factor. *Immunity* **32**, 790–802 (2010).
70. Pernigoni, N. et al. Commensal bacteria promote endocrine resistance in prostate cancer through androgen biosynthesis. *Science* **374**, 216–224 (2021).
71. Dobin, A. et al. STAR: ultrafast universal RNA-seq aligner. *Bioinformatics* **29**, 15–21 (2013).
72. Harrow, J. et al. GENCODE: the reference human genome annotation for the ENCODE project. *Genome Res.* **22**, 1760–1774 (2012).
73. Love, M. I., Huber, W. & Anders, S. Moderated estimation of fold change and dispersion for RNA-seq data with DESeq2. *Genome Biol.* **15**, 550 (2014).
74. Oertlin, C. et al. Generally applicable transcriptome-wide analysis of translation using anota2seq. *Nucleic Acids Res.* **47**, e70 (2019).
75. Franceschini, A. et al. STRING v9.1: protein–protein interaction networks, with increased coverage and integration. *Nucleic Acids Res.* **41**, D808–D815 (2013).
76. Swaim, C. D., Scott, A. F., Canadeo, L. A. & Huibregtse, J. M. Extracellular ISG15 signals cytokine secretion through the LFA-1 integrin receptor. *Mol Cell* **68**, 581–590 (2017).
77. Sadik, C. D., Miyabe, Y., Sezin, T. & Luster, A. D. The critical role of C5a as an initiator of neutrophil-mediated autoimmune inflammation of the joint and skin. *Semin. Immunol.* **37**, 21–29 (2018).
78. Lauria, F. et al. SMN-primed ribosomes modulate the translation of transcripts related to spinal muscular atrophy. *Nat. Cell Biol.* **22**, 1239–1251 (2020).
79. Tebaldi, T. et al. Widespread uncoupling between transcriptome and translatome variations after a stimulus in mammalian cells. *BMC Genomics* **13**, 220 (2012).
80. Lauria, F. et al. riboWaltz: optimization of ribosome P-site positioning in ribosome profiling data. *PLoS Comput. Biol.* **14**, e1006169 (2018).
81. Robinson, M. D., McCarthy, D. J. & Smyth, G. K. edgeR: a Bioconductor package for differential expression analysis of digital gene expression data. *Bioinformatics* **26**, 139–140 (2010).
82. Livak, K. J. & Schmittgen, T. D. Analysis of relative gene expression data using real-time quantitative PCR and the 2(-ΔΔC(T)) method. *Methods* **25**, 402–408 (2001).
83. Welti, J. et al. Targeting bromodomain and extra-terminal (BET) family proteins in castration-resistant prostate cancer (CRPC). *Clin. Cancer Res.* **24**, 3149–3162 (2018).
84. Gil, V. et al. HER3 is an actionable target in advanced prostate cancer. *Cancer Res.* **81**, 6207–6218 (2021).
85. Zhong, Q. et al. Image-based computational quantification and visualization of genetic alterations and tumour heterogeneity. *Sci Rep.* **6**, 24146 (2016).
86. Antonarakis, E. S. et al. An immunohistochemical signature comprising PTEN, MYC, and Ki67 predicts progression in prostate cancer patients receiving adjuvant docetaxel after prostatectomy. *Cancer* **118**, 6063–6071 (2012).

Acknowledgements

We acknowledge all the members of the A.A. laboratory for scientific discussions and critical reading. We acknowledge all the patients who participated in the study protocols. I.G. was, in part, funded by a SAKK Translational Urogenital Cancer Meeting Award. This work was supported by ERC consolidator (CoG683136) grant, Prostate Cancer Foundation (PCF Challenge Award 19CHAL08), Swiss Card-Onco-Grant of Alfred and Annemarie von Sick, Horten Foundation, Prix Robert Wenner, Ligue Suisse contre le Cancer and ISREC Foundation (to A.A.).

Author contributions

A.A. and D.B. conceived and designed the project. D.B., A.P., M.M. and N.P. performed experiments. M.T. performed the bioinformatic analysis. B.C. contributed to data discussion and revision of the manuscript. E.P. and G.A. took care of genotyping the animals, performed the in vivo treatments and tumor measurement. S.M. performed the immunohistochemical experiments. M.D. and A.A. developed the $Pten^{pc-/-}$; $CDCP1^{pc+/+}$ mouse model. M.C. analyzed the Incucyte-derived data. I.G. and A.Revandkar developed the $Pten^{pc-/-}$;$Timp1^{-/-}$ mouse model. T.T. performed the bioinformatic analysis related to the 5′ UTR length and folding energy. D.D., F.L. and G.V. performed and analyzed the Ribo-seq. A.V. performed the in vivo treatments and tumor measurement. M.M. revised the manuscript. A.C. performed preliminary immunophenotyping experiments. M.B. supervised M.T. A. Rinaldi checked the quality of the RNA. S.B. provided the AZD5069 compound. J.H.R. and H.M. provided the human tissue microarray of the cohort 1. M.S. and M.F. provided the human tissue microarray of the cohort 2. S.S., M.C., W.Y., A.S. and J.d.B. selected and provided human CRPC and patient-derived xenograft samples. M.G., A.B., C.M. and L.T. provided the $Pten^{-/-}$; $Trp53^{-/-}$ RapidCap cell line. N.D. performed preliminary bioinformatic analysis. D.B. and A.A. interpreted the data and wrote the paper.

Competing interests

S.B. is affiliated with IMED Oncology AstraZeneca, Li Ka Shing Centre, Cambridge, UK and provided the AZD5069 compound. Johann de Bono has served on Advisory Boards for Roche and AstraZeneca and he is an employee of the ICR, which has received funding or other support for his research work from AstraZeneca and which has a commercial interest in PI3K/AKT pathway inhibitors (no personal income). Johann de Bono and Andrea Alimonti are principal investigators of the NCT03177187 trial which was partially supported by AstraZeneca and Astellas Pharma. The remaining authors declare no competing interests.

Additional information

Extended data is available for this paper at https://doi.org/10.1038/s43018-023-00594-z.

Supplementary information The online version contains supplementary material available at https://doi.org/10.1038/s43018-023-00594-z.

Correspondence and requests for materials should be addressed to Andrea Alimonti.

Peer review information *Nature Cancer* thanks Tracy McGaha, Ping Mu and the other, anonymous, reviewer(s) for their contribution to the peer review of this work.

[1]Institute of Oncology Research, Oncology Institute of Southern Switzerland, Bellinzona, Switzerland. [2]Faculty of Biomedical Sciences, Università della Svizzera Italiana, Lugano, Switzerland. [3]Yale Cancer Center and Department of Internal Medicine, Yale University School of Medicine, New Haven, CT, USA. [4]Institute of Biophysics, CNR Unit at Trento, Povo, Italy. [5]Bioinformatics Core Unit, Swiss Institute of Bioinformatics, Bellinzona, Switzerland. [6]Computational Oncology Unit, Department of Oncology, Istituto di Richerche Farmacologiche 'Mario Negri' IRCCS, Milano, Italy. [7]IMED Oncology AstraZeneca, Li Ka Shing Centre, Cambridge, UK. [8]Department of Pathology and Molecular Pathology, University Hospital Zurich (USZ), Zurich, Switzerland. [9]Veneto Institute of Oncology, IOV-IRCCS, Padua, Italy. [10]Institute of Cancer Research and Royal Marsden NHS Foundation Trust, London, UK. [11]Cold Spring Harbor Laboratory, Cold Spring Harbor, New York, NY, USA. [12]2cSysBioMed, TI, Contra, Switzerland. [13]Department of Medicine (DIMED), Surgical Pathology Unit, University of Padua, Padua, Italy. [14]The Royal Marsden Hospital, London, UK. [15]Department of Medicine, Venetian Institute of Molecular Medicine, University of Padova, Padova, Italy. [16]Department of Health Sciences and Technology, Eidgenössische Technische Hochschule (ETH) Zürich, Zurich, Switzerland. [17]Present address: Ima Biotech, Lille, France. [18]Present address: Evotec, Toulouse, France. [19]Present address: Imperial College London, London, UK. [20]Present address: Institute of Molecular Health Sciences, ETH Zurich, Zurich, Switzerland. [21]Present address: Harvard Medical School, Massachusetts General Hospital Cancer Center, Boston, MA, USA. [22]Present address: Department of Urology, Universitätklinikum Bonn, Bonn, Germany. [23]Present address: Biosun Pharmed, Kordan, Iran. ✉e-mail: andrea.alimonti@ior.usi.ch

https://doi.org/10.1038/s43018-023-00594-z

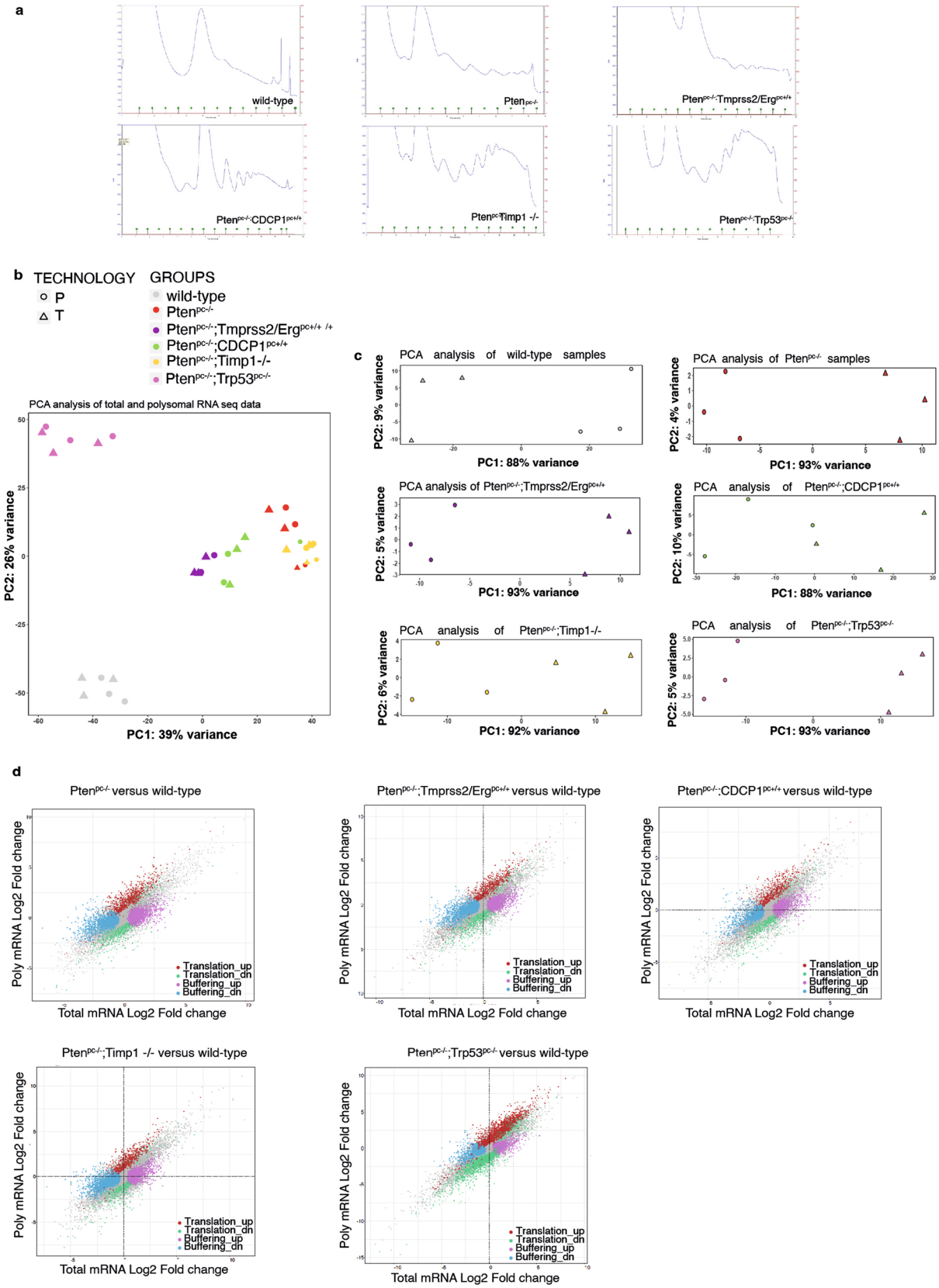

Extended Data Fig. 1 | See next page for caption.

https://doi.org/10.1038/s43018-023-00594-z

Extended Data Fig. 1 | Polysome profiling analysis in Pten-null-driven prostate cancer. a, Polysome profiles of wild-type prostate, $Pten^{pc-/-}$, $Pten^{pc-/-}$;TMPRSS2/$Erg^{pc+/+}$, $Pten^{pc-/-}$;$CDCP1^{pc+/+}$, $Pten^{pc-/-}$;Timp1−/− and $Pten^{pc-/-}$;$Trp53^{pc-/-}$ prostate cancer. RNA-seq was performed on polysome-bound RNAs and total RNA derived from the prostate of three mice for each genetic background for a total of 18 samples. **b**, PCA plots of total (T) and polysomal RNA (P) fractions for each analyzed genetic background (n = 3 mice for each genetic background for a total of 18 samples). **c**, PCA plots of total and polysomal RNA fractions for each genetic background analyzed, corrected for the batch effect (n = 3 mice for each genetic background for a total of 18 samples). **d**, Scatter plots of fold-changes for polysome-associated and total mRNA levels for the comparisons between the indicated genetic backgrounds and wild-type prostates showing mRNAs with upregulated translation efficiency (red), downregulated translation efficiency, buffering up (pink), buffering down (blue) (n = 3 mice for each genetic background for a total of 18 samples). Details are provided in Supplementary Table 1 and Supplementary Table 2.

https://doi.org/10.1038/s43018-023-00594-z

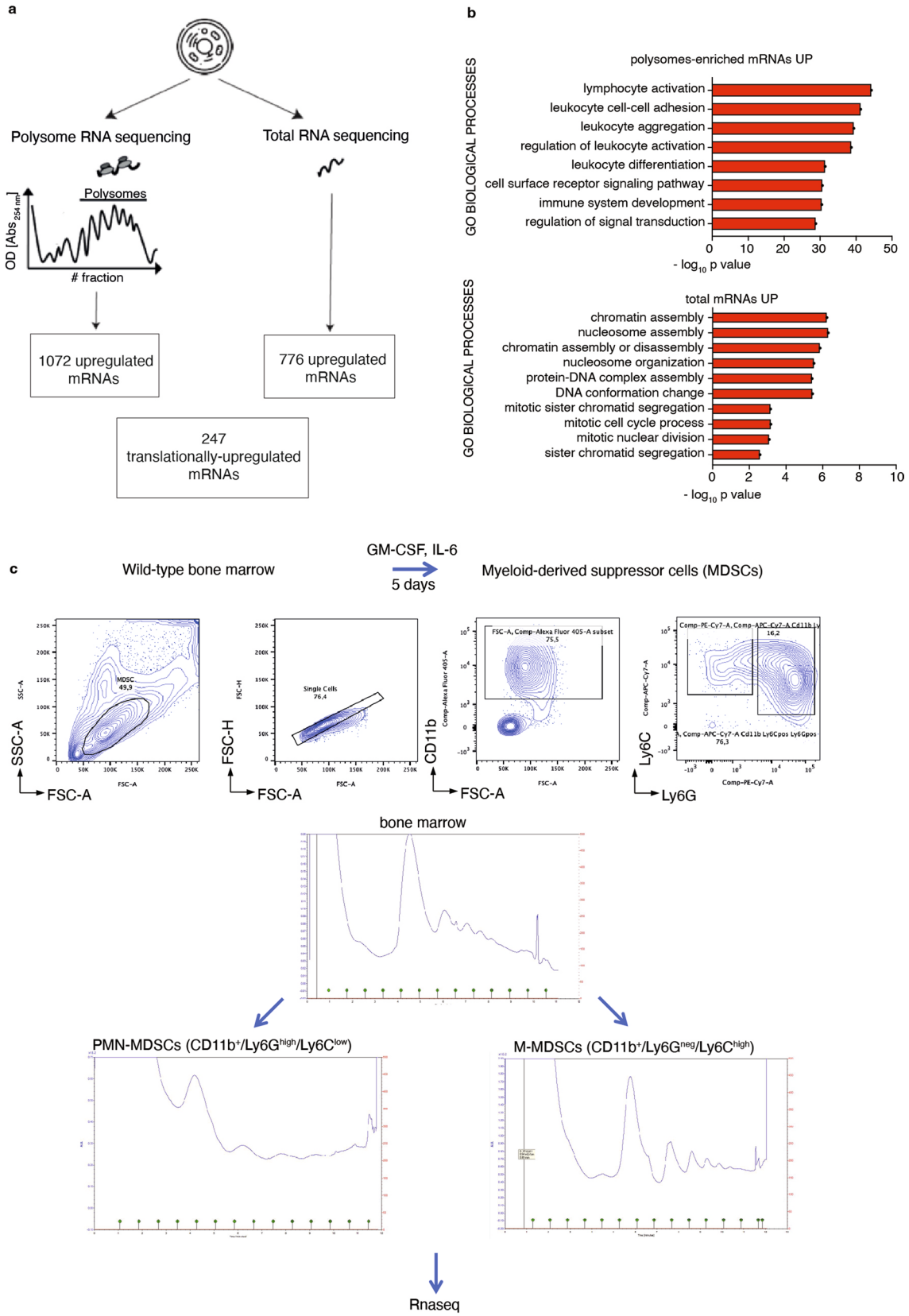

Extended Data Fig. 2 | See next page for caption.

https://doi.org/10.1038/s43018-023-00594-z

Extended Data Fig. 2 | Polysome profiling analysis in Pten-null-driven prostate cancer and bone marrow-derived MDSCs. a, Schematic representation of the polysome profiling analysis performed by selecting mRNAs changes in common among the five different genetic backgrounds analyzed ($Pten^{pc-/-}$, $Pten^{pc-/-}$; TMPRSS2/$Erg^{pc+/+}$, $Pten^{pc-/-}$;$CDCP1^{pc+/+}$, $Pten^{pc-/-}$;Timp1−/− and $Pten^{pc-/-}$;$Trp53^{pc-/-}$ prostate cancer) and wild-type prostate. Using this approach, 1072 polysomes-bound mRNAs were upregulated in the polysomal RNA pool (threshold Log2 FC > 1.0; FDR < 0.05), 776 total mRNA were upregulated in the total RNA pool (threshold Log2 FC > 1.0; FDR < 0.05) and 247 mRNAs were found translationally up-regulated (threshold for polysomal mRNA expression Log2 FC ≥ 1.0; FDR < 0.05: threshold for translation efficiency Log2 FC ≥ 0.5; FDR < 0.1) in each genetic background compared to wild-type prostate. **b**, Gene Ontology biological processes enriched among the upregulated mRNAs in the polysomes-bound pool (upper panel) and in the total RNA pool (lower panel) in $Pten^{pc-/-}$, $Pten^{pc-/-}$;TMPRSS2/$Erg^{pc+/+;}$ $Pten^{pc-/-}$;$CDCP1^{pc+/+}$, $Pten^{pc-/-}$;Timp1−/− and $Pten^{pc-/-}$;$Trp53^{pc-/-}$ prostate cancer compared to wild-type prostate, determined by DAVID software (n = 3 mice for each genetic background for a total of 18 samples). Log_{10} adjusted *p*-values by using the linear step-up method of Benjamini is reported. **c**, Scheme of the differentiation protocol of bone marrow-derived MDSCs; FACS plot of the gating strategy of bone marrow-derived MDSCs, sorted in $CD11b^{+}$/$Ly6G^{high}$/$Ly6C^{low}$ PMN-MDSCs and $CD11b^{+}$/$Ly6G^{neg}$/$Ly6C^{high}$ M-MDSCs after 5 days of differentiation with 40 ng/ml GM-CSF and 40 ng/ml IL-6 in RPMI plus 10% FBS medium (top); polysome profiles of undifferentiated bone marrow (middle) $CD11b^{+}$/$Ly6G^{high}$/$Ly6C^{low}$ PMN-MDSCs (bottom left) and $CD11b^{+}$/$Ly6G^{neg}$/$Ly6C^{high}$ M-MDSCs (bottom right). RNA-seq was performed on polysome-bound RNAs and total RNA derived from three biological replicates.

https://doi.org/10.1038/s43018-023-00594-z

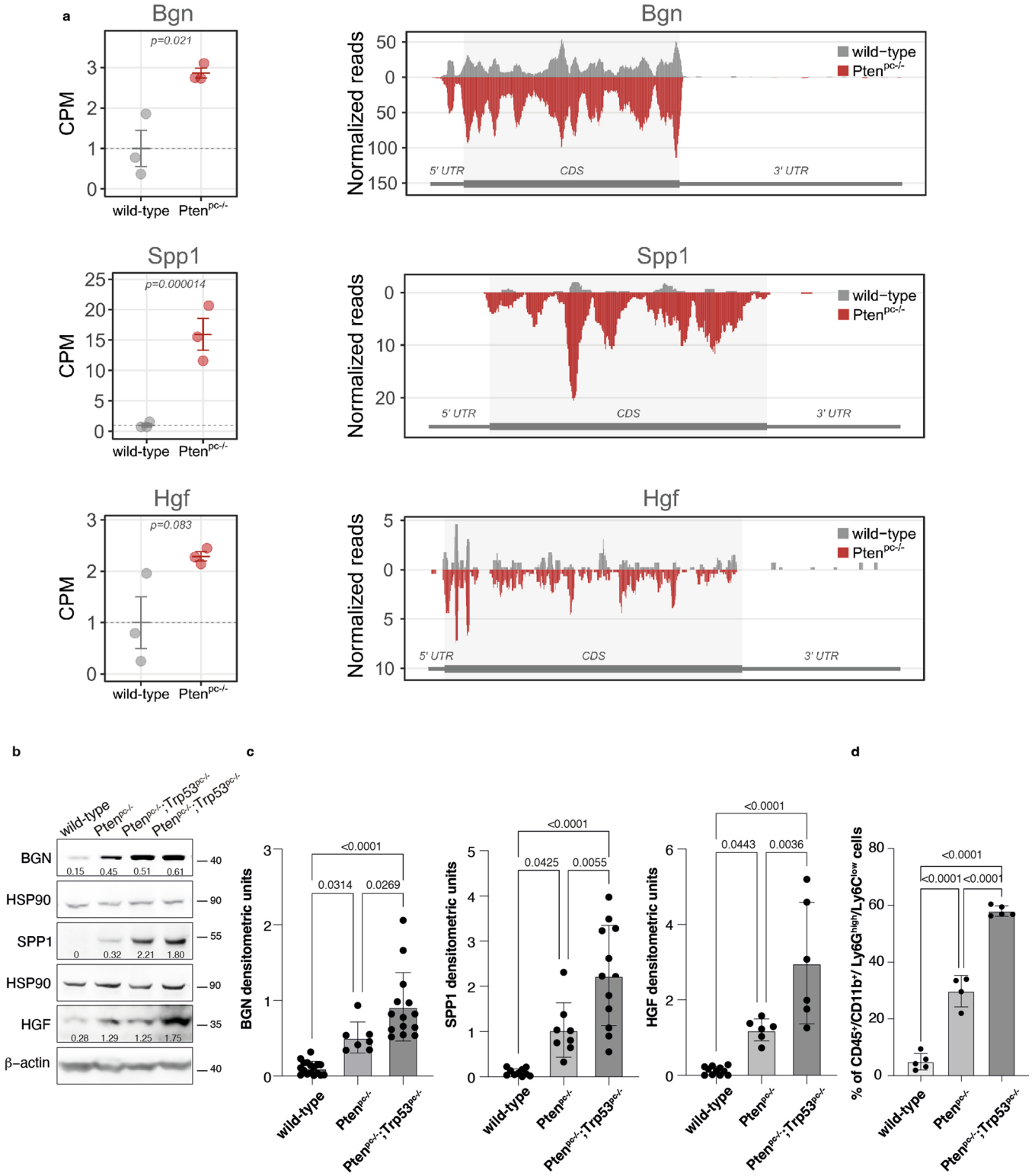

Extended Data Fig. 3 | BGN, SPP1 and HGF are upregulated in Pten null-driven prostate cancer compared to wild-type prostate. a, Graphs showing the CPM of *Bgn*, *Spp1* and *Hgf* in wild-type prostate and Pten$^{pc-/-}$ prostate cancer determined by Ribo-seq analysis (left panel). Data are presented as mean values +/− SEM of n = 3 mice for each genotype. P values were computed by one-tailed quasi-likelihood F-test and are indicated at the top of the graph. Ribosome occupancy in wild-type prostate (grey) and Pten$^{pc-/-}$ prostate cancer (red) determined by Ribo-seq analysis (right panel). Each profile represents the mean normalized coverage among n = 3 mice for each genotype. The structure of the transcript, showing the boundaries of CDS and UTR regions, is outlined below each profile. **b**, Western blot showing the protein levels of BGN, SPP1 and HGF in wild-type prostates, Pten$^{pc-/-}$ and Pten$^{pc-/-}$;Trp53$^{pc-/-}$ prostate cancers. Densitometry values normalized to the respective loading control are indicated for each band. See quantification for the indicated number of mice in Ext Data Fig. 3c. **c**, Densitometric analysis of BGN, SPP1 and HGF in wild-type prostates, Pten$^{pc-/-}$ and Pten$^{pc-/-}$;Trp53$^{pc-/-}$ prostate cancers (from the left, BGN n = 17, n = 7, n = 14; SPP1 n = 10, n = 8, n = 12; HGF n = 11, n = 6, n = 6). Data are mean ± SD. **d**, Percentage of tumor-infiltrating CD45^{+}/CD11b^{+}/ Ly6G^{high}/Ly6C^{low} cells (PMN-MDSCs) in wild-type, Pten$^{pc-/-}$ and Pten$^{pc-/-}$;Trp53$^{pc-/-}$ prostate cancers (from the left, n = 5, n = 4, n = 5 derived from the analysis of Fig. 1a. Data are mean ± SD. Statistical analysis between all groups in (c) and (d): (ordinary one-way ANOVA followed by Tukey's multiple comparisons test).

https://doi.org/10.1038/s43018-023-00594-z

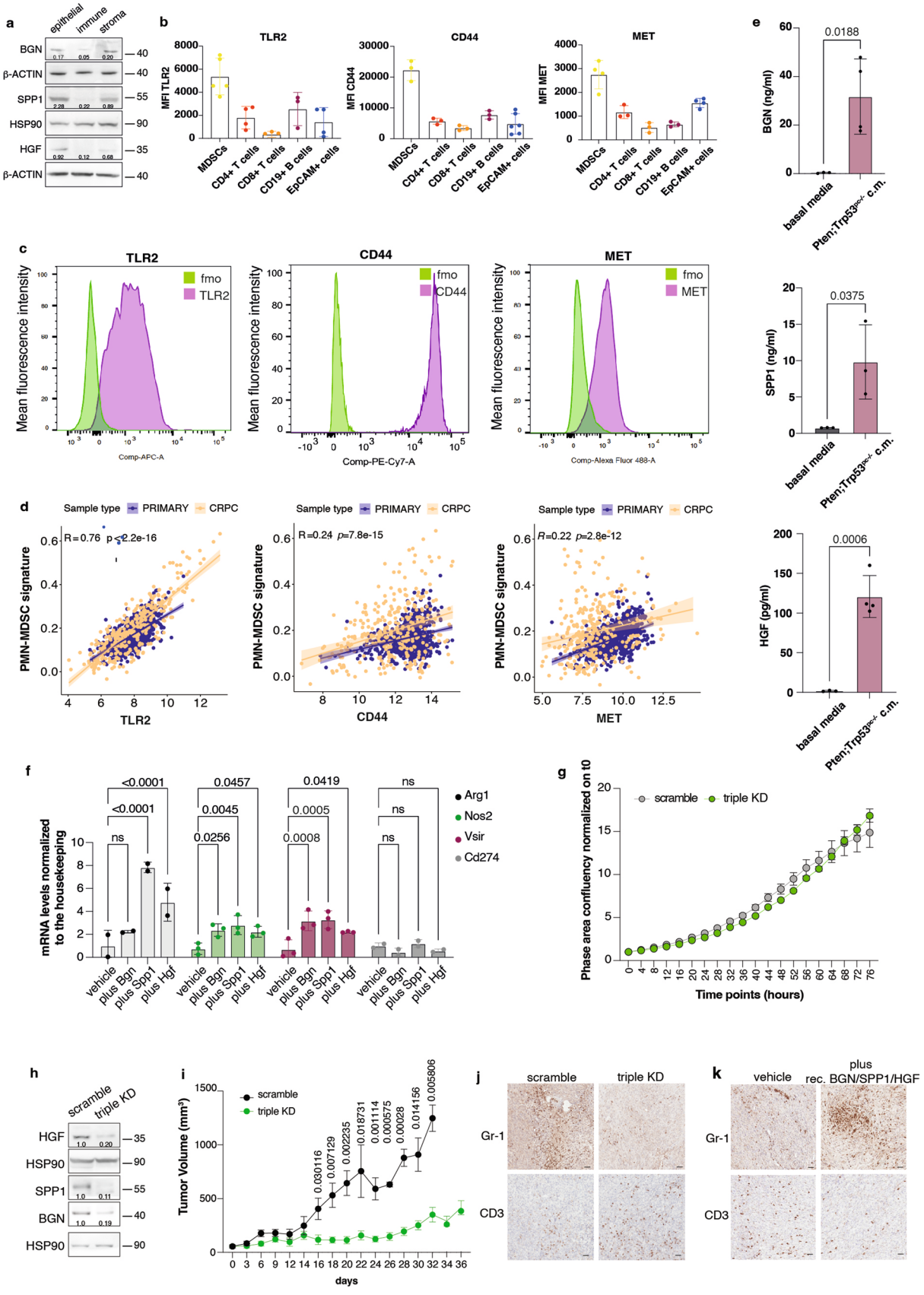

Extended Data Fig. 4 | See next page for caption.

https://doi.org/10.1038/s43018-023-00594-z

Extended Data Fig. 4 | TLR2, CD44 and MET expression correlates with the PMN-MDSCs signature in human prostate cancer and CRPC. a, Western blot showing the protein levels of BGN, SPP1 and HGF in epithelial (EpCAM+ cells), immune (CD45+ cells) and stromal fraction (EpCAM-, CD45- cells) of $Pten^{pc-/-}$;$Trp53^{pc-/-}$ prostate cancer. Densitometry values normalized to the respective loading control are indicated for each band. The experiment was repeated two independent times with similar results. **b**, Mean fluorescence intensity (MFI) of the indicated receptors in tumor-infiltrating immune cells subsets and EpCAM+ cells in $Pten^{pc-/-}$;$Trp53^{pc-/-}$ prostate cancers. At least n = 3 biologically independent samples. Data are mean ± SD. **c**, FACS plots of TLR2, CD44 and MET receptor expression in bone marrow-derived MDSCs; green signal: MDSCs stained with fluorescence minus one control, violet signal: MDSCs stained with the specific antibody. **d**, Correlation of TLR2 (left panel), CD44 (middle panel) and MET (right panel) expression with the PMN-MDSCs signature in primary prostate cancer and CRPC. Pearson correlation and p value are indicated at the top of the graph. TLR2: 95 % confidence interval 0.734- 0.785; CD44: 95 % confidence interval: 0.180-0.295; MET: 95 % confidence interval: 0.156-0.273 **e**, BGN, SPP1 and HGF protein levels determined in $Pten^{-/-}$;$Trp53^{-/-}$ (RapidCap)-derived conditioned medium by ELISA assay. n = 3 biologically independent samples. Data are mean ± SD. Statistical analysis (unpaired two-sided Student's t-test). **f**, *Arg1*, *Nos2*, *Vsir* and *Cd274* mRNA expression levels in bone marrow-derived MDSCs pretreated with recombinant BGN, SPP1 and HGF for 24 hours. n = 2 (*Arg1*), n = 3 (*Nos2*), n = 3 (*Vsir*), n = 2 (*Cd274*) biologically independent samples. Data are mean ± SD. Statistical analysis (two-way ANOVA followed by Dunnett's multiple comparisons test). **g**, Growth curve of scramble and *Hgf*/*Spp1*/*Bgn* triple KD $Pten^{-/-}$;$Trp53^{-/-}$ (RapidCap) cells. Data are mean ± SEM. The experiment was repeated two independent times with similar results. **h**, Western blot showing HGF, SPP1 and BGN protein levels in scramble and triple KD $Pten^{-/-}$;$Trp53^{-/-}$ (RapidCap)- cell lines used for the in vivo experiments. Densitometry values normalized to the respective loading control are indicated for each band. **i**, Tumor growth of scramble and *Hgf*/*Spp1*/*Bgn* triple KD in $Pten^{-/-}$;$Trp53^{-/-}$ (RapidCap) - allografts (for all groups, n = 5 in each group). Data are mean ± SEM. Statistical analysis (multiple unpaired student t test). **j**, Representative IHC of Gr-1 and CD3 in scramble and *Hgf*/*Spp1*/*Bgn* triple KD $Pten^{-/-}$;$Trp53^{-/-}$ (RapidCap)- allografts. Scale bar 50 µm. (n = 5 mice in each group). **k**, Representative IHC of Gr-1 and CD3 in vehicle-treated (n = 4 mice) and recombinant Bgn/Spp1/Hgf-treated (n = 6 mice) TRAMP-C1 allografts. Scale bar 50 µm.

https://doi.org/10.1038/s43018-023-00594-z

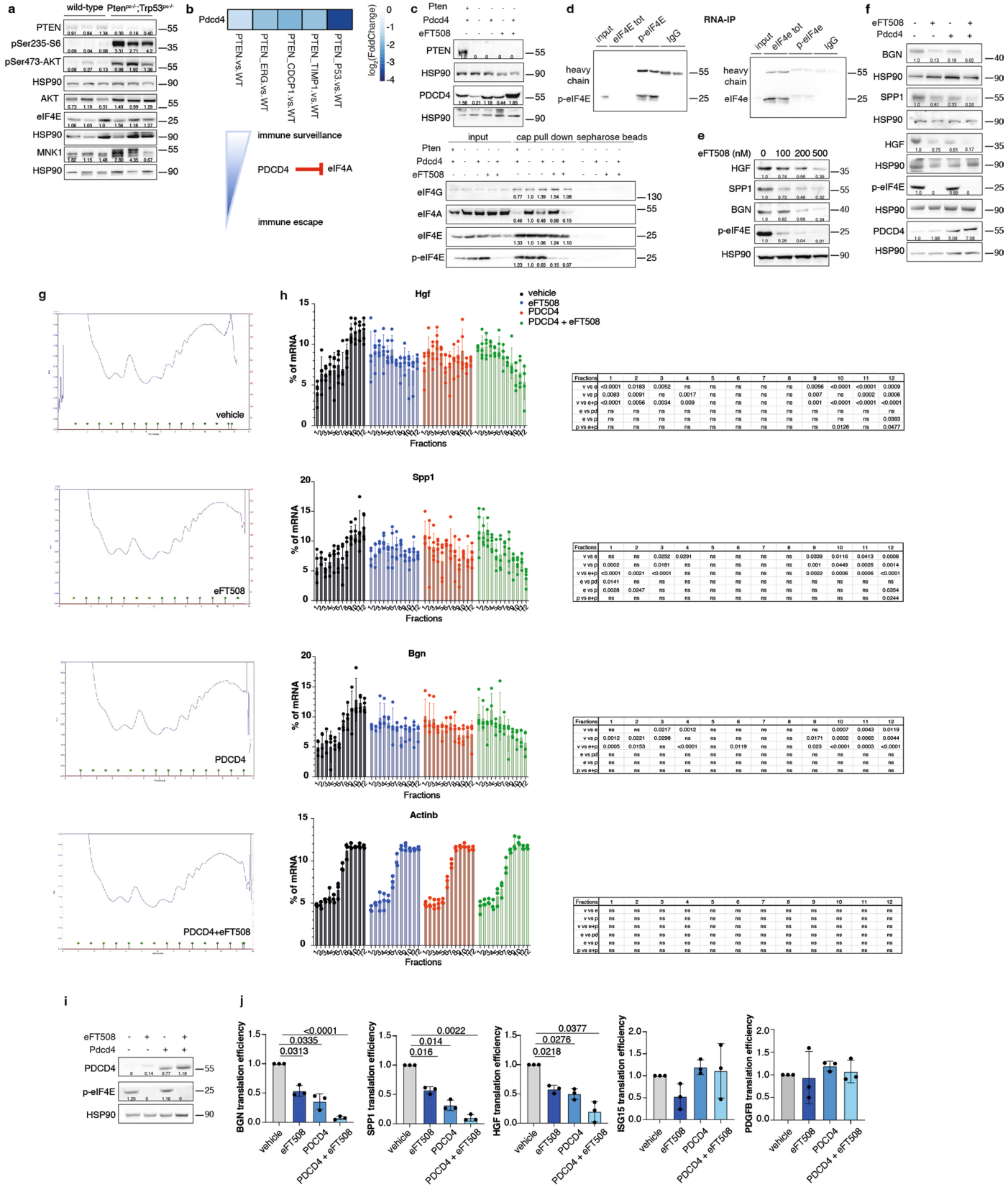

Extended Data Fig. 5 | See next page for caption.

https://doi.org/10.1038/s43018-023-00594-z

Extended Data Fig. 5 | PDCD4 inhibits eIF4F complex formation and cooperates with eFT508 to reduce *Hgf*, *Spp1* and *Bgn* levels. a, Western blot showing the protein levels of PTEN, pSer473-AKT, AKT total, pSer235-S6, eIF4E, MNK1 and representative HSP90 in wild-type prostate and $Pten^{pc-/-}$;$Trp53^{pc-/-}$ prostate cancer. The experiment was performed once with n = 3 mice for each group. **b**, Heatmap showing PDCD4 mRNA levels in the indicated genetic background of prostate cancer compared to wild-type prostate (total mRNA expression determined by RNA-seq). **c**, Western blot showing the levels of Pten and PDCD4 in the indicated settings (top). Cap pull-down assay showing the levels of eIF4G, eIF4A, eIF4E and p-eIF4E in input, cap pull-down and sepharose control beads. Densitometry values of the cap pull-down normalized to the input are indicated for each band (bottom). **d**, Western blot showing the levels of p-eIF4E and eIF4E after RNA immunoprecipitation with the respective antibody in Pten-sh TC1 prostate cancer cells. **e**, Western blot showing the levels of HGF, SPP1, BGN, p-eIF4E and representative HSP90 in Pten-sh TC1 cell line upon the indicated concentration of eFT508. **f**, Western blot showing the levels of HGF, SPP1, BGN, p-eIF4E, PDCD4 and representative HSP90 in Pten-sh TC1 cell line upon 500 nM eFT508 treatment and PDCD4 rescue. **g**, Polysome profiles of vehicle, 500 nM eFT508-treated, Pdcd4-overexpressing Pten-sh cells and eFT508-treated / Pdcd4-overexpressing Pten-sh cells. **h**, Distribution of *Hgf*, *Spp1* and *Bgn* mRNA levels in the fractions derived from the sucrose gradient fractionation in Pten-sh TC1 cells, determined by qRT-PCR (n = 5 independent experiments for *Hgf* and *Spp1*; n = 4 independent experiments for *Bgn*; n = 3 independent experiments for *Actinb*). The percentages of *Hgf*, *Spp1* and *Bgn* mRNA distributed in each fraction are shown. v = vehicle; e = eFT508; p = pdcd4; e + p = eFT508 + pdcd4. Data are mean ± SD. Statistical analysis between all groups (ordinary two-way ANOVA followed by Tukey's multiple comparisons test). **i**, Western blot showing the levels of PDCD4 and p-eIF4E in human PC3 prostate cancer cell line. **j**, Translation efficiency (polysomal mRNA expression/ total mRNA expression) of *HGF*, *SPP1*, *BGN*, *ISG15* and *PDGFB* upon 500 nM eFT508 treatment and PDCD4 rescue in human PC3 prostate cancer cell line (n = 3 independent experiments). Data are mean ± SD. Statistical analysis between all groups: (RM one-way ANOVA followed by Tukey's multiple comparisons test). Densitometry values normalized to the housekeeping are indicated for each band in (a) and (e-f) and (i). The experiment was repeated at least two independent times with similar results in (c-f) and (i).

https://doi.org/10.1038/s43018-023-00594-z

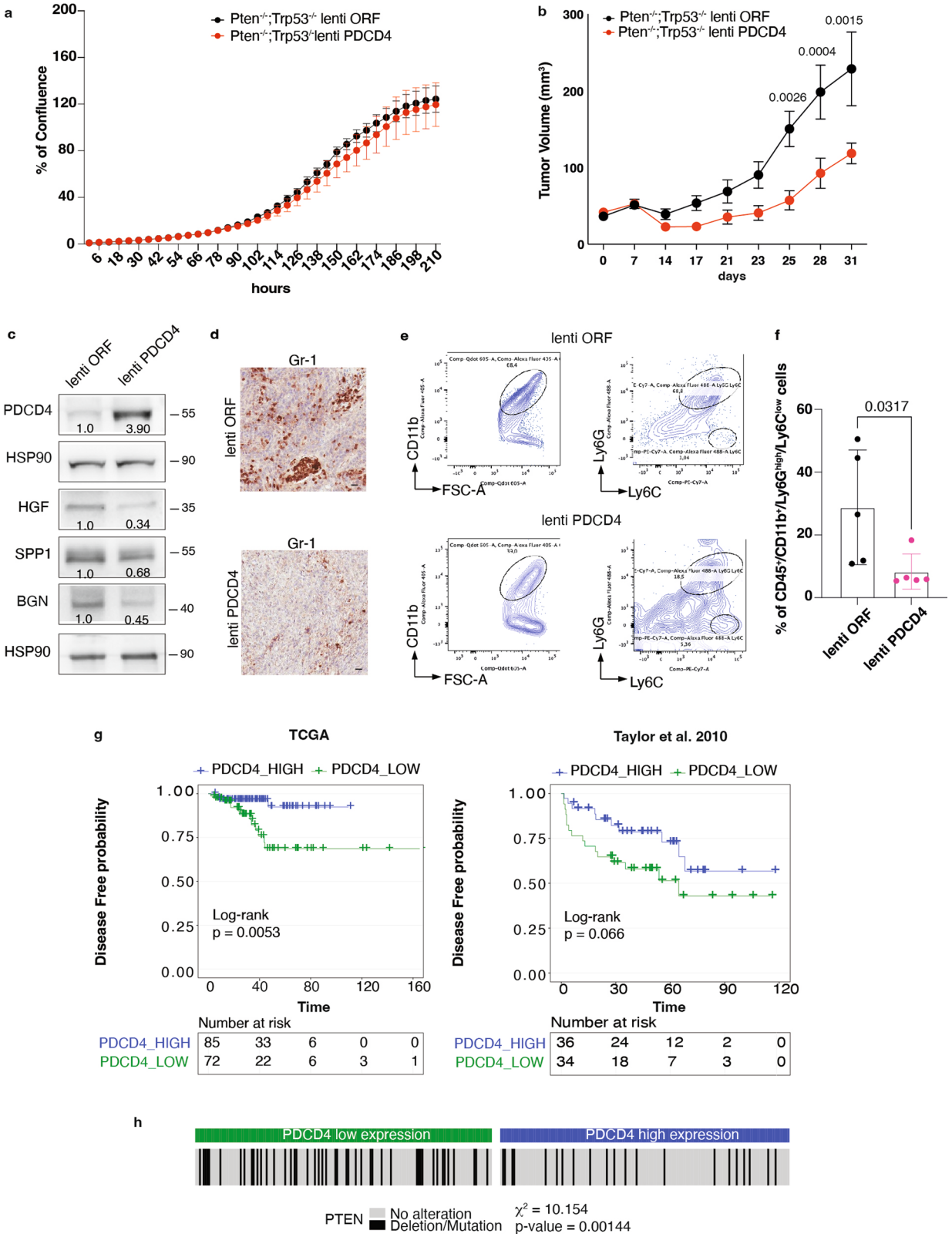

Extended Data Fig. 6 | See next page for caption.

https://doi.org/10.1038/s43018-023-00594-z

Extended Data Fig. 6 | Prostate-specific Pdcd4 rescue inhibits tumor-infiltrating PMN-MDSCs and its loss is associated with decreased disease-free survival in human prostate cancer. a, Growth curve of control vector (lenti ORF) and PDCD4 -overexpressing (lenti PDCD4) $Pten^{-/-}$;$Trp53^{-/-}$ (RapidCap) prostate cancer cells, determined by the Incucyte system. Data are mean ± SEM. The experiment was repeated two independent times with similar results. **b**, Tumor growth of C57BL6 mice injected with 2.5×10^6 control vector or PDCD4 -overexpressing $Pten^{-/-}$;$Trp53^{-/-}$ (RapidCap) prostate cancer cells (lenti ORF n = 10; lenti Pdcd4 n = 7 mice). Data are mean ± SEM. Statistical analysis: (two way ANOVA followed by Šídák's multiple comparisons test). **c**, Western blot showing the protein levels of PDCD4, SPP1, HGF, BGN and representative HSP90 in control vector and PDCD4 -overexpressing $Pten^{-/-}$;$Trp53^{-/-}$ (RapidCap) murine prostate cancer cells. Densitometry values normalized to the housekeeping are indicated for each band. The experiment was repeated two independent times with similar results. **d**, Representative IHC of Gr-1-positive cells in control vector or PDCD4 -overexpressing $Pten^{-/-}$;$Trp53^{-/-}$ (RapidCap) allografts. Scale bar 50 µm. (n = 5 mice in each group). **e**, Representative FACS plot of $CD45^+$/$CD11b^+$/$Ly6G^{high}$/$Ly6C^{low}$ cells (PMN-MDSCs) inside the $CD45^+$/$CD11b^+$ population. **f**, Percentage of tumor-infiltrating $CD45^+$/$CD11b^+$/$Ly6G^{high}$/$Ly6C^{low}$ (PMN-MDSCs) in control vector and PDCD4-overexpressing $Pten^{-/-}$;$Trp53^{-/-}$ (RapidCap) allografts determined by flow cytometric analysis (n = 5 mice in each group). Data are mean ± SD. Statistical analysis (Mann-Whitney test). **g**, Correlation between PDCD4 mRNA levels and disease-free probability in the indicated human prostate cancer datasets. **h**, Correlation between PDCD4 mRNA expression levels and Pten deletion/mutation in the human prostate cancer TCGA dataset. Statistical analysis: chi-square test.

https://doi.org/10.1038/s43018-023-00594-z

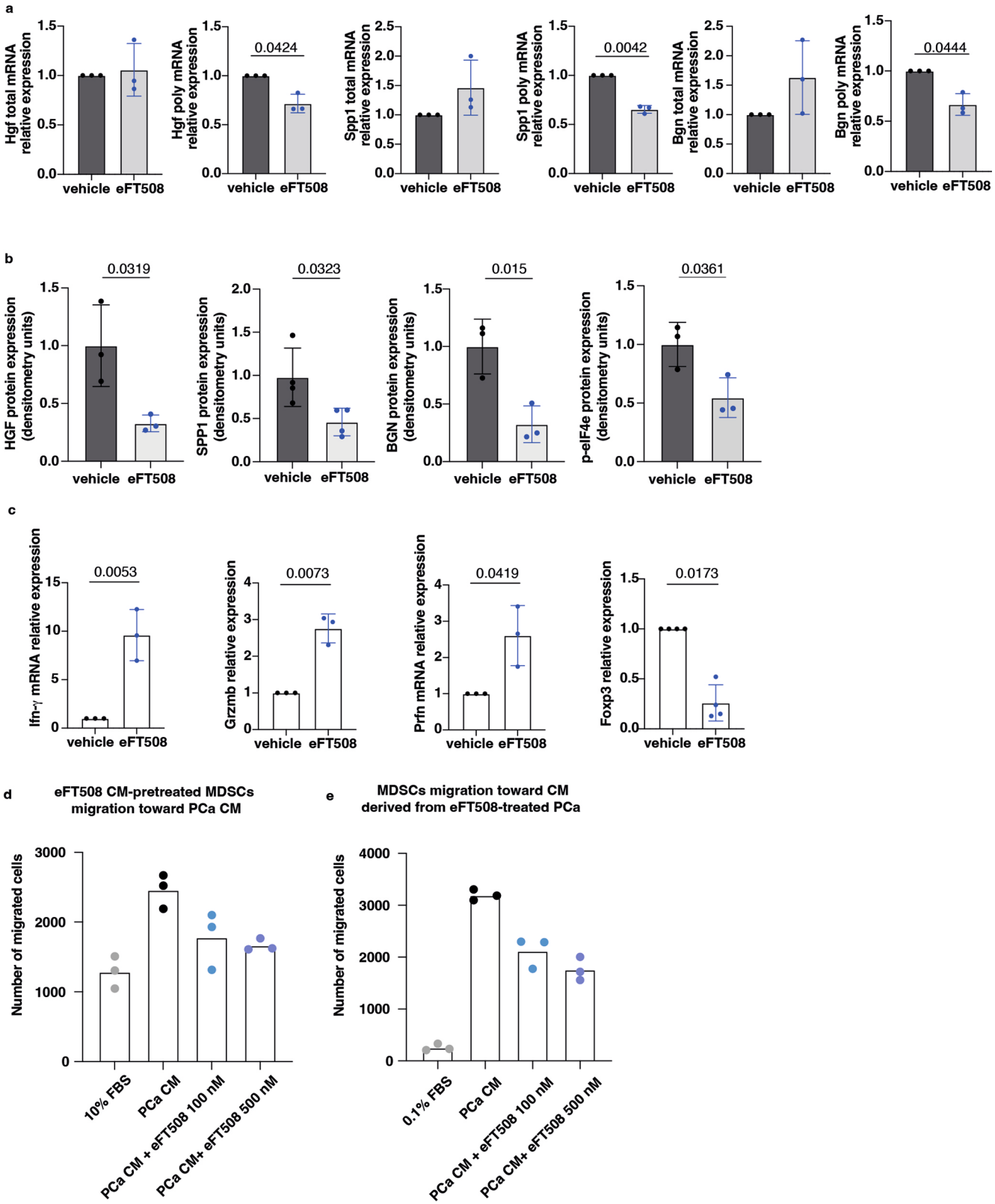

Extended Data Fig. 7 | See next page for caption.

https://doi.org/10.1038/s43018-023-00594-z

Extended Data Fig. 7 | eFT508 inhibits translation of *Hgf*, *Spp1* and *Bgn* and impairs PMN-MDSCs migration in prostate cancer. a, *Hgf*, *Spp1* and *Bgn* mRNA levels in polysomes-bound mRNAs and total mRNAs fraction in prostate cancer of eFT508-treated and vehicle-treated $Pten^{pc-/-}$;$Trp53^{pc-/-}$ mice determined by qRT- PCR (n = 3 mice in each group). Data are mean ± SD. Statistical analysis (two-tailed ratio paired t-test). **b**, Densitometry of BGN, SPP1 and HGF protein expression levels in prostate cancer of eFT508-treated or vehicle-treated $Pten^{pc-/-}$;$Trp53^{pc-/-}$ mice (BGN and HGF, n = 3 mice ; SPP1, n = 4 mice). Data are mean ± SD. Statistical analysis (unpaired two-sided Student's t-test). **c**, Ifng, Granzyme B (*GrzmB*), Perforin (*Prfn*) and *FoxP3* mRNA levels in prostate cancer of eFT508-treated compared to vehicle-treated $Pten^{pc-/-}$;$Trp53^{pc-/-}$ mice determined by qRT- PCR (Ifng, *GrzmB* and *Prfn*, n = 3 mice, *Foxp3* n = 4 mice). Data are mean ± SD. Statistical analysis (two-tailed ratio paired t-test). **d**, Number of migrated MDSCs tested in a transwell migration assay: MDSCs, previously exposed to 10% FBS, vehicle, 100 nM or 500 nM eFT508-treated $Pten^{pc-/-}$;$Trp53^{pc-/-}$ (RapidCap)-derived conditioned media for 24 hours, were allowed to migrate through a 5 µm-transwell to the bottom well for 6 hours toward $Pten^{-/-}$;$Trp53^{-/-}$ (RapidCap)-derived conditioned media. The number of migrated cells was determined by flow cytometric analysis. Experiment in technical replicates performed twice with similar results. **e**, Number of migrated MDSCs tested in a transwell migration assay: MDSCs were allowed to migrate through a 5 µm-transwell to the bottom well for 6 hours toward 0.1% FBS media, vehicle, 100 nM or 500 nM eFT508-treated $Pten^{-/-}$;$Trp53^{-/-}$ (RapidCap)-derived conditioned media. The number of migrated cells was determined by flow cytometric analysis. Experiment in technical replicates performed twice with similar results.

https://doi.org/10.1038/s43018-023-00594-z

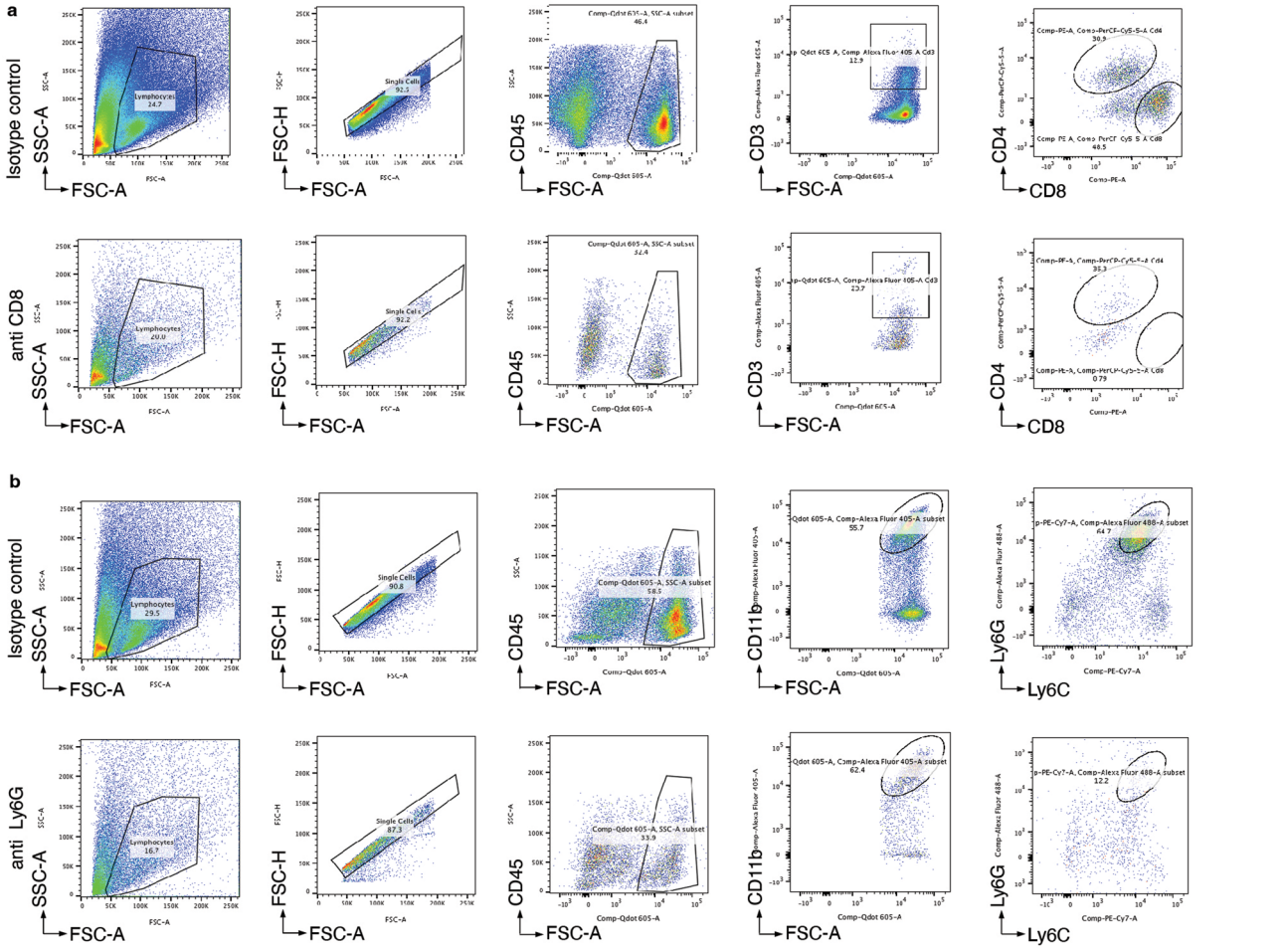

Extended Data Fig. 8 | eFT508 restores T cell activation in the Pten$^{pc-/-}$;Trp53$^{pc-/-}$ mouse model. a, Representative FACS plots of the CD45$^+$/CD3 population and CD45$^+$/CD3$^+$/CD8$^+$ cells upon isotype control and anti-CD8 depleting antibody. **b**, Representative FACS plots of the CD45$^+$/CD11b$^+$ population and CD45$^+$/CD11b$^+$/Ly6G^{high}/Ly6C^{low} (PMN-MDSCs) upon isotype control and anti-Ly6G depleting antibody. **c**, Ifng, *GrzmB* and *Foxp3* mRNA levels in eFT508-treated and vehicle-treated Pten$^{-/-}$;Trp53$^{-/-}$ (RapidCap) allografts determined by qRT- PCR (vehicle group, n = 4; eFT508 group, n = 4, n = 5, n = 5 mice, respectively). Data are mean ± SD. Statistical analysis (unpaired two-sided Student's t-test). **d**, Growth curve analysis of Pten$^{-/-}$;Trp53$^{-/-}$ (RapidCap) murine prostate cancer cells, LnCap and PC3 human prostate cancer cell line treated with vehicle or 1 µM, 2 µM, 5 µM eFT508, determined by the Incucyte system. Data are mean ± SEM. The experiment was repeated two independent times with similar results.

https://doi.org/10.1038/s43018-023-00594-z

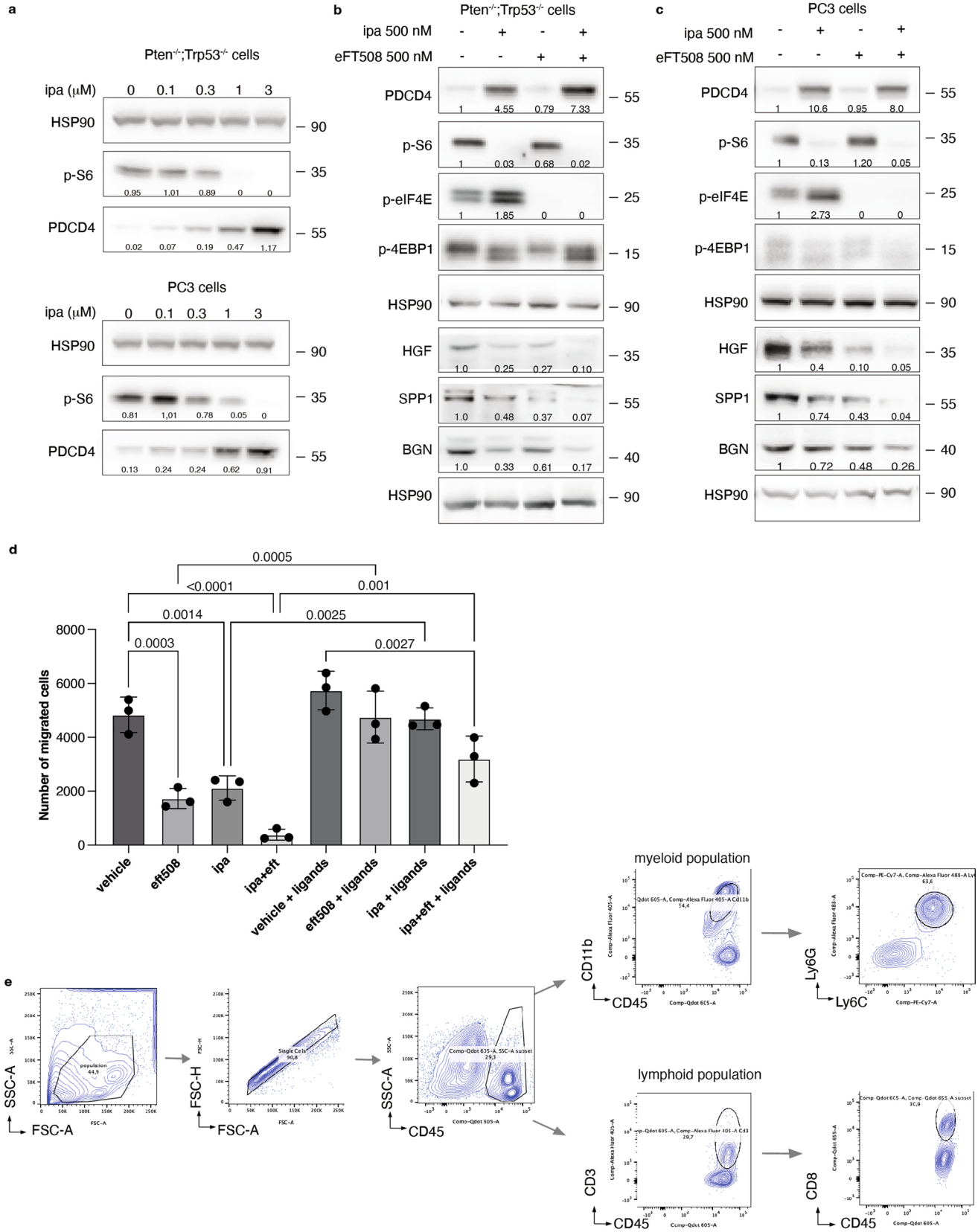

Extended Data Fig. 9 | See next page for caption.

https://doi.org/10.1038/s43018-023-00594-z

Extended Data Fig. 9 | AKT inhibition increases PDCD4 levels and cooperates with eFT508 to reduce HGF, SPP1 and BGN protein levels in Pten$^{-/-}$;Trp53$^{-/-}$ prostate cancer cells. a, Western blot analysis showing the protein levels of PDCD4 and phospho-S6 in Pten$^{-/-}$;Trp53$^{-/-}$ (RapidCap) and PC3 prostate cancer cell line upon treatment with the indicated concentration of ipatasertib. Densitometry values normalized to the loading control are indicated at the bottom for each band. The experiment was repeated two independent times with similar results. **b**, Western blot analysis showing the protein levels of PDCD4, p-S6, p-eIF4E, p-4EBP1, HSP90 (upper panel) and HGF, SPP1, BGN and representative HSP90 (lower panel) in Pten$^{-/-}$;Trp53$^{-/-}$ (RapidCap) murine prostate cancer cell line upon treatment with vehicle, 500 nM eFT508, 500 nM ipatasertib or the dual treatment. Densitometry values normalized to the loading control are indicated at the bottom for each band. The experiment was repeated two independent times with similar results. **c**, Western blot analysis showing the protein levels of PDCD4, p-S6, p-eIF4E, p-4EBP1, HSP90 (upper panel) and HGF, SPP1, BGN and representative HSP90 (lower panel) in PC3 human prostate cancer cell line upon treatment with vehicle, 500 nM eFT508, 500 nM ipatasertib or the dual treatment. Densitometry values normalized to the loading control are indicated for each band. The experiment was repeated two independent times with similar results. **d**, Transwell migration assay performed with bone marrow-derived MDSCs tested for the capability to migrate toward PCa medium conditioned with the indicated treatments. n = 3 biological replicates. The experiment was repeated two independent times with similar results. Data are mean ± SD. Statistical analysis between all groups (ordinary one-way ANOVA followed by Tukey's multiple comparisons test). **e**, Representative FACS plot of the gating strategy for the quantification of CD45$^+$/CD11b$^+$/Ly6G^{high}/Ly6C^{low} (PMN-MDSCs) (left) and CD45$^+$/CD3$^+$/CD8$^+$ cells (right) in Pten$^{pc-/-}$;Trp53$^{pc-/-}$ prostate tumors.

https://doi.org/10.1038/s43018-023-00594-z

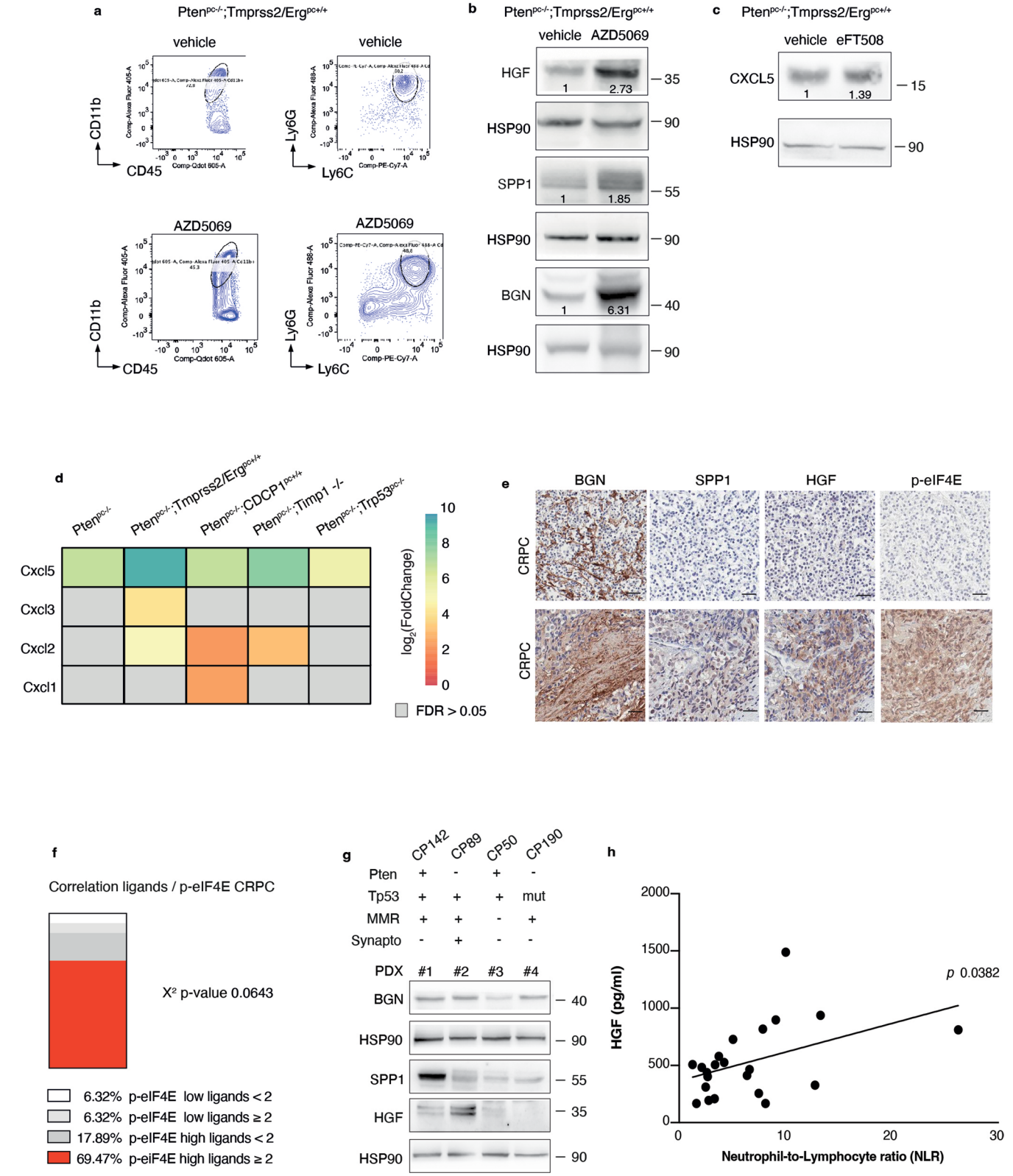

Extended Data Fig. 10 | See next page for caption.

https://doi.org/10.1038/s43018-023-00594-z

Extended Data Fig. 10 | BGN, SPP1 and HGF are highly expressed in CRPC and correlate with p-eIF4E protein levels. a, Representative FACS plots of $CD45^+$/$CD11b^+$ population and $Ly6G^{high}$/$Ly6C^{low}$ cells (PMN-MDSCs) inside the $CD45^+$/$CD11b^+$ population in AZD5069-treated and vehicle-treated $Pten^{pc-/-}$;Tmprss2/$Erg^{pc+/+}$. **b**, Western blot analysis showing the protein levels of HGF, SPP1 and BGN in $Pten^{pc-/-}$;Tmprss2/$Erg^{pc+/+}$ prostate tumors upon treatment with vehicle or AZD5069. Densitometry values normalized to the housekeeping are indicated for each band. The experiment was performed once. **c**, Western blot analysis showing the protein levels of CXCL5 in $Pten^{pc-/-}$;Tmprss2/$Erg^{pc+/+}$ prostate tumors upon treatment with vehicle or eFT508. Densitometry values normalized to the housekeeping are indicated for each band. The experiment was repeated two independent times with similar results. **d**, Heatmap depicting the mRNA levels of CXCL-chemokines in prostate tumors of the indicated genotypes compared to wild-type prostates (total mRNA expression determined by RNA-seq; n = 3 mice for each genetic background). **e**, Representative IHC of BGN, SPP1, HGF and p-eIF4E showing negative (upper panel) and positive (lower panel) cases in CRPC in cohort 1. Scale Bar 50 µm. **f**, Correlation between the co-expression of ≥ 2 ligands and p-eIF4E in CRPC in cohort 1 (n = 101). Two-sided Fisher's exact test. **g**, Western blot showing the protein levels of BGN, SPP1 and HGF and representative HSP90 in CRPC patient-derived xenografts. (n = 4). **h**, Correlation between plasma HGF levels (pg/ml), determined by ELISA assay, and neutrophil-to-lymphocyte ratio (NLR) in CRPC patients. Statistical analysis: simple linear regression.

nature portfolio

Corresponding author(s): Andrea Alimonti

Last updated by author(s): 9 June 2023

Reporting Summary

Nature Portfolio wishes to improve the reproducibility of the work that we publish. This form provides structure for consistency and transparency in reporting. For further information on Nature Portfolio policies, see our Editorial Policies and the Editorial Policy Checklist.

Statistics

For all statistical analyses, confirm that the following items are present in the figure legend, table legend, main text, or Methods section.

n/a	Confirmed	
☐	☒	The exact sample size (*n*) for each experimental group/condition, given as a discrete number and unit of measurement
☐	☒	A statement on whether measurements were taken from distinct samples or whether the same sample was measured repeatedly
☐	☒	The statistical test(s) used AND whether they are one- or two-sided *Only common tests should be described solely by name; describe more complex techniques in the Methods section.*
☒	☐	A description of all covariates tested
☐	☒	A description of any assumptions or corrections, such as tests of normality and adjustment for multiple comparisons
☐	☒	A full description of the statistical parameters including central tendency (e.g. means) or other basic estimates (e.g. regression coefficient) AND variation (e.g. standard deviation) or associated estimates of uncertainty (e.g. confidence intervals)
☐	☒	For null hypothesis testing, the test statistic (e.g. *F*, *t*, *r*) with confidence intervals, effect sizes, degrees of freedom and *P* value noted *Give P values as exact values whenever suitable.*
☒	☐	For Bayesian analysis, information on the choice of priors and Markov chain Monte Carlo settings
☒	☐	For hierarchical and complex designs, identification of the appropriate level for tests and full reporting of outcomes
☐	☒	Estimates of effect sizes (e.g. Cohen's *d*, Pearson's *r*), indicating how they were calculated

Our web collection on statistics for biologists contains articles on many of the points above.

Software and code

Policy information about availability of computer code

Data collection	RNA Sequencing: Illumina NextSeq 500/550 (Illumina). Flow cytometry: BD Fortessa flow cytometer (BD Biosciences). FACS-sorting: BD FACSAria III. IHC image acquisition: Aperio ScanScope (Leica Biosystem). BCA proten quantification: Epoch microplate spectrophotometer. Western blot acquisition: Fusion Solo S. In vitro cell growth analysis: Incucyte image system. Polysome profiles acquisition: BioLogic LP system and BioLogic LP Dataview 2.0 (BioRad). Real-Time PCR: StepOne plus Real-Time PCR system (Applied Biosystem).
Data analysis	Gene expression analysis: FastQC v0.11.8. STAR v.2.5.1b. RStudio v1.3.1093. DESeq2 V1.34.0. Anota2seq v1.18.0. All the plots were generated using ggplot2 v3.3.5. (Wickham H (2016). ggplot2: Elegant Graphics for Data Analysis. Springer-Verlag New York. ISBN 978-3-319-24277-4, https://ggplot2.tidyverse.org.), ggpubr v0.4.0. and Pheatmap v1.0.12. David 6.8. software Immunohistochemistry: ImageScope, v12.3.2.8013, Leica Biosystem. Western blot analysis: ImageJ 1.52p. Flow cytometry analysis: BD FACSDiva software 6.0; FlowJo software 10.1. Cell growth analysis:

Incucyte software v.2020B.
Data and statistical analysis:
Microsoft Excel 2018. GraphPad Prism v8.4.2.

For manuscripts utilizing custom algorithms or software that are central to the research but not yet described in published literature, software must be made available to editors and reviewers. We strongly encourage code deposition in a community repository (e.g. GitHub). See the Nature Portfolio guidelines for submitting code & software for further information.

Data

Policy information about availability of data

All manuscripts must include a data availability statement. This statement should provide the following information, where applicable:

- Accession codes, unique identifiers, or web links for publicly available datasets
- A description of any restrictions on data availability
- For clinical datasets or third party data, please ensure that the statement adheres to our policy

Gene expression data (RNA-seq) that support the findings of the present study have been deposited in :
ArrayExpress: E-MTAB-9624 (RNA-seq on total RNA of wild-type, Pten pc-/-; Pten pc-/-; P53 pc -/-);
Gene Expression Omnibus under accession no. GSE202910 =
RNA-seq on total RNA of Pten pc-/; TMPRSS2/Erg pc+/+; Pten pc-/-; Cdcp1 pc +/+; Pten pc-/-; Timp1 -/-
RNA-seq on polysomal RNA of Pten pc-/; TMPRSS2/Erg pc+/+; Pten pc-/-; Cdcp1 pc +/+; Pten pc-/-; Timp1 -/-.
The data published in the Array Express are the results of the RNAseq on total RNA of the same samples for which the results of the RNAseq on polysomal RNA are published on GEO database, and they are processed at the same time.

Gene Expression Omnibus under accession no. GSE202907 =
RNA-seq on total RNA of undifferentiated bone marrow, PMN-MDSCs (Cd11b+/Ly6Ghigh/Ly6Clow) and M-MDSCs (Cd11b+/Ly6Gneg/Ly6Chigh).
RNA-seq on polysomal RNA of undifferentiated bone marrow, PMN-MDSCs (Cd11b+/Ly6Ghigh/Ly6Clow) and M-MDSCs (Cd11b+/Ly6Gneg/Ly6Chigh).

The datasets used in this study are:
Uniprot: https://www.uniprot.org/; Human Protein Atlas: https://www.proteinatlas.org/; STRING: https://string-db.org/; David 6.8: https://david.ncifcrf.gov/; iTALK https://www.biorxiv.org/content/10.1101/507871v1.full.

The human prostate cancer transcriptomic data were derived from the TCGA Research Network (http://cancergenome.nih.gov/) and from: Taylor, B. S. et al. Integrative genomic profiling of human prostate cancer. Cancer Cell 18, 11-22 (2010). https://doi.org:10.1016/j.ccr.2010.05.026.

Human research participants

Policy information about studies involving human research participants and Sex and Gender in Research.

Reporting on sex and gender	All the patients samples used in the study derived from males.
Population characteristics	The patient samples used in Cohort 1 (n= 545) of Figure 7 were from benign prostate hyperplasia, primary adenocarcinoma and castration-resistant prostate cancer, as described in ref. 45 and ref. 80. The mean age was 65.03± 8.34 The patient samples used in Cohort 2 (n=69) of Figure 7 were primary adenocarcinoma derived from the same patient. The mean age was 67.17 ± 7.56. Patients-derived xenografts were obtained as described previously (https://doi.org/10.1158/1078-0432.CCR-17-3571). All samples used in Extended Data Figure 10h (n=22) were obtained from patients affected by castration-resistant prostate cancer.
Recruitment	All patients had given written informed consent and were enrolled in institutional protocols approved by the Royal Marsden NHS Foundation Trust Hospital (London, UK) ethics review committee (reference no. 04/Q0801/60) and by the Padova Province (Padova, Italy) Clinical Experimentation Ethics Committee (reference no. 5480/AO/22). Human biological samples were sourced ethically and their research use was in accord with the terms of the informed consent provided. Case selection was therefore independent and blinded to baseline characteristics, treatments received, clinical outcome and molecular characterization to reduce any potential self-selection bias.
Ethics oversight	Royal Marsden NHS Foundation Trust Hospital (London, UK) ethics review committee (reference no. 04/Q0801/60); Padova Province (Padova, Italy) Clinical Experimentation Ethics Committee (reference no. 5480/AO/22). Patients did not receive compensation.

Note that full information on the approval of the study protocol must also be provided in the manuscript.

Field-specific reporting

Please select the one below that is the best fit for your research. If you are not sure, read the appropriate sections before making your selection.

☒ Life sciences ☐ Behavioural & social sciences ☐ Ecological, evolutionary & environmental sciences

For a reference copy of the document with all sections, see nature.com/documents/nr-reporting-summary-flat.pdf

Life sciences study design

All studies must disclose on these points even when the disclosure is negative.

Sample size	No statistical method was used to predetermine sample size. For animal studies, sample size was defined based on past experience with the models. For ethical reasons, the minimum number of animals necessary was used.
Data exclusions	No data were excluded from the analysis. All samples meeting proper experimental conditions were included.
Replication	The experiments were done with the number of replicates indicated in the figure legends.
Randomization	Animals were allocated randomly to each treatment group. Samples from different treatment groups were processed identically, and animals in different treatment groups were exposed to the same environment. For experiments other than those involving animals, the samples were allocated randomly into experimental groups.
Blinding	Data collection and analysis were not performed blind to the conditions of the experiments.

Reporting for specific materials, systems and methods

We require information from authors about some types of materials, experimental systems and methods used in many studies. Here, indicate whether each material, system or method listed is relevant to your study. If you are not sure if a list item applies to your research, read the appropriate section before selecting a response.

Materials & experimental systems

n/a	Involved in the study
☐	☒ Antibodies
☐	☒ Eukaryotic cell lines
☒	☐ Palaeontology and archaeology
☐	☒ Animals and other organisms
☒	☐ Clinical data
☒	☐ Dual use research of concern

Methods

n/a	Involved in the study
☒	☐ ChIP-seq
☐	☒ Flow cytometry
☒	☐ MRI-based neuroimaging

Antibodies

Antibodies used	Flow cytometry= CD45 (Biolegend, code 103140, clone 30-F11, lot no. B235438; 1:200); Ly-6G (Biolegend, code 127626, clone 1A8, lot no. B194432; 1:200); Ly-6C (Biolegend, code 128017, clone HK1.4, lot no. B243043; 1:200); Ly-6C (Biolegend, code 128008, clone HK1.4; 1:200); CD11b (Biolegend, code 101235, clone M1/70, lot no. B233927; 1:200); F4/80 (Biolegend, code 123152, clone BM8, lot no. 4305911; 1:100), B220 (Biolegend, clone 103228, RA3-6B2, lot no. B210434; 1:200), CD3 (Biolegend, code 100341, clone 145-2C11, lot no. B241616; 1:200), CD8 (Biolegend, code 100742, clone 53-6.7, lot no. B193838; 1:200), CD8 (Invitrogen, code 12-0081-83, clone 53-6.7, 1:200), CD4 (Biolegend, code 100433, clone GK1.5, lot no. B240053; 1:200), NK1.1 (Biolegend, code 108710, clone PK136, lot no. 4291566; 1:200), EpCAM (Thermo Fisher Scientific, code 11-5791-82; clone G8.8, 1:200), Met (Thermo Fisher Scientific; code 11-8854-82; eBioclone 7; 1:100), Tlr2 (Biolegend; code 153008; clone QA1601, 1:200), Cd44 (Biolegend; code 103029, clone IM7; 1:200). Samples were acquired on a BD Fortessa flow cytometer (BD Biosciences). Data were analyzed using FlowJo software (TreeStar). For the polysome profiling analysis, MDSCs were sorted using a FACS Aria III cell sorter (BD Biosciences), after staining with CD11b (Biolegend, code 101235, clone M1/70, 1:200)); Ly-6G (Biolegend, code 127618, clone 1A8, 1:200) and Ly-6C (Biolegend, code 128026, clone HK1.4; 1:200). Western Blot: PTEN (Cell Signaling Technology, catalog 9552S; 1:1000); HSP90 (Cell Signaling Technology, catalog 4877S; 1:1000); β-actin (Sigma, catalog A5316; 1:5000); AKT (Cell Signaling Technology, catalog 9272S; 1:1000); p-AKT-S473 (Cell Signaling Technology, catalog 9171S; 1:1000); p-S6-Ser235/236 (Cell Signaling Technology, catalog 4857; 1:1000), eIF4G1 (Cell Signaling Technology, catalog 8701S; 1:1000); eIF4A1 (Cell Signaling Technology, catalog 2013T; 1:1000); Pdcd4 (Cell Signaling Technology, catalog 9535S; 1:1000); p-eIF4e (Abcam; ab7626; 1:1000), eIF4e (Thermo Scientific; code MA1089; clone 5D11; 1:1000), p-4EBP1(Cell Signaling Technology; catalog 2855; 1:1000), p-Mnk1 (Cell Signaling Technology, catalog 2111S; 1:1000), Mnk1 (Cell Signaling Technology, catalog 2195S; 1:1000), Hgf (Thermo Scientific; PA5-79361; 1:1000), Hgf (Cell Signaling technology; catalog 52445 clone D6S7D; 1:500) Spp1 (R&D system, MAB808-100; 1:1000), Spp1 (Abcam catalog ab283656; RM1018, 1:1000), Bgn (Abcam; ab109369; 1:1000), Cxcl5 (Genetex; GTX53165; 1:1000). Mouse IHC= anti-peIF4e (ab7626; Abcam, 1:100), anti-Pdcd4 (Cell Signaling Technology, catalog 9535S; 1:400), anti-Ly6G (Gr1) (BD Pharmingen; clone 1A8, catalog 551459, 1:1500) and anti-Cd3 (Dako, catalog A0452; 1:800). Human IHC= anti-Hgf (LS-Bio; LS-C3402101, 1:300), anti-Spp1 (IBL-America, #18625, 1:200), anti-Bgn (R&D system; AF-2667, 1:400), anti-peIF4e (ab7626; Abcam, 1:100) and anti-Cd33 (Leica D04C023; PA0555, clone PWS44, 1:500). In vivo experiments: InVivoPlus anti-mouse CD8 antibody (BioXCell; BP0061-5MG-A), InVivoPlus anti-mouse Ly6G BioXCell, BP0075-1-5MG-A); InVivoMab rat IgG2b isotype control (BioXCell; BE0090-5MG-A).
Validation	The validation of each primary antibody for the species and applications is available from the manufacturer's websites. For flow cytometry analysis and Western Blot analysis, standardized dilution previously set up in the laboratory or by the investigator was

used. For murine and human IHC, preliminary tests with increasing dilutions and different unmasking pH solutions were performed.

Eukaryotic cell lines

Policy information about cell lines and Sex and Gender in Research

Cell line source(s)	HEK-293T CRL-3216™ATCC® , TRAMP-C1 cell line ATCC® CRL-2730™ , PC-3 ATCC® CRL-1435™ , LNCaP clone FGC ATCC® CRL-1740™. Pten null; P53 null (RapidCap) cell lines were obtained as described in ref. 68 from Dr. Lloyd Trotman laboratory. Where indicated, cells were engineered as described in the method sections.
Authentication	All the cell lines used were purchased from ATCC. No further authentications were performed.
Mycoplasma contamination	Cells were routinely tested for mycoplasma with MycoAlert Mycoplasma Detection kit (Lonza, Cat. LT07-218).
Commonly misidentified lines (See ICLAC register)	No commonly misidentified cell lines were used in the study.

Animals and other research organisms

Policy information about studies involving animals; ARRIVE guidelines recommended for reporting animal research, and Sex and Gender in Research

Laboratory animals	All mice were maintained under specific pathogen-free conditions in the IRB facility (Bellinzona, Switzerland). Experiments were performed according to the state guidelines and approved by the local ethical committee (''Dipartimento della Sanità e Socialità, Esperimenti su animali'' Canton Ticino), authorization number TI13/2015, TI25/2016, TI51/2018 e TI08/2021. The local ethics committee approved the conduction of the in vivo experiments with maximal tumor sizes of 1500 mm3. The maximal tumor size/burden was not exceeded. Male C57BL/6 were purchased from Charles River (Calco, Italy) and acclimatized for four weeks before experimentation. Mice were maintained in a 12 hour light (7 am-7pm) and 12 hour dark cycles (7pm-7 am) environment. The temperature is 21 +/- 2 degrees and humidity is 55% +/- 5%. Pten pc-/- mice were generated as described in ref. 5 and genotyped as follows: female Pten loxP/loxP mice were crossed with male Pten loxP/WT;PB-Cre4 transgenic mice and genotyped for Cre using the following primers: primer 1 (5'-AAAAGTTCCCCTGCTGATGATTTGT-3') and primer 2 (5'-TGTTTTTGACCAATTAAAGTAGGCTGTG-3') for PTEN loxP/loxP: primer 1 (5' TGATGGACATGTTCAGGGATC 3') and primer 2 (5'CAGCCACCAGCTTGCATGA 3') for Probasin-CRE. TMPRSS2/Erg pc+/+ mice were obtained as described in ref. 42 Female Pten loxP/loxP ;Trp53loxP/loxP mice, generated as described in ref. 43, were crossed with male PB-Cre4 transgenic mice for the prostate-specific deletion of Pten and Trp53 . To obtain the prostate-specific overexpression of CDCP1 and deletion of Pten, female CDCP1, obtained as described in ref. 44, and/or Pten loxP/loxP mice were crossed with male Probasin-Cre4 (Pb-Cre4) transgenic mice. Prostate-specific Pten pc-/- transgenic mice were crossed with Timp1-/- mice (Jackson Laboratory, 6243) to generate Timp1 knockout in Pten pc-/-, as described in ref.45.
Wild animals	No wild animals were used in this study.
Reporting on sex	All the animals used in this study are male mice.
Field-collected samples	No field-collected samples were used in the study.
Ethics oversight	The animal experiments were approved by the local ethical committee (''Dipartimento della Sanità e Socialità, Esperimenti su animali'' Canton Ticino), authorization number TI13/2015, TI25/2016, TI51/2018 e TI08/2021. Mice undergoing treatment were administered control vehicles or therapeutic doses of the appropriate agents. Any mouse suffering distress or greater than 15% weight loss during treatment was euthanized by CO2 asphyxiation. At the completion of the study, mice were euthanized by CO2 asphyxiation. Tissues and blood were collected for histology, mRNA analysis, protein analysis and single-cell suspensions for flow cytometry.

Note that full information on the approval of the study protocol must also be provided in the manuscript.

Flow Cytometry

Plots

Confirm that:

☒ The axis labels state the marker and fluorochrome used (e.g. CD4-FITC).

☒ The axis scales are clearly visible. Include numbers along axes only for bottom left plot of group (a 'group' is an analysis of identical markers).

☒ All plots are contour plots with outliers or pseudocolor plots.

☒ A numerical value for number of cells or percentage (with statistics) is provided.

Methodology

Sample preparation	To obtain single-cell suspensions, murine prostates were cut into small pieces with scissors, digested in collagenase D (5 µg/ml, Roche, Cat. 11088858001) for 1 hour at 37 °C, incubated in Trypsin and DNase (20 µg/ml, Roche, Cat.4716728001) for five minutes and smashed onto a cell strainer (Falcon®, Cat.352340). To obtain bone marrow cells, femurs were flushed with ice-cold PBS and red blood cells were lysed with ACK buffer (Gibco, Cat. A10492-01). Bone marrow cells were cultured and differentiated into myeloid-derived suppressor cells as described in Methods. Prostate single cell suspensions or MDSCs were blocked for Fc receptor binding with CD16/CD32 antibody (Biolegend, cose 101302, clone 93) for 15 min and stained with the antibodies indicated in Methods: CD45 (Biolegend, clone 30-F11, lot no. B235438; 1:200); Ly-6G (Biolegend, clone 1A8, lot no. B194432; 1:200); Ly-6C (Biolegend, clone HK1.4, 1:200), CD11b (CD11b, clone M1/70, 1:200); F4/80 (Biolegend, clone BM8,1:100), B220 (Biolegend, clone RA3-6B2, 1:200), CD3 (Biolegend, clone 145-2C11, 1:200), CD8 (Biolegend, clone 53-6.7, 1:200), CD4 (Biolegend, clone GK1.5, 1:200), NK1.1 (Biolegend, clone PK136, 1:200), EpCAM (Thermo Fisher Scientific, code 11-5791-82; clone G8.8, 1:200), Met (Thermo Fisher Scientific; code 11-8854-82; eBioclone 7; 1:100), Tlr2 (Thermo Fisher Scientific; code 11-8854-82; eBioclone 7; 1:100), CD44 (Biolegend; code 103029, clone IM7; 1:200). Samples were acquired at BD Fortessa cytometer (BD Biosciences). Data were analyzed using FlowJo software (LLC). For gating, isotype controls or fluorescence-minus-one controls were used.
Instrument	BD Fortessa flow cytometer (BD Biosciences)
Software	FlowJo software (10.6)
Cell population abundance	PMN-MDSCs and Mo-MDSCs were sorted accordingly to the gating strategy reported in Extended Data Figure 2c.
Gating strategy	Cells were gated on SSC-A, FSC-A gate and FSC-H, FSC-A gate. The frequency of different cell subsets analyzed was reported as the frequency within the CD45+ cells.

☒ Tick this box to confirm that a figure exemplifying the gating strategy is provided in the Supplementary Information.